Two stages of skarn formation - two tin enrichments: the Hämmerlein polymetallic skarn deposit, western Erzgebirge, Germany

---

kumulative Dissertation
zur Erlangung des akademischen Grades
„doctor rerum naturalium" (Dr. rer. Nat.)
in der Wissenschaftsdisziplin „Geochemie"

eingereicht an der
MATHEMATISCH-NATURWISSENSCHAFTLICHEN FAKULTÄT
INSTITUT FÜR ERD- UND UMWELTWISSENSCHAFTEN DER UNIVERSITÄT POTSDAM

von
Marie G. Lefebvre
Potsdam, im März 2019

Datum der Disputation: 05.03.2019

Supervisor: **Prof. Dr. Rolf. L. Romer**
1. Referee GFZ German Research Centre for Geosciences, Potsdam, Germany
University of Potsdam, Institute of Earth and Environmental Science, Germany

2. Referee: **Univ. Prof. Mag. Rer. Nat. Dr. Mont. Frank Melcher**
Montanuniversität, Chair of Geology and Economic Geology, Leoben, Germany

3. Referee: **Prof. Dr. Uwe Altenberger**
University of Potsdam, Institute of Earth and Environmental Science, Germany

Published online at the
Institutional Repository of the University of Potsdam:
https://doi.org/10.25932/publishup-42717
https://nbn-resolving.org/urn:nbn:de:kobv:517-opus4-427178

Zusammenfassung

Skarn-Lagerstätten befinden sich auf allen Kontinenten und wurden zu unterschiedlichen Zeiten vom Präkambrium bis zum Tertiär gebildet. Typischerweise wird die Bildung eines Skarns durch die Intrusion eines Granits in karbonatreiche Sedimentgesteine induziert. Während der Kontaktmetamorphose reagieren die Fluide aus dem Granit mit dem sedimentären Wirtgestein, was zur Bildung von Kalksilikaten auf Kosten von Karbonaten führt. Diese neu gebildeten Minerale entwickeln sich im Allgemeinen in einer metamorph zonierten Aureole mit Granat im proximalen und Pyroxen im distalen Bereich. Erzelemente die in magmatischen Fluiden enthalten sind werden aufgrund der veränderten Fluidzusammensetzung ausgefällt. Die Temperaturabsenkung des gesamten Systems, hervorgerufen durch die Abkühlung von magmatischen Fluiden sowie durch das Eindringen meteorischen Wassers, führen zu teilweisen oder vollständigen Umwandlung prograder Minerale.

Die Skarn-Lagerstätte Hämmerlein hat eine mehrstufige Geschichte mit Skarnsbildung während der regionalen Metamorphose und Retrogression der primären Skarn-Minerale während der Intrusion von Graniten. Zinn wurde während beiden Ereignissen mobilisiert. Die 340 Ma alten zinnhaltigen Skarnminerale zeigen, dass Zinn in Sedimenten bereits vor dem Graniteintrag vorhanden war, und dass die erste Sn-Anreicherung während der Bildung des Skarns durch Fluide der Regionalmetamorphose stattfand. In einem zweiten Schritt um 320 Ma wurden Zinn-haltige Fluide durch die Intrusion des Eibenstockgranits freigesetzt. Diese Fluide überprägten den Skarn. Das freisetzen und das neu zugefügte Zinn ist in Kassiterit gebunden und führten dem System zusätzliches Zinn zu, wobei Zinn aus den Skarn-Kalksilikaten remobilisiert wurde.

Im Vergleich zu Tonstein oder Mergel sind die Skarn mit Sn, W, In, Zn, und Cu angereichet. Diese Metalle sind während der Regionalmetamorphose und der Granitplatznahme zu unterschiedlichen Teilen zugeführt worden. Darüber hinaus zeigen die verschiedenen isotopen und chemischen Daten der Skarn-Proben, dass der Granit selektiv einige Elemente wie Sn hinzugefügt, und dass es keinen sichtbar granitischen Beitrag zur sedimentären Signatur des Skarns gab.

Das Beispiel Hämmerlein zeigt, dass es möglich ist einen zinnreichen Skarn ohne zugehörigen Granit zu bilden, wenn Zinn von zinnhaltigen Sedimenten während einer Regionalmetamorphose mit wässrigen metamorphen Fluiden transportiert worden ist. Diese Skarne sind wirtschaftlich uninterssant wenn das Zinn nur in den Skarn-Mineralen enthalten ist. Spätere Umwandlung des Skarns (die Quelle der Wärme und Fluiden ist nicht unbedingt ein Granit) kann jedoch zur Bildung von sekundärem Kassiterite (SnO_2) führen, womit der Skarn plötzlich wirtschaftlich hoch interessant sein kann.

Abstract

Skarn deposits are found on every continents and were formed at different times from Precambrian to Tertiary. Typically, the formation of a skarn is induced by a granitic intrusion in carbonates-rich sedimentary rocks. During contact metamorphism, fluids derived from the granite interact with the sedimentary host rocks, which results in the formation of calc-silicate minerals at the expense of carbonates. Those newly formed minerals generally develop in a metamorphic zoned aureole with garnet in the proximal and pyroxene in the distal zone. Ore elements contained in magmatic fluids are precipitated due to the change in fluid composition. The temperature decrease of the entire system, due to the cooling of magmatic fluids and the entering of meteoric water, allows retrogression of some prograde minerals.

The Hämmerlein skarn deposit has a multi-stage history with a skarn formation during regional metamorphism and a retrogression of primary skarn minerals during the granitic intrusion. Tin was mobilized during both events. The 340 Ma old tin-bearing skarn minerals show that tin was present in sediments before the granite intrusion, and that the first Sn enrichment occurred during the skarn formation by regional metamorphism fluids. In a second step at ca. 320 Ma, tin-bearing fluids were produced with the intrusion of the Eibenstock granite. Tin, which has been added by the granite and remobilized from skarn calc-silicates, precipitated as cassiterite.

Compared to clay or marl, the skarn is enriched in Sn, W, In, Zn, and Cu. These metals have been supplied during both regional metamorphism and granite emplacement. In addition, the several isotopic and chemical data of skarn samples show that the granite selectively added elements such as Sn, and that there was no visible granitic contribution to the sedimentary signature of the skarn

The example of Hämmerlein shows that it is possible to form a tin-rich skarn without associated granite when tin has already been transported from tin-bearing sediments during regional metamorphism by aqueous metamorphic fluids. These skarns are economically not interesting if tin is only contained in the skarn minerals. Later alteration of the skarn (the heat and fluid source is not necessarily a granite), however, can lead to the formation of secondary cassiterite (SnO_2), with which the skarn can become economically highly interesting.

Acknowledgements

I would like to thank my supervisor Prof. Dr. Rolf L. Romer for his guidance, advice, patience and criticism during those three years (and a bit more) of PhD.

I also acknowledge the Inorganic and Isotopes Geochemistry section of the German Research Centre for Geosciences for their help with analytical work and the financial support of field work and conferences. I especially thank the head of the section, Prof. Dr. Sarah Gleeson, for her support. I would like to express my gratitude to PD Dr. Johannes Glodny for his help and teaching concerning isotopes geochemistry. I also thank Bettina Hübner for her precious help and guidance in the lab.

I am thankful to Dr. Franziska Wilke and Oona Appelt for support with microprobe analysis, Dr. Anja Maria Schleicher, Andrea Gottsche, and Sabine Tonn for their help during XRF and ICP-AES analysis, Uwe Dittmann and Elke Lewerenz for their help with thin sections preparation.

I am grateful to Dr. Marco Roscher, from Saxore Bergbau GmbH, who gave us access to Hämmerlein and allowed us to use his chemical data. I also thank him and PD Dr. Uwe Kroner, from TU Freiberg, for their advice and corrections for the papers we have written together.

I would also like to thank my office mate Dr. Mathias Wolf for the very nice atmosphere we had in our office. We spent three years of our lives to ask ourselves “Where is the tin?” and it is priceless.

I cannot write those acknowledgments without mentionning Christian Meeßen, Melanie Lorenz, and the entire first generation of the StRATEGy program. You are all amazing friends and my time in Germany would have been really boring without you.

I am grateful to my family who always supported me since the day I decided I wanted to be a geologist 15 years ago. It has been difficult, but it was worth it. I hope I will continue to make you proud for a long time.

Finally, I would like to thank Louis Desanois for his unwavering support. I do not know if I would have been able to finish this PhD without you. I hope I can become as strong as you, and be your support for our future adventures.

Contents

List of figures

List of tables

1. Chapter 1: Introduction

1.1. Generalities on skarns

Skarns are some of the most important mineralization in the crust and have mainly be mined for metals like Fe, Cu, W, Pb, Mo, Zn, Au, Ag, REE, U, B, F, and Sn. They occur on all continent, in various geological environments, and are dated from Precambrian to Tertiary. Most of skarn deposits which are described in the literature are formed by contact metamorphism. Their mineralogy is mainly dominated by calc-silicate minerals such as garnet and pyroxene. Different metals can be enriched with the skarnification process and form a deposit. These define the seven main types of skarns: Au, Cu, Fe, Mo, W, Zn, and Sn skarns.

1.1.1. Skarns: terminology

"Skarn" is an old Swedish word which referred to very hard calc-silicate rocks (i.e. mainly composed of garnet, pyroxene and amphibole) associated with chalcopyrite and magnetite deposits. Nowadays, this term is widely used to refer to metasomatic replacement of carbonate rocks by calc-silicate minerals during regional and/or contact metamorphism. Most of skarn occurrences generally formed by contact metamorphism with a granitic intrusion into carbonate rocks. The thermic anomaly causes chemical, textural, and mineralogical transformations, and forms a metamorphic aureole with an extension depending on the size of the intrusive body. Other parameters, like the chemicals compositions of the protolith and the magma, or the pressure, can be involved during this contact metamorphism.

Fluid circulation occurs during the formation of the intrusion, which implies that the metamorphism does not present isochemical features anymore. The system is then open and metasomatic reactions can occur, i.e. pervasive cationic exchange between the host rocks (intrusion and protolith) and the external environment. Three different kinds of fluids are implied in those reactions: (1) fluids with a purely magmatic origin, (2) fluids produced by dehydration and decarbonation of the host rocks, and (3) meteoric fluids. Depending on whether fluids are moving or not, metasomatic transfers occur respectively (1) by percolation when a pressure gradient make the fluid move across permeable rocks, or (2) by diffusion induced by a chemical potential gradient between the rocks.

Skarnification is a dynamic process in terms of time and space, which evolves between metamorphism and metasomatism, and occurs in carbonated environments. The strong gradient of temperature and the wide circulation cells of fluids generated by ascension of the magma contributes to a continuous metamorphism/metasomatism in the system. The process continues with retrograde alterations as temperature decreases and the chemical composition of the whole system changes.

1.1.2. Classification

Several classifications are proposed to distinguish the wide variety of skarns. A first distinction is based on their chemical composition between calcic and magnesian skarns, depending on whether they formed

from the replacement of limestone or dolomite (Einaudi et al., 1981; Burt, 1982). Another classification based on the oxidation state of skarns also exists (Einaudi et al., 1981). In this classification, assemblages of oxidized skarns are dominated by andradite, diopside, epidote, chlorite, quartz, calcite, and pyrite. On the other hand, reduced skarns are mainly composed of grossular, pyroxene, biotite, plagioclase, and pyrrhotite.

Skarnification is often associated with the concentration and deposition of metals, which depend on several parameters, including the chemistry of the intrusion and the oxidation state of fluids. Therefore, the economic and more widely used classification is based on the dominant metal occurring in skarn deposits: Au, Cu, Fe, Mo, Sn, W, or Zn (Einaudi and Burt, 1982; Meinert et al., 2005). This study will be focused on the tin occurrence in the Hämmerlein polymetallic deposit. Therefore, generalities on Sn-skarns will be detailed in the next paragraphs.

1.2. Identity card of Sn-skarns

1.2.1. Morphology

Tin skarns can be subdivided according to several criteria such as their distance to the granite, the nature of the skarn (calcic or magnesian), the amount of skarnified rock, the type of mineralization (oxide-rich or sulfide-rich), and the occurrence of greisen. Generally, tin skarns are associated with relatively shallow magmatic bodies emplaced close to or within carbonate rocks. The morphology of the skarn depends on the geometry of the contact between the magmatic body and the host rocks, but also on the morphology of the host rocks themselves (Chen et al., 1992). Most tin skarns show a stratabound or stratiform geometry following the sedimentary layers of the host rocks. Transfers of heat and fluids from the magmatic body to hosting carbonates induce the formation of a zonation of the host rock with proximal garnet and distal pyroxene at the contact between skarn and marble. Variations in this zonation depends on the magma chemistry, wall rocks composition, and oxidation state of the fluids.

1.2.2. Mineralogy

Garnet from tin skarns mainly show compositions ranging from pure andradite to grossular and can present significant content of almandine and spessartine. Al-free garnet bear significant amounts of tin (up to 6 wt%, Dobson 1982) due to the substitution of Fe^{3+} by Sn^{4+} and Fe^{2+} (Eadington and Kinealy 1983). Tin-skarn pyroxene mostly present hedenbergitic compositions (Newberry 1979) and may also incorporate tin (Lefebvre et al., 2019). Amphibole also occur in Sn-skarns and show mostly hastingsite, ferroedenite, and/or ferropargasite compositions (Newberry, 1998). They may also show relatively high contents of F and Cl (up to 1%, Kwak, 1983; Newberry et al., 1997), but also of Sn (Lefebvre et al., 2019).

The main tin ore mineral is cassiterite (SnO_2). However, tin can be incorporated into silicate minerals of the skarn, such as garnet, pyroxene, sphene, amphibole, or idocrase (Kwak and Askins, 1981; Dobson

1982; Lefebvre et al., 2019), and cannot be recovered. Retrograde alteration and/or greisenization of the skarn are likely to liberate tin from those silicates and allow it to precipitate as cassiterite or in sulfide ore.

A late greisen alteration of the skarn (= destruction of feldspar from the granitic body in association with the skarn) is characteristic of tin-skarns. It occurs in superimposition upon the intrusion, early skarn, and carbonates. The greisenization is characterized by a high fluorine activity and crystallization of new minerals in late veins of by replacement (e.g. fluorite, topaz, muscovite, tourmaline, quartz…).

1.3. Genesis conditions

1.3.1. Environment

1.3.1.1.Petrogenesis of the intrusions

Granitic rocks in association with tin skarns are highly evolved tin-bearing S-type granites (Chappell and White, 1974), with a syenogranitic composition (Einaudi et al., 1981). Most of those granites show fine-grained porphyritic or porphyry facies and present a strong alteration and abundant veins. Sn-skarn associated granites present a strong crustal signature and are the most peraluminous granites that can be found in association with skarns (Meinert, 1995). They generally form by partial melting of continental crust. Newberry (1998) reported some occurrences of basaltic dykes in the vicinity of skarn associated granites and show a compositionally bimodal suite. Furthermore, Ni anomalies, that have been reported in some granites (Meinert, 1995), seem to be inherited from underlying mafic magma, which may have caused the initial crustal melting.

1.3.1.2.Host rocks lithologies

The main condition for the formation of a skarn is the occurrence of a carbonated sedimentary host rocks, like limestone, dolomite rock, or a mixture of carbonates with marl or schist. If the protolith is mainly composed of limestone, it will lead to the formation of a calcareous skarn, otherwise a dolomite-rich protolith will form a magnesian skarn. The nature of the host rock has a strong influence on the reaction of fluids in the system. Decarbonation and devolatilization of the host rocks increase the amount of CO_2 in mineralizing fluids, and induce, at ~2 kbar, a phase separation between H_2O-rich and H_2O-CO_2 fluids. Metals are then more likely to precipitate from those mineralizing fluids.

1.3.2. P-T-X conditions of the skarnification

1.3.2.1.Determination of P-T-X conditions

Within a very reactive skarn system, geochemistry allows to estimate the P-T-X conditions of the skarn formation. Several geochemical methods can be used such as fluid inclusions, mineral phase equilibrium, minerals chemistry, and isotopes. The present study mainly focused on the three last. Mineral phase equilibrium modeling allowed to verify if the estimates of temperature and pressure were

correct. Minerals chemistry was used to determine how the skarn forming event distributed the elements into the system. Isotopes has been used to determine the age of the skarn formation (Rb-Sr isotopic system), and also to determine the source of fluids that were involved during the skarnification process (Pb, Sr, Nd, Li, and B isotopes).

1.3.2.2.Pressure and temperature

Pressure is very important for the skarnification process, however it is a parameter that may be difficult to estimate. It depends on the depth of the skarn formation, but, nowadays, many skarn deposits are outcropping and/or have been reworked during several tectonic events. Furthermore, skarns generally undergo a retrograde metasomatism/metamorphism that superimposes to the prograde assemblages.

Some characteristics of the skarn (morphology, ductile or brittle deformation) may help to determine the pressure of formation, and are related to the intrusion. Skarns generally form at relatively shallow depth, i.e. between 1 and 4.5 km (Einaudi et al., 1981).

The temperature of formation depends on the temperature of the fluids but also on the distance to the intrusion. Homogenization temperature Th of fluid inclusions are interpreted as the initial temperature of the fluid. Inclusions in prograde skarn minerals may reach temperatures above 700°C (Meinert et al., 2005). However, proximal skarns like tin-skarns generally form at temperature between 400 and 650°C (Kwak 1986). This temperature decreases with time as the granite and its fluids cool down.

1.3.2.3.Chemical conditions

Hydrothermal fluids that are generated by the intrusion are H_2O-rich fluids. Their interaction with the carbonate host rock to form the skarn allows the release of CO_2 into the system, causing a phase separation between H_2O-rich and H_2O-CO_2 fluids. Tin is mainly transported as Cl-complexes (Heinrich 1990) but can also form complexes with F (Malyshev and Korzhanovskaya, 1989). Release of CO_2 from the host rock, decrease of temperature, HCl occurrence in fluids, and increase in pH or oxygen fugacity (Eugster and Wilson, 1985; Pabalan, 1986; Wilson and Eugster, 1990; Taylor and Wall, 1993; Mueller and Seward, 2001; Mlynarczyk et al., 2003; Schmidt, 2018) are several parameters that can allow the precipitation of cassiterite from Cl- or F-complexes.

Granite and its emanating fluids are not the only influence on chemical and isotopic signatures of the skarn. The host rock composition also has to be considered to entirely understand skarn formation processes. With the interactions between hydrothermal fluids and carbonates rocks, major, trace, and rare earth elements are added to the system while others are removed. However, analysis of elements that are immobile during hydrothermal processes (REE, Lottermoser 1992) may be used to have an idea of the composition of the sedimentary protolith. Furthermore, isotopic (e.g. Li and B) studies of whole rocks and individual skarn minerals are used to trace the different fluid sources, by comparing with isotopic signatures of likely reservoirs (i.e. sedimentary rocks, granite, seawater, meteoric water…).

Isotopic geochronology (e.g. Rb-Sr) of skarns rocks and minerals are also used to determine the timing of skarn formation, and the age of mineralization.

1.4. Tin mineralization in the western Erzgebirge

1.4.1. Types of tin mineralization

1.4.1.1.Greisens

Tin-greisens are the result of the alteration of granitic units (here the Eibenstock granite) by hydrothermal fluids during the several pulses of the granite emplacement. This alteration mainly causes the destruction of feldspar crystals and the formation of new minerals such as mica, topaz, tourmaline, but also ore minerals like cassiterite. Greisens are generally located within the Eibenstock granite but the alteration also affected metasediments in the vicinity of the granite. This resulted in the formation of mineralized metasomatized phyllite.

All greisens are mainly composed of quartz and white mica. Some relicts from the primary granitic assemblage are still visible with polylithionite, strongly chloritized biotite, and rare strongly altered feldspar crystals. Cassiterite, in association with muscovite, represents the mineralizing event. In metasomatized phyllite, this assemblage is completed by tourmaline and apatite. Mineralized veins are also visible within the greisen. They show coarse-grained cassiterite in association with arsenopyrite, sericite, löllingite, wolframite, topaz, pyrite and fluorite (Rojík 2005).

1.4.1.2.Skarns

Four types of skarn occur in Hämmerlein: garnet, amphibole, pyroxene, and magnetite skarn. Their succession differs at different locations of the deposit. The three first types are mainly composed of calc-silicate minerals (garnet, amphibole, and pyroxene) with quartz and show a microcrystalline structure. Chlorite forms as a secondary phase with the alteration of amphibole and biotite. It is systematically associated with apatite. The main ore mineral, cassiterite, mainly occurs in the amphibole skarn and at the contact between amphibole and magnetite skarns. The fourth type of skarn is composed of massive magnetite with disseminated sulfides such as chalcopyrite.

1.4.1.3.Pegmatites

Tin-rich pegmatites are also occurring in the Erzgebirge. The rare metal granite-pegmatite system of the Ehrenfriedersdorf is one example. The whole system formed by a more or less continuous evolution from a magmatic stage to a high temperature hydrothermal stage, via a pegmatitic stage (Breiter et al., 1999). Pegmatites occur as marginal pegmatites called stockscheider at the roof of the granite cupolas, and as pegmatite-aplite dykes which cut the granite contact. Several tectonic and magmatic pulses have been recorded in stockscheiders and aplites, representing the evolution of the residual melt. The Sn-

enrichment has been interpreted as a late magmatic event linked to the aqueous-rich residual melt (Breiter et al., 1999). Furthermore, Sn is enriched in KCl-dominated fractions of the pegmatites.

1.4.2. Hämmerlein skarns and the Eibenstock granite associated greisens

The Hämmerlein polymetallic skarn is located in the western part of the Erzgebirge, close to the border between Germany and Czech Republic. It was discovered and mined during the second half of the 20th century mainly for tin, but also for zinc and indium. The current resources estimation is 101 500 t Sn with a cut-off grade of 0.2 wt% Sn. Zinc and indium content have been estimated at 200 200 t and 2 149 t respectively. Few studies have already been carried on the Hämmerlein deposit (Malyshev and Korzhanovskaya, 1989; Shapenko and Šmidel, 1991; Malyshev et al., 1997), but they mainly focused on the ore minerals and their deposition processes. Processes resulting in the skarn formation were not detailed and the entire story of the skarn and its mineralization was not explained.

Two major tectonic and hydrothermal events occurred in the Hämmerlein area: (1) a regional metamorphism that reached its peak at ca. 340 Ma during the Variscan orogeny, and (2) the intrusion of the Eibenstock granite at ca. 320 Ma. By following the general model for skarn formation, one can say that the granite intrusion is likely responsible of the Hämmerlein skarn formation and its mineralization, as well as the Eibenstock associated greisens. However, it is interesting to know how the regional metamorphism influenced the chemical processes which resulted in the skarn formation. Furthermore, the mineralization itself may have been impacted by the regional metamorphism.

To understand and build the story of the Hämmerlein polymetallic skarn deposit formation, several methods were used: (1) mineral and bulk rock chemistry, to chemically characterize the different lithologies and see which elements were mobilized during the different events. (2) Rb-Sr dating were processed to know the age of the skarn and greisen, and link them to the regional or contact metamorphism. (3) Finally, Sm-Nd, Pb-Pb, B, and Li isotopes were used to trace origin of skarn forming fluids and/or mineralizing fluids.

Chapter 2 of the thesis focuses first on mineral assemblages that constitute Hämmerlein skarns and greisen associated to the Eibenstock granite. Primary and secondary assemblages were determined with microscope observations and microprobe analyses. The second part of this chapter presents Rb-Sr isotopic data of mineral fractions from skarns and greisen. Those data were used to calculate the ages of skarns, greisen, and Sn mineralization, and link them to their corresponding tectonic event.

Chapter 3 presents P-T-XCO_2 modellings for the four skarn types of Hämmerlein, which were calculated from their bulk rock composition. To determine which tectonic event was responsible of the skarn assemblages formation, models have been made with T-XCO_2 variations at a constant pressure of 2 kbar for contact metamorphism conditions and at 5 kbar for regional metamorphism conditions. Rb-Sr ages, previously discussed in chapter 2, were also used to support the accuracy of the right model.

Chapter 4 focuses, in the first part, on the whole chemistry of skarns, schists, and gneisses of Hämmerlein. Those data were used to determine the contribution of the protolith on the current composition, and also composition changes induced by fluids circulation during the granite intrusion and mineralization. The second part of this chapter presents Sr, Nd, and Pb isotopic compositions of skarns, schists, and gneisses, and their comparison with likely isotopic reservoirs, i.e. granites of the Erzgebirge, metamorphic rocks of the Erzgebirge and their Paleozoic sedimentary protolith. This comparison aims to determine which reservoir influenced the Hämmerlein rocks composition, and the source of mineralizing fluids. B and Li signatures of skarns, schists, gneisses, and greisens, and their comparison with the same reference reservoirs, allow to be more precise as to the estimation of the fluids sources.

2. Chapter 2: The Hämmerlein skarn-hosted polymetallic deposit and the Eibenstock granite associated greisen, western Erzgebirge, Germany: Two phases of mineralization – two Sn sources

Abstract

The Hämmerlein polymetallic deposit is hosted in skarn, schists, and gneisses that reached their metamorphic peak at ~340 Ma during the Variscan orogeny. The deposit is spatially closely associated with one of the most voluminous granites of the Erzgebirge, the Eibenstock granite which intruded the metamorphic units at ~320 Ma, and locally also developed greisen mineralization. Cassiterite is the main ore mineral in the Hämmerlein skarn and in greisen mineralizations associated with the Eibenstock granite. The age of skarn formation is bracketed by multi-mineral Rb-Sr isochron ages of the gneisses (~340 Ma) and the end of ductile deformation (>330 Ma). The dated calc-silicate minerals of the skarn have elevated Sn contents, which implies that some Sn was present in the system during regional metamorphism, i.e., well before the emplacement of the Eibenstock granite. Tin in the >330 Ma old skarn silicates possibly was mobilized from the metamorphic wall rocks. Retrogression of the skarn mineral assemblage may have released some Sn that formed cassiterite in an assemblage with chlorite and fluorite. The Sr isotope signatures of fluorite indicate that this late assemblage is not related to cooling of the metamorphic rocks, but to the emplacement of the Eibenstock granite, which introduced additional Sn into the skarn. Thus, mineralization in the Hämmerlein deposit includes Sn that was introduced during two different events from different sources.

Keywords

Erzgebirge, Hämmerlein, tin, skarn, greisen, ore deposits, Eibenstock granite

Published as

Lefebvre MG, Romer RL, Glodny J, Kroner U, Roscher M (2019) The Hämmerlein skarn-hosted polymetallic deposit and the Eibenstock granite associated greisen, western Erzgebirge, Germany: Two phases of mineralization – two Sn sources. Mineralium Deposita 54:193–216

2.1. Introduction

The Hämmerlein polymetallic skarn deposit is located in the western Erzgebirge, in the northern part of the Bohemian Massif. The area is dominated by schists and gneisses that mostly represent Cambro-Ordovician sedimentary protoliths, metamorphosed at ~340 Ma during the Variscan orogeny. The Hämmerlein mineralization is hosted in a unit that formerly was referred as Jàchymov Group, and that includes mica-schists with skarns, gneisses, and amphibolites. The high-pressure – low temperature metamorphic units are intruded by the S-type, high-F, high-P_2O_5 Li-mica Eibenstock granite which is exposed to the west of the deposit. Hämmerlein was discovered in the course of uranium mining activities and prospected during the second half of the 20th century for tin, but also for indium and zinc.

The current resources estimation for Hämmerlein is 101 500 t Sn with a cut-off grade of 0.2 wt% Sn. Indium and zinc contents have also been estimated at 2 149 t and 200 200 t, respectively.

Most earlier studies focused mainly on the ore minerals and their deposition at Hämmerlein (Malyshev and Korzhanovskaya, 1989; Shapenko and Šmidel, 1991; Malyshev et al. 1997), but there are no studies on the skarn formation itself. Based on petrographic observations, mineral and bulk rock chemistry, P-T-XCO_2 modelling, and Rb-Sr dating, the aim of this study is to understand whether the regional metamorphism or the Eibenstock granite intrusion is responsible of the skarn formation, when in its history the mineralization took place, and where exactly the tin was preferentially deposited. We demonstrate that the Hämmerlein skarn formed during the Variscan regional metamorphism, and that it was later overprinted during the intrusion of the Eibenstock granite. Furthermore, we demonstrate that Sn was incorporated into the skarn during its formation and was redistributed during the emplacement of the granite along with a new input of Sn into the skarn. Greisen mineralization is directly related to the emplacement of the Eibenstock granite.

2.2. Geological Setting

2.2.1. Tectonic context

The Variscan orogenic belt formed by the collision of Laurussia with Gondwana in the late Paleozoic (Franke 1989; Matte 1986), starting with the closure of the Rheic Ocean (collision of Armorica and the Teplá-Barrandian Unit with Laurussia) and followed by intra-continental subduction of thinned continental crust and its sedimentary cover (Kroner and Romer, 2013). In the Bohemian Massif, these deeply subducted continental rocks reached peak metamorphic conditions at about 340 Ma (Rötzler et al., 1998) and eventually were emplaced into the middle and upper crust, where they form high-strain belts of metamorphic nappes (Kroner and Romer, 2013). The Erzgebirge in the Saxo-Thuringian Zone of the Variscan orogeny (Fig. 1a) is part of the allochthonous domain (Kroner et al., 2007) and represents a stack of medium to ultra-high pressure metamorphic nappes that were rapidly exhumed (Rötzler and Plessen, 2010). The metamorphic nappes have been intruded by a wide range of geochemically contrasting post-kinematic granites, some of which show closely-associated important tin mineralization (Förster et al., 1999).

The metamorphic nappes of the Erzgebirge are dominated by rocks of the former Gondwana margin (Mingram 1998) that have been subducted and exhumed during the early Carboniferous (Willner et al., 1997; Rötzler et al., 1998). The former Gondwana margin consisted of a Cadomian basement with important Cambrian granodiorites (Linnemann et al., 2004) and early Ordovician magmatic complexes (Tichomirowa and Leonhardt, 2010), and its Cambro-Ordovician to Silurian volcanosedimentary cover units. These basement units and their volcanosedimentary cover behaved differently during the Variscan orogeny: (i) the basement rocks were subducted to medium-pressure conditions and are now exposed in the gneiss domes of the Erzgebirge. The tectonostratigraphically lowermost units are exposed in the

eastern Erzgebirge (Freiberg Gneiss Dome) and are dominated by granodioritic orthogneisses derived from a ~550 Ma old protolith (Kröner et al., 1995). The medium pressure units of the Reitzenhain Gneiss Dome in the central Erzgebirge are sandwiched between nappes that experienced higher grade metamorphism during the Variscan orogeny. The Reitzenhain gneisses have protolith ages of c. 490 Ma (Tichomirowa and Leonhardt, 2010). (ii) The volcanosedimentary cover rocks are dominated by Paleozoic protoliths (conglomerates, greywackes, pelites, marbles, rhyolites, and metabasites) (Rötzler and Plessen, 2010). The various nappes reached peak conditions at ~ 340 Ma and became rapidly exhumed to middle and upper crustal levels. This is indicated by the emplacement of the 325 to 318 Ma old post-kinematic granites, which formed in the middle crust and were emplaced in the upper crust (< 2 kbar) (Förster et al., 1999).

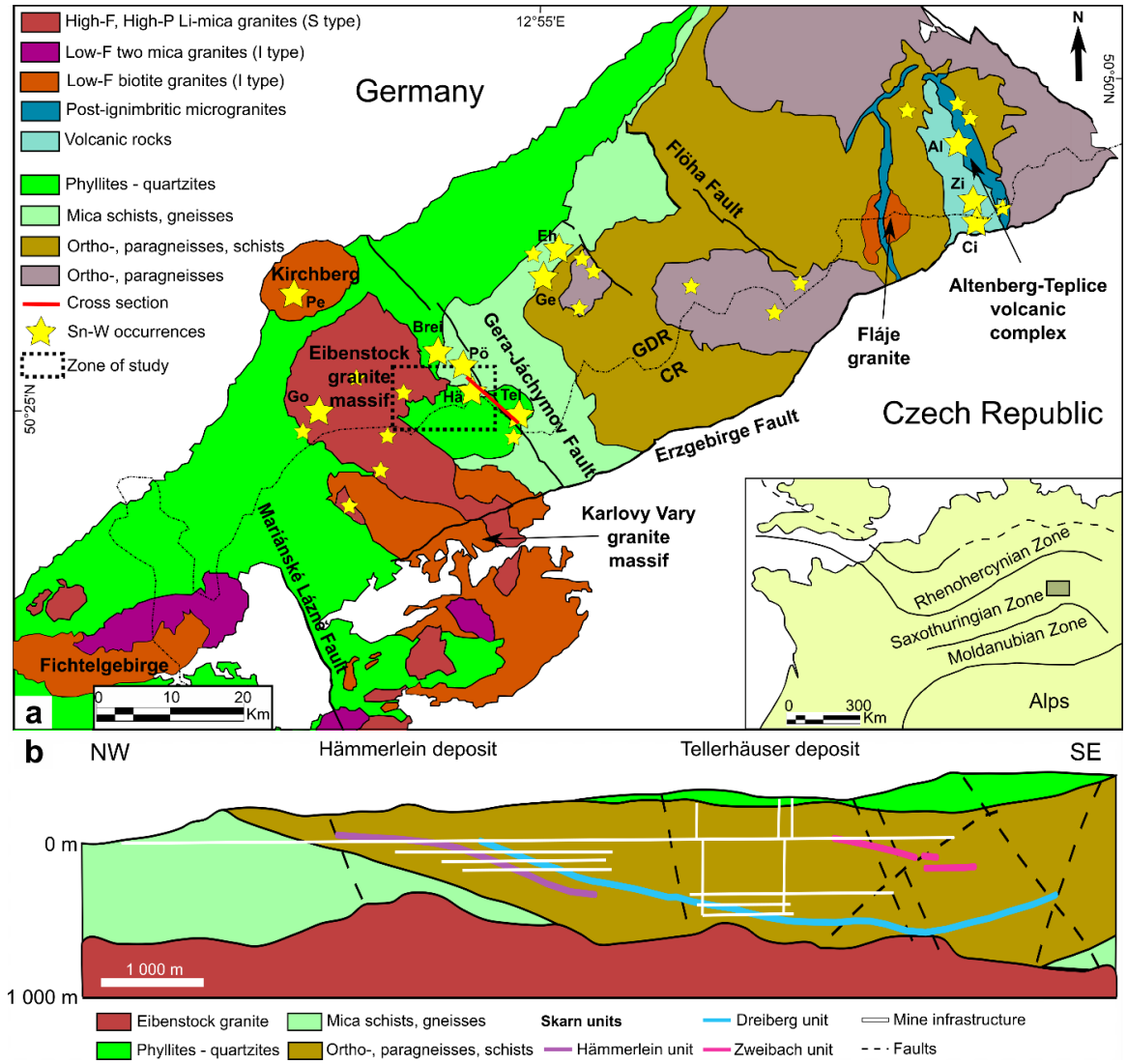

Figure 1: a: Simplified geological map of the Erzgebirge-Vogtland-Fichtelgebirge area showing the distribution of the various tin and tungsten deposits. Most of the ore deposits are spatially associated with granites (deposit locations according to Štemprok and Blecha, 2015. Al: Altenberg, Brei: Breitenbrunn, Ci: Cínovec/Zinnwald, Eh: Ehrenfriedersdorf, Ge: Geyer, Go: Gottesberg, Hä: Hämmerlein, Pe: Pechtelsgrün, Pö: Pöhla-Globenstein, Tel: Tellerhäuser). Insert: Domains of the Variscan orogen in Central Europe. b: Simplified cross-section of the Hämmerlein-Tellerhäuser deposit; modified after Schuppan and Hiller (2012) and Anglo Saxony Mining (2015).

There are three age groups of granitic rocks: (i) 340-330 Ma old intrusions (Meissen, Berbersdorf) along crustal scale shear zones and in contact with UHT metamorphic units were emplaced synchronous with the emplacement of the metamorphic nappes (Förster and Romer, 2010; Wenzel et al., 1997); (ii) 325-318 Ma old post-kinematic granitic intrusions (e.g. Eibenstock, Kirchberg) represent crustal melts and derive their geochemical variability from the lithologic and geochemical heterogeneity of the stacked continental crust (Förster et al., 1999; Förster and Romer, 2010); and (iii) 305-280 Ma old intrusions and volcanic complexes (Gottesberg) with variable input of mantle-derived material are bound to extensional structures of the Central European Extensional Province that developed in response to reorganization of the regional stress field after the Variscan orogeny (Kroner and Romer, 2013; Kroner et al., 2016). Most tin and tungsten mineralization of the Erzgebirge is thought to be related to 325-318 Ma old granites (Förster et al., 1999) that formed by melting of quartzo-feldspathic rock mixed with micaceous metapelite enriched in Sn and W (Breiter 2012).

2.2.2. Post-kinematic granites

The 325-318 Ma old post-kinematic granites are classified in three groups: (1) low-F biotite granites (Kirchberg), (2) low-F two-mica granites (Fichtelgebirge), and (3) high-F, high-P_2O_5 Li-mica granites (Eibenstock) (Förster et al., 1999; Förster and Romer, 2010). The composite Eibenstock granite is the "type" pluton for the high-F, high-P_2O_5 Li-mica granites. This granite commonly is mainly equigranular, but may locally show a porphyritic texture with a coarse grained assemblage with K-feldspar and minor quartz phenocrysts (Förster et al., 1999). There are no significant differences in the chemical composition between porphyric and non-porphyric varieties.

The Eibenstock granite constitutes the northern part of the Eibenstock-Nejdek pluton (Breiter 1993), a 25 by 22 km large complex in the western Erzgebirge (Fig. 1a). This complex is the most voluminous granitic body of the Erzgebirge, and it was emplaced in a late/post-collisional regime into paragneisses and schists, i.e., medium and low grade metamorphic rocks of the nappe pile of the Erzgebirge (Förster et al., 1999).

The granite is Si-rich, peraluminous, reduced and has a crustal isotopic signature (Sr_i values range from 0.711 to 0.713, Velichkin et al., 1994), and is associated with Sn-W mineralization (Förster et al., 1999). The Paleozoic metamorphic units (gneisses, mica schists) have played a role in the formation of the granite (Breiter et al., 1999). The Eibenstock granite is a multi-stage granite intrusion which have been dated between ~320 Ma (U-Pb dating by Förster 1998; Pb-Pb dating on zircon by Kempe et al., 2004) for the major part of the granite, and ~310 Ma (U-Pb dating on zircon by Tichomirowa et al., 2016) for some younger intrusions.

There are two types of mica in this granite. The trioctahedral ones are rich in Li and Fe and accompanied by topaz. Dioctahedral Li-rich micas typically overgrow trioctahedral micas and feldspars. Accessory minerals include schorl, topaz, apatite, rutile, and zircon. Rutile may host several wt% of Ta, Nb, Sn and

W. In addition, the Eibenstock granite locally also has cassiterite, scheelite and wolframite (Förster et al., 1999).

2.3. Skarn and greisen assemblages

2.3.1. Skarn assemblage

The Hämmerlein deposit is a polymetallic skarn, hosted in the metasedimentary rocks of the Erzgebirge nappe pile, which is intruded by a suite of post-kinematic granites and eventually overprinted by the late- to postorogenic Gera-Jàchymov fault zone (Fig. 2). This NW-SE striking, recurrently reactivated fracture zone is causally related with major uranium mineralizations of the region (Schuppan and Hiller, 2012). The Hämmerlein host rocks are dominated by schists (Shapenko and Šmidel, 1991) that are intercalated with layers of metacarbonates affected by the skarn formation, amphibolites, gneisses, quartzitic, and carbon-rich schists (Schuppan and Hiller, 2012) (Fig. 1b). Although metacarbonates are seen as the protolith for the skarn formation (Schuppan and Hiller, 2012) it is worth noting that there are no relics of metacarbonates within the skarn layers. The foliated skarn is in tectonic contact with intensively deformed quartz-rich mica schists and gneisses (Fig. 3).The mica schists contain layers with tin-rich biotite (up to 0.1%) (Malyshev et al., 1997; Malyshev and Korzhanovskaya, 1989). The metamorphic wall rocks of the Hämmerlein deposit form the roof of the Eibenstock intrusion (Fig. 1b).

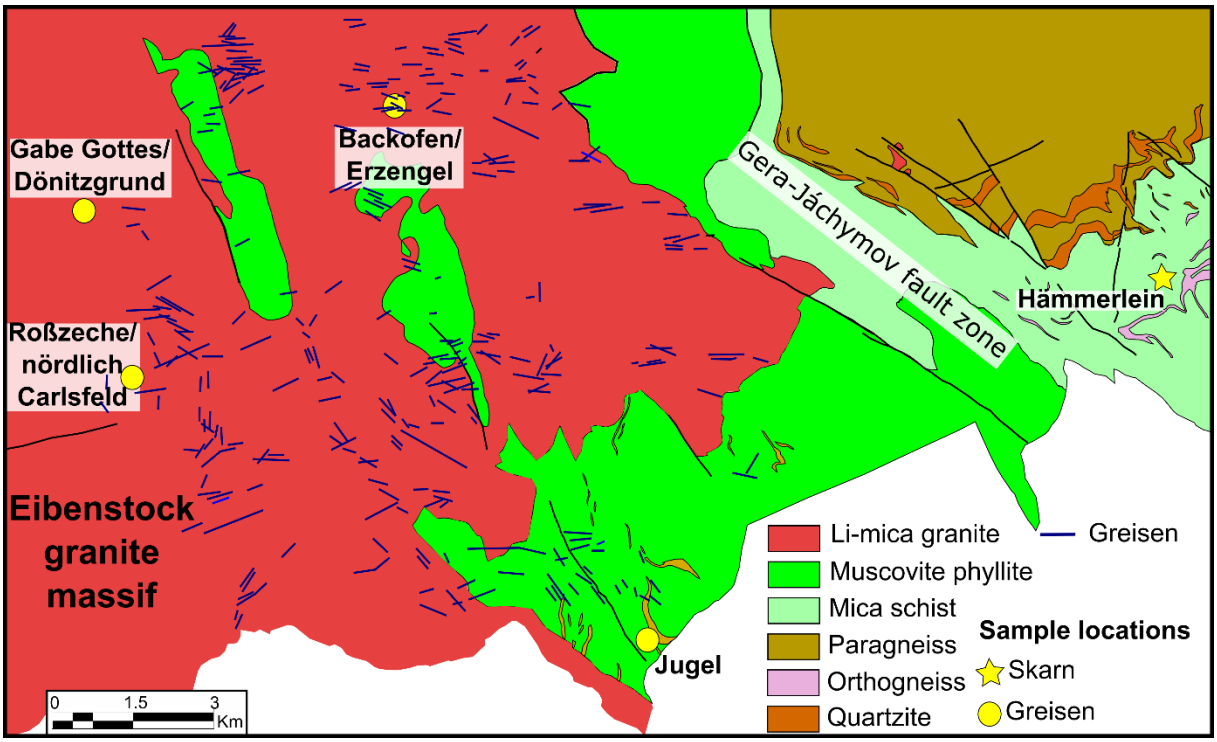

Figure 2: Simplified geological map of the studied area showing the location of Hämmerlein and the locations of the dated greisen samples. The Hämmerlein deposit is hosted in micaschists, whereas greisen mineralizations are located along faults within the muscovite phyllite unit or within the Eibenstock granite (modified after Leonhardt et al,. 1999, 2004, 2010).

There are three types of mineralization in the Hämmerlein deposit: (i) skarn with magnetite mineralization, (ii) skarn with strata-bound tin and sulfide mineralization (mainly sphalerite), and (iii) hydrothermal uranium-bearing veins (Schuppan and Hiller, 2012). Skarn mineralization is controlled by SW-NE striking faults (Schuppan and Hiller, 2012). In contrast, hydrothermal uranium mineralization is connected with N-S and NW-SE striking faults and is related to multiple reactivations of the Gera-Jàchymov zone at 280 Ma and later (Förster 1996). The source of Sn in the skarn deposit has been enigmatic. Even though a close spatial relation has been established between the greisen deposits and granite, the relation between skarn Sn mineralization and granite is less clear. The granite and the skarn are close together (Fig. 1b) but there is no contact between them.

There are four types of skarn at Hämmerlein, garnet skarn, amphibole skarn, pyroxene skarn, and magnetite skarn that show different successions at different locations of the deposit (Table 1). The three calc-silicate skarns are microcrystalline and the most obvious difference between them is the color of their matrix, which depends on their content of garnet (brownish-red matrix for the garnet skarn), amphibole (greyish-green for the amphibole skarn), and pyroxene (light brownish-green for the pyroxene skarn). The fourth type of skarn is a magnetite skarn which is mainly composed of massive magnetite partially interspersed with irregular, up to 5 cm large patches of chalcopyrite.

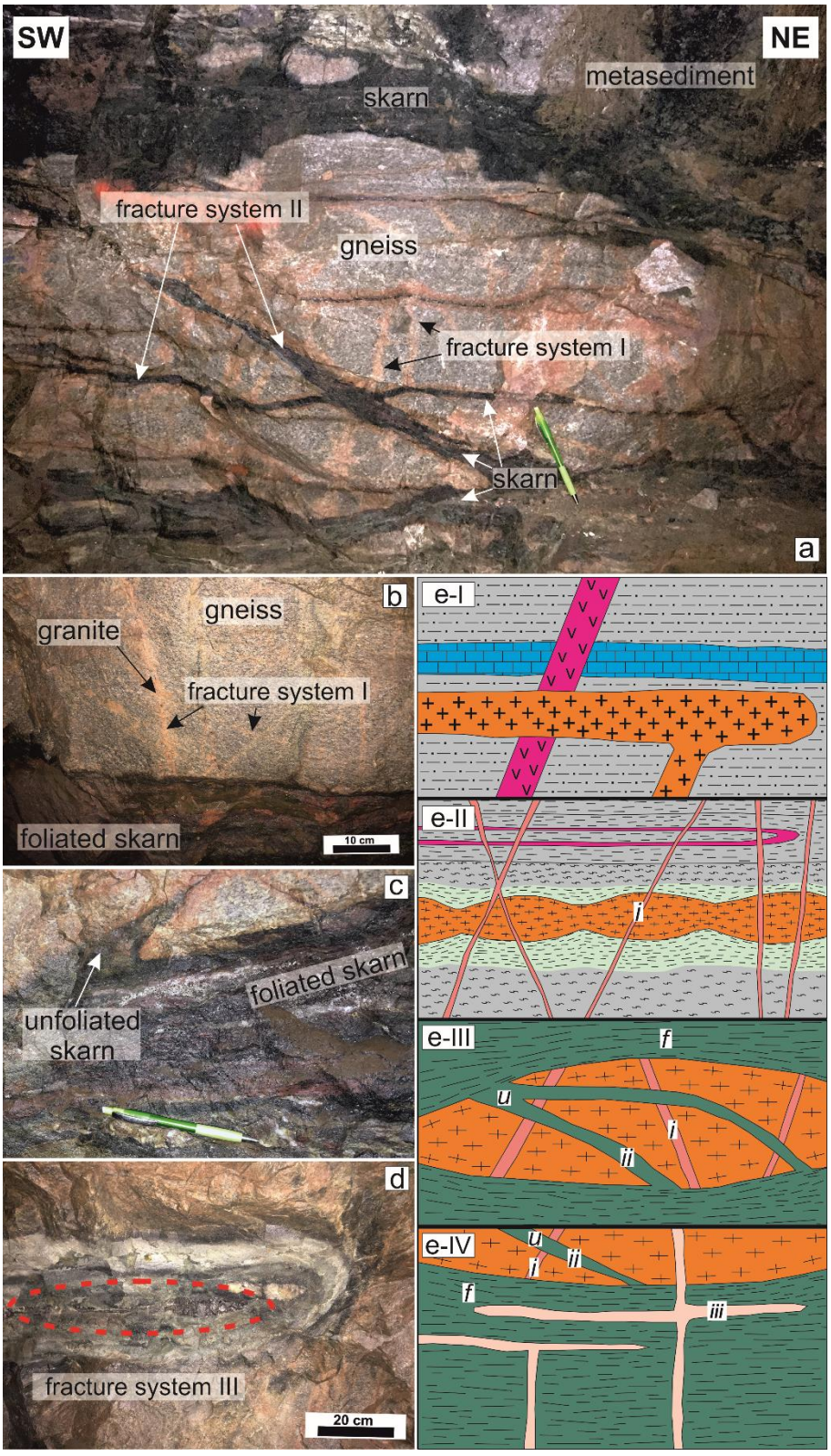

Figure 3: Tectonic evolution of the synmetamorphic skarn of the Hämmerlein deposit. a: Lenses of gneiss mantled by pervasively foliated amphibole/pyroxene skarn layers are part of the metasedimentary/metavolcanic suite of the Erzgebirge nappe pile. Two fracture systems transect the foliation of the gneiss. The older fractures contains granitic segregations and were cut and partly reactivated by tension gashes containing unfoliated skarn. b: Crosscutting relationship of the foliated skarn and the fracture system I indicating that the foliation of the skarn is younger than both the fractures and the foliation of the gneiss. c: Emplacement of the skarn utilizing fracture system 2. This indicates a high viscosity contrast between the skarn and the gneiss as well as fluid overpressure. The skarn inside the gneiss is protected from the subsequent ductile deformation

affecting the skarn mantle of the gneiss lenses which remains under low differential stress at this stage. The fluid overpressure led to the formation of tension gashes and the subsequent emplacement of the low viscosity skarn. d: After cooling of the metasedimentary sequence a third generation of fractures crosscuts the entire sequence and is related to chloritization of the wall rock. e: Schematic sketch of the formation of the synmetamorphic skarn layers. e-I: early Paleozoic sediments (siliciclastic and carbonate rocks), are intruded by dikes and sills. e-II: Subsequent regional metamorphic overprint due to nappe stacking during the Variscan continental collision led to medium grade metamorphism and a pervasive deformation of the lithologies. Competence contrast between the orthogneisses and the metasediments resulted in pinch and swell structures in the gneiss. Fluid overpressure probably caused the formation of the oldest fractures with granitic segregations. e-III: Due to the viscosity contrast between gneiss and the surrounding lithologies ongoing ductile deformation is localized in the metasediments including the evolving skarn layers. The gneiss preserves earlier deformation increments, i.e. the gneiss foliation as well as the granitic dikes. Fluid overpressure in combination with low differential stress inside gneiss culminated in the formation of a second fracture system. The emplacement of the skarn inside the gneiss indicates low viscosity of the skarn at this stage. e-IV: A third fracture system postdates the metamorphic processes and is related to hydrothermal processes associated with the intrusion of the Eibenstock granite below the metasediments. Abbreviations: f – foliated skarn; u – unfoliated skarn; i, ii, iii – fracture system 1-3

Table 1: Description of the skarn samples from Hämmerlein and of the greisen associated to the Eibenstock granite (skarn samples location in Gauss-Krüger coordinates, zone 4).

Sample name	Lithology	Location	Characteristics
Hämmerlein skarn samples			
CSV1	Contact between pyroxene skarn and gneiss	5 593 093 mN 4 559 547 mE	This sample is mainly composed of prograde pyroxene and recrystallized quartz. Rare bigger altered crystals of quartz and feldspar are visible. In the gneiss, pyroxene forms veinlets. Elongate crystals of muscovite together with apatite occur within fractures cutting pyroxene veinlets.
ASb, HAS2	Contact between garnet and amphibole skarns	5 593 125 mN 4 559 500 mE	Samples are formed by chloritized amphibole and quartz. Some garnet and rare feldspar crystals occur within the prograde amphibole-quartz assemblage. Clusters of green amphibole surrounding remnant calcite also occur. Cassiterite occurs at contacts between chloritized amphibole and magnetite as coarse grains (up to 10 mm).
HAS3	Contact between amphibole skarn and gneiss	5 593 194 mN 4 559 409 mE	This sample is similar to sample HAS2 but here smaller cassiterite (~10 µm) occurs disseminated in the skarn prograde assemblage and is associated with chlorite.
HGS1	Contact between garnet and amphibole skarn	5 593 000 mN 4 559 500 mE	The garnet skarn is composed of prograde garnet and quartz crystals. In the amphibole skarn, some secondary chlorite also occurs in the skarn in association with apatite.
HMS1	Magnetite skarn	5 593 000 mN 4 559 500 mE	The main component of the sample is variably martitized massive magnetite. Patches of chalcopyrite and pyrite occur in the magnetite. Indium-sphalerite exsolutions appear in chalcopyrite.
HPS1	Contact between pyroxene and amphibole skarn	5 593 000 mN 4 559 500 mE	The pyroxene skarn is mainly composed of prograde pyroxene and quartz crystals. Some lenses of coarse pyroxene (~1 cm) occur in the pyroxene-quartz assemblage. Some secondary calcite veinlets crosscut both the matrix and the lenses.
Greisen samples			
BO1	Granite	Backofen/Sosa	Two types of mica occur in a matrix mainly composed of quartz. Ferroan polz-lithionite phenocrysts (~2 mm) are disseminated into the matrix and small fan-shaped muscovite (~200 µm) occurs at quartz phenocrysts boundaries.
EE2	Granite	Erzengel/Sosa	
GG1	Granite	Gabe Gottes/Dönitzgrund	
GG3	Granite	Gabe Gottes/Dönitzgrund	This sample is similar to samples BO1, EE2, and GG1 but here no large ferroan poly-lithionite occur and only small fan-shaped muscovite crystals are visible.
JG1 and JG2	Phyllite	Jugel NW	Some muscovite-tourmaline-cassiterite assemblages occur in fractures in the quartz matrix. Chloritized biotite may occur in association with this assemblage in fractures.
RZ2	Granite	Roßzeche/nördlich Carlsfeld	The matrix is mainly composed of quartz and biotite. Ferroan poly-lithionite phenocrysts occur disseminated in the matrix and small fan-shaped muscovite are visible at quartz phenocrysts boundaries.

Garnet skarn (samples HAS2 and HGS1) is mainly composed of garnet and quartz. Garnet crystals are still visible in the amphibole skarn where the two skarn types are in contact (Fig. 4a). Garnet does not seem to be altered into chlorite, whereas coexisting amphibole is strongly altered. At the contact with gneiss, some muscovite and strongly chloritized biotite occur in the garnet skarn. Chlorite that formed by the alteration of biotite typically is associated with apatite.

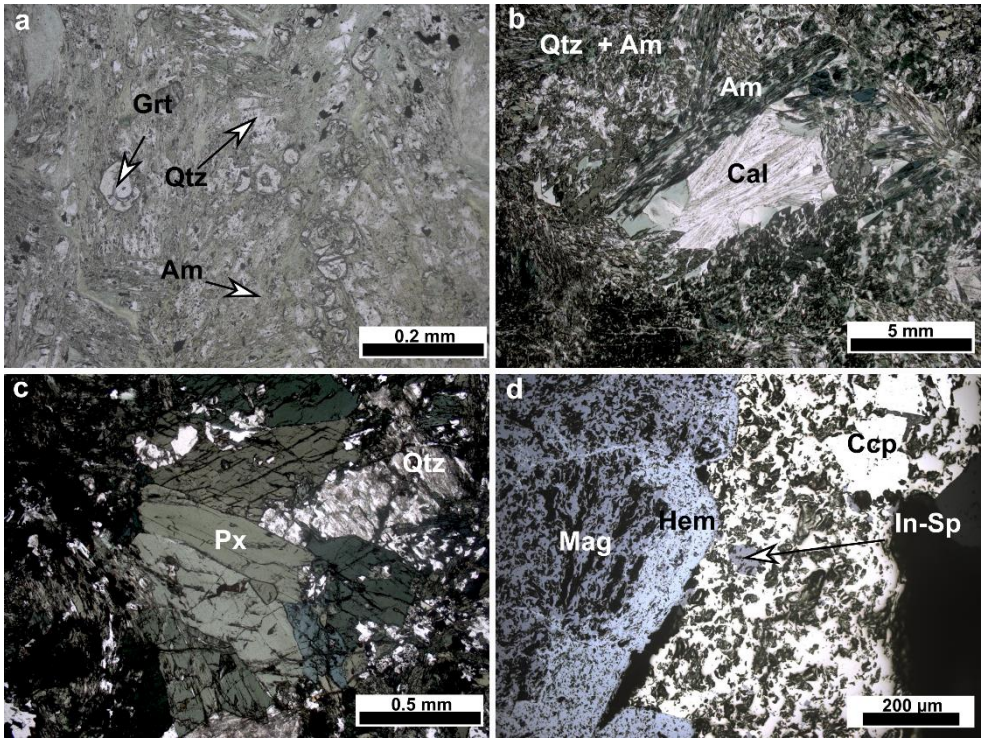

Figure 4: Thin sections showing the typical mineral assemblages of the various skarn types. a: contact between garnet and amphibole skarns (sample HAS2) with garnet disseminated into the amphibole skarn mainly composed of amphibole and quartz, b: amphibole skarn (sample HAS1) with calcite surrounded by amphibole in a quartz-amphibole assemblage, c: pyroxene skarn (sample HPS1) with a pyroxene-quartz assemblage, and d: magnetite skarn (sample HMS1) in reflected light showing a cluster of chalcopyrite in the magnetite-hematite assemblage. Indium-rich sphalerite occurs as inclusions in chalcopyrite. Am: amphibole, Cal: calcite, Ccp: chalcopyrite, Grt: garnet, Hem: hematite, In-Sp: In-sphalerite, Mag: magnetite, Px: pyroxene, Qtz: quartz.

Amphibole skarn (samples HAS1, HAS2, and HAS3) is mainly composed of chloritized amphibole, quartz, and some rare feldspar. Some relics of calcite are surrounded by amphibole (Fig. 4b) showing that calcite was a precursor phase for the skarn formation. As feldspar crystals are rare and strongly altered, they may reflect early phases or be inherited from the protolith. Amphibole and quartz formed from this protolith during the prograde stage of the skarn formation. Chlorite occurs along grain boundaries, as pseudomorphs after amphibole, and in veinlets, where it is associated with tourmaline and rare muscovite. Chlorite alteration and late veins of muscovite-tourmaline are not part of the skarn assemblage, but reflect a later event of retrogression or alteration. In contrast, apatite occurs mainly as inclusions in feldspar crystals, which are remnants of the protolith, and, thus apatite may have formed at the same time as feldspar and be inherited from the protolith. Cassiterite occurs in two different forms:

(i) coarse grained cassiterite (up to 10 mm) at the contact between chloritized amphibole and magnetite (at contact to the magnetite skarn, e.g. sample HAS2) and (ii) fine-grained cassiterite (~10 μm) that is disseminated in the amphibole-quartz assemblage. Both types of cassiterite are associated with chlorite. Cassiterite formed during the later retrogression or alteration event that also led to the chloritization of the original skarn minerals.

Pyroxene skarn (sample CSV1) is mainly composed of pyroxene crystals (Fig. 4c) and recrystallized quartz with some rare bigger crystals of feldspar and quartz. At the contact between pyroxene skarn and gneiss, pyroxene forms altered veinlets in the gneiss (e.g. sample CSV1). Fractures within the gneiss may contain elongate crystals of muscovite which are accompanied by small apatite crystals. Muscovite and apatite seem to have formed later than pyroxene as they occur in fractures that locally cut the pyroxene veinlets. Locally, pyroxene skarn and gneiss are closely interbedded, forming a rock (e.g. sample HPS1) that is mainly composed of quartz and feldspar associated with small pyroxene crystals. Lenses of bigger pyroxene typically are surrounded by quartz. Veins of calcite cut both the quartz-feldspar assemblage and lenses of pyroxene, thus, showing that calcite formed as a retrograde phase whereas pyroxene is part of the prograde assemblage.

The magnetite skarn is mainly composed of massive magnetite that is variably martitized at the rim of the crystals. There are irregular patches of chalcopyrite and pyrite within the magnetite (sample HMS1). Chalcopyrite may bear exsolutions of In-sphalerite (Fig. 4d). Minor arsenopyrite and Bi-Cu minerals occur disseminated in the magnetite skarn. Late fractures in the rock contain quartz and chlorite.

The textural relation between skarn and gneisses is complex, due to the overprinting of older structures by younger ones and the contrasting rheological behavior of gneisses, schists, and skarn. The regional metamorphic layering is characterized by pervasive foliated metasedimentary rocks and foliated skarn incorporating lenses of orthogneiss. Within the ductile deformed gneiss, there are local granitic segregations along fractures that crosscut the older foliation of the gneiss (Fig. 3a). These local granitic segregations may reflect fluid channels and possibly formed due to local fluid-overpressure near metamorphic peak conditions. Fluid overpressure led to the formation of a second fracture system with associated amphibole skarn within the gneiss partly reactivating the first fractures (Fig. 3a). Amphibole skarn that cuts the foliation of the gneisses is not foliated, whereas amphibole skarn at the margin of gneiss lenses is pervasively foliated. Pervasive deformation of amphibole skarn is concentrated outside of the gneiss, because of the viscosity contrast between the skarn (low viscosity) and the gneiss (higher viscosity). Hence, the subparallel foliations of the gneiss and the skarn reflects two distinct synmetamorphic, deformational events interrupted by brittle fracturing. The various skarns and the two fracture systems developed when the entire sequence still was in the temperature field of ductile deformation. A third fracture system cutting across the entire metasedimentary sequence evolved in the brittle upper crust and contains significant hydrothermal tin mineralization. Because cooling of the Erzgebirge below the ductile-brittle transition occurred no later ca. 330 Ma (e.g. Werner and Lippolt,

2000), the formation of ductile-deformed amphibole skarn as well as related fractures are distinctly older than the emplacement of the post-kinematic intrusion of the Eibenstock granite and the associated youngest fractures (Fig. 3e).

2.3.2. Greisen assemblage

Sn-greisens are generally located within or close to the Eibenstock granite (Fig. 2). The greisen formed after the coarse-grained phase of the granite (Rojík 2005). Tin-bearing greisens typically are concentrated along the granite margin, but also occur along SE-striking zones within the Eibenstock granite. Greisens cut all textural types of Eibenstock granite. Tin mineralization rarely crosses the outer contact of the granite (Rojík 2005).

Greisens follow short subvertical joints and form grouped bands separated into parallel-packed zones. The center of the greisen typically is mineralized with cassiterite veinlets. The main greisen mineralization includes several generations of greisen with higher ore grades at the contacts.

There are several types of greisen (Table 1). All of them are composed of quartz and fine-grained mica with disseminated strongly altered feldspar. The various greisen occurences mainly differ in the nature of accessory minerals. The samples from Backofen, Erzengel, and Gabe Gottes (BO1, EE2, and GG1, respectively; Fig. 2) show two types of white mica: (i) up to 2 cm large ferroan poly-lithionite phenocrysts associated with feldspar and quartz phenocrysts which seem to be remnants of the primary granite and (ii) fine-grained second generation, up to 200 µm large alteration-related muscovite crystals at the boundaries of feldspar and ferroan poly-lithionite phenocrysts. Sample GG3 (Gabe Gottes) does not show ferroan poly-lithionite phenocrysts, but only fine grained mica. In this sample, phenocrysts seem to have been altered completely and the only mica present belongs to the second generation. Cassiterite forms ~250 µm large crystals that occur together with second-generation mica (Fig. 5b). Cassiterite may have formed at the same time as the alteration that formed the second generation of mica. Samples from the Jugel metasomatized phyllite (JG1 and JG2) show the assemblage muscovite-tourmaline-cassiterite in fractures within a quartz-feldspar assemblage. Muscovite forms small fan-shaped grains and tourmaline crystals reach up to 500 µm (Fig. 5c). Locally, there is up to 200 µm large apatite (sample EE2, Fig. 5a) together with second generation muscovite. The assemblage muscovite-tourmaline-apatite-cassiterite reflects a late-stage event that also resulted in the almost complete chloritization of biotite.

Mineralized veins associated with the greisen show coarse-grained aggregates of cassiterite in the center together with löllingite, arsenopyrite, wolframite, sericite, topaz, and minor pyrite, and fluorite, and rare feldspar. There are also veinlets between greisen bands with a similar mineral assemblage. They contain cassiterite, hematite, K-feldspar, quartz, wolframite, topaz, fluorite, and muscovite (Rojík 2005).

2.4. Materials and methods

Mineral compositions were determined using a JEOL Hyperprobe JXA-8500F at GFZ Potsdam. Natural and synthetic standards were used for the calibration. Analyses were performed with an accelerating voltage of 15 kV, beam current of 12 nA and a beam diameter of 5 µm.

Mineral separation has been carried out for Rb-Sr and U-Pb analysis. Mineral concentrates of white mica, K-feldspar, albite, amphibole, garnet, apatite, tourmaline, epidote, sulfides and fluorite were produced. The first crushing was performed in a steel mortar. Mineral enrichment has been done with a FRANTZ magnetic separator and heavy liquids. White mica fractions sieved to different size ranges had been grounded in pure ethanol in an agate mortar and then sieved again to remove adherent matrix and inclusions. All separates had been checked and purified by hand-picking. For Rb-Sr analysis, mineral separates had been spiked with mixed ^{87}Rb-^{84}Sr tracers to determine Rb and Sr concentrations. Rb- Sr and U-Pb data were measured on a TRITON multicollector thermal ionization mass spectrometer (TIMS) at GFZ Potsdam following the routine described in Glodny et al. (2002) and Romer and Hahne (2010) respectively.

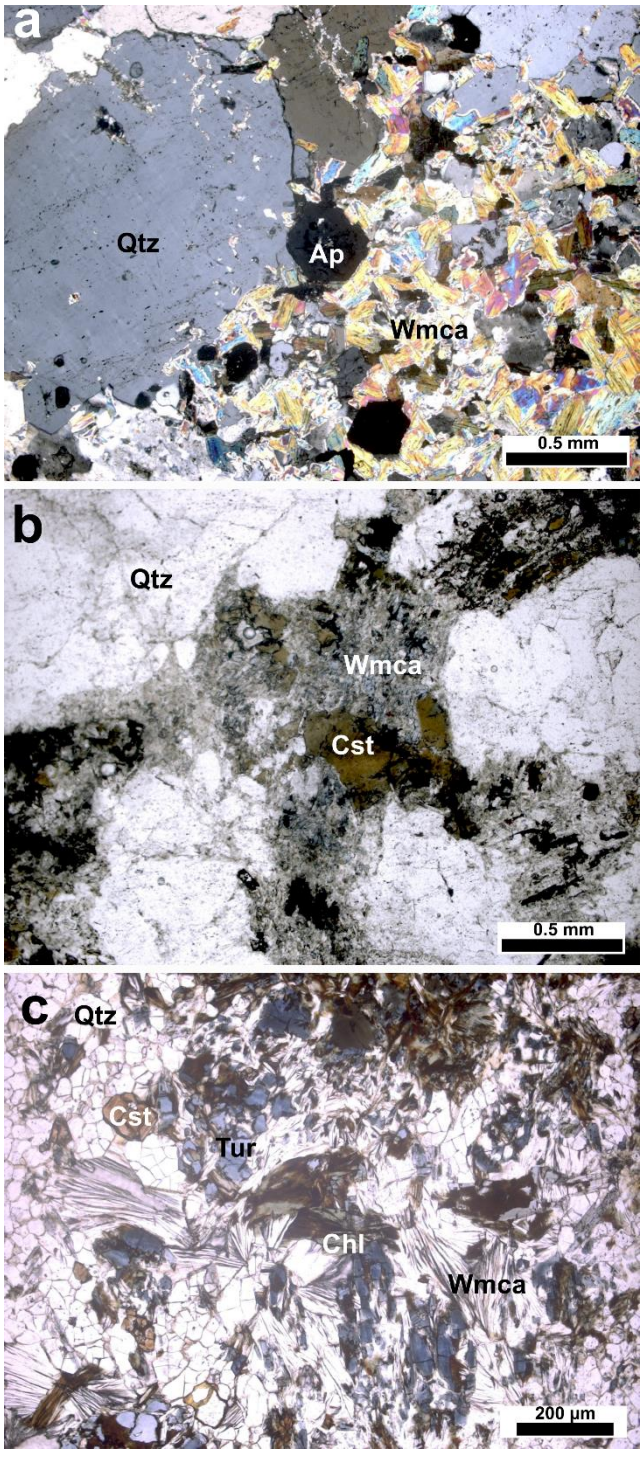

Figure 5: Typical greisen mineral assemblages: a: White mica- apatite assemblage embedded in the quartz (sample EE2), b: White mica-cassiterite assemblage in the quartz (sample GG3), c: White mica-chlorite-tourmaline-cassiterite assemblage (sample JG2). Ap: apatite, Chl: chlorite, Cst: cassiterite, Qtz: quartz, Tur: tourmaline, Wmca: white mica.

2.5. Results

2.5.1. Mineral chemistry

The greisen samples contain one generation of small fan-shaped white mica, except for samples from Backofen, Erzengel, and Gabe Gottes (BO1, EE2, and GG1 respectively) that show two generations. In these samples, the first generation of ferroan poly-lithionite forms large white mica crystals (1-3 cm) whereas the second

generation of muscovite forms small fan-shaped aggregates. In skarn samples, there is only one generation of mica. We characterized mica for the various greisen, metasomatized phyllites, and skarn samples by EPMA (Table 2 and Electronic supplementary material 1). We use the classification of Tischendorf et al. (2001), which is based on the substitution of Li and Al for Mg and Fe, respectively, to group white mica from the various greisen and skarn samples (Fig. 6). The majority of samples plot in the compositional fields of (ferroan) muscovite and ferroan poly-lithionite. However, there are several distinct differences between first and second generation mica. For the Backofen greisen (BO1), first generation white mica shows a ferroan poly-lithionite composition, whereas second generation mica falls mainly in the field of muscovite and ferroan muscovite. At the Erzengel location (EE1), first generation greisen mica has mainly a ferroan poly-lithionite composition. The second generation shows a muscovite composition. In Gabe Gottes greisen (GG1), first generation mica shows a compositional range extending from ferroan poly-lithionite to lithian sidero-phyllite, whereas the second generation shows a muscovite composition with some Fe-rich crystals that plot in the ferroan muscovite field (Fig. 6). This classification highlights the occurrence of two generations of mica in the greisen sample GG3 from Gabe Gottes, in the metasomatized phyllite sample JG1 from Jugel, and in the amphibole skarn (HAS3) of Hämmerlein. One generation shows a ferroan poly-lithionite composition, which can be close to zinnwaldite for Gabe Gottes and Jugel. The other generation has a muscovite composition in Gabe Gottes and Jugel, whereas it shows a ferroan muscovite composition in the amphibole skarn of Hämmerlein. The only generation of mica occurring in pyroxene skarn (CSV1) of Hämmerlein shows a ferroan muscovite composition. Figure 7 highlights the compositional contrast between the two generations of greisen mica in terms of major and trace elements. In greisen samples, first generation white mica contains less Al than the second generation (~20 wt% vs. ~34 wt%). In contrast, Mg and Li contents of first generation white mica are higher than those of second generation white mica (~0.9 wt% vs. ~0.2 wt% Mg and ~2.2 apfu vs. 0.2 apfu Li). Fluorine is higher in the first generation greisen white mica, whereas Na content is higher in the second generation greisen white mica (Fig. 7). Tin is present in most greisen white mica samples with ~0.03 wt% Sn in first generation white mica and up to 0.13 wt% Sn in second generation white mica. Note, Sn contents in skarn white mica are below the detection limit of the electron microprobe (Table 2).

Table 2: Representative electron microprobe analyses of muscovite from greisen mineralizations spatially associated with the Eibenstock granite and from skarns from Hämmerlein.

	Greisen and metasomatized phyllites										Skarn/gneiss	
	BO1 1st gen.	BO1 2nd gen.	EE2 1st gen.	EE2 2nd gen.	GG1 1st gen.	GG1 2nd gen.	GG3 1st gen.	GG3 2nd gen.	JG1	JG2	CSV1	HAS3
SiO_2	47.65	47.58	45.80	47.10	45.84	46.83	46.77	46.85	46.70	46.33	48.79	48.41
TiO_2	0.28	0.07	0.20	0.03	0.17	0.04	0.09	0.04	0.07	0.01	0.29	0.34
Al_2O_3	24.85	32.24	21.05	33.22	28.36	31.29	32.12	34.32	30.74	33.52	26.42	25.83
FeO	8.93	3.87	12.53	3.19	7.52	5.22	4.52	2.48	4.18	3.53	6.67	7.97
MgO	0.37	0.06	0.87	0.16	0.57	0.18	0.18	0.09	1.44	0.36	0.42	0.36
CaO	0.04	0.02	bdl	0.02	bdl	0.06	0.02	0.10	bdl	0.04	0.02	0.03
K_2O	10.17	10.56	10.17	10.62	10.58	10.17	10.79	10.47	10.61	10.55	10.40	10.30
Na_2O	0.07	0.15	0.10	0.14	0.08	0.18	0.22	0.27	0.28	0.27	0.12	0.11
MnO	0.16	0.08	0.22	0.09	0.16	0.04	0.05	0.05	0.01	0.03	0.18	0.21
BaO	0.06	0.07	0.12	0.03	0.11	0.15	0.04	0.08	0.07	0.14	0.11	0.07
P_2O_5	0.02	0.06	bdl	0.01	bdl	bdl	0.06	0.05	bdl	0.01	0.01	bdl
SnO_2	0.03	0.13	bdl	0.08	0.03	0.04	0.03	0.08	0.15	0.11	bdl	bdl
Li_2O	4.11	0.63	3.58	0.70	3.59	0.44	3.86	0.55	3.84	0.20	0.22	4.31
Cl	0.01	0.01	0.01	0.01	0.01	bdl	bdl	0.01	bdl	0.02	bdl	bdl
F	4.99	1.42	8.22	1.55	1.78	1.09	1.80	1.29	1.80	0.60	0.65	1.25
H_2O	bdl	3.78	0.26	3.73	0.32	3.87	0.21	3.87	0.19	4.15	4.00	3.71
Total	101.74	100.73	102.87	100.68	99.12	99.60	100.76	100.60	100.08	99.87	98.30	98.90
Si	6.4	6.4	6.5	6.3	6.2	6.4	6.1	6.2	6.1	6.3	6.8	6.4
Al (T)	1.6	1.6	1.5	1.7	1.8	1.6	1.9	1.7	1.9	1.7	1.2	1.6
K	1.7	1.8	1.8	1.8	1.8	1.8	1.8	1.8	1.8	1.8	1.8	1.7
Na	bdl	bdl	bdl	bdl	bdl	bdl	0.1	0.1	0.1	0.1	bdl	bdl
Al (M)	2.4	3.5	2.0	3.5	2.7	3.4	3.0	3.6	2.8	3.6	3.1	2.5
Fe	1.0	0.4	1.5	0.4	0.8	0.6	0.5	0.3	0.5	0.4	0.8	0.9
Mg	0.1	bdl	0.2	bdl	0.1	bdl	bdl	bdl	0.3	0.1	0.1	0.1
Li	2.2	0.3	2.0	0.4	1.9	0.2	2.0	0.3	2.0	0.1	0.1	2.3
F	2.1	0.6	3.7	0.7	0.8	0.5	0.7	0.5	0.7	0.3	0.3	0.5

Li_2O calculated after Tischendorf et al. (1997) Analytical data in wt %; mineral formula calculation results are given in apfu. Bdl: below detection limit. Additional analyses are given in the Electronic supplementary material 1.

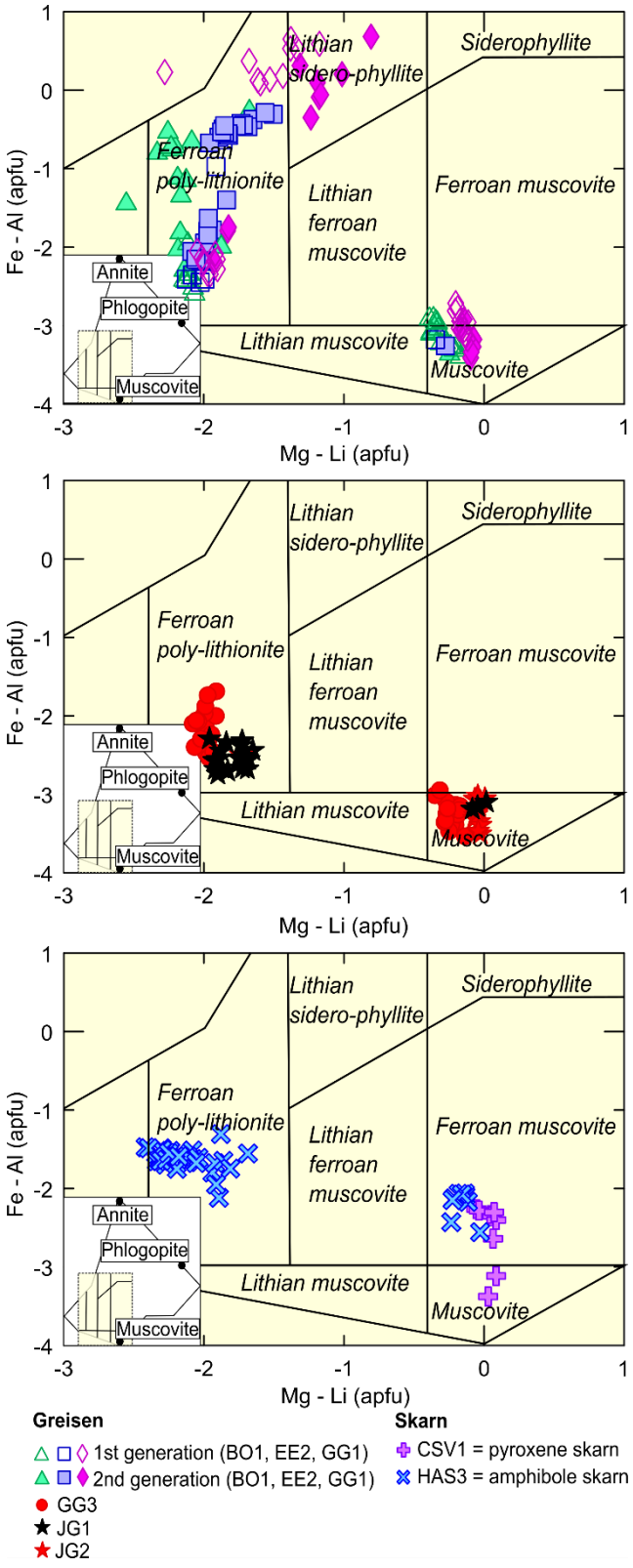

Figure 6: Composition of white mica from the Hämmerlein skarn (a) and greisen mineralization associated with the Eibenstock granite (Backofen BO1, Erzengel EE2, and Gabe Gottes GG1 with two populations of micas (b) and Gabe Gottes GG3 and Jügel JG1/JG2 with one population (c)) in terms of FeAl vs MgLi (FeAl = Fe_{tot} + Mn + Ti - Al^{VI} ; MgLi = Mg – Li in apfu). Data source: see Electronic supplementary material 1. The insert represents the entire classification diagram (diagram modified from Tischendorf et al., 2001).

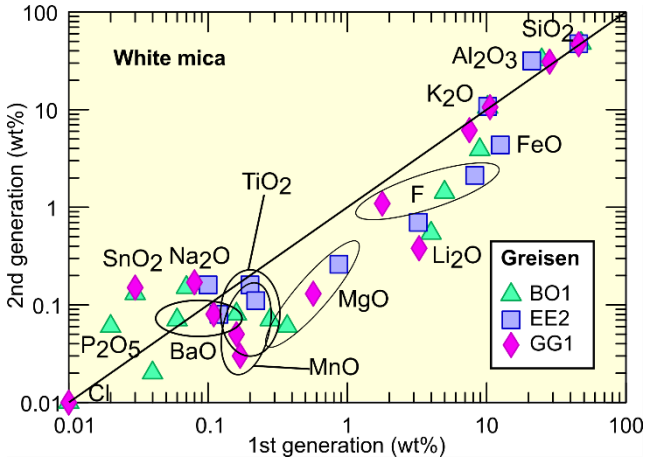

Figure 7: Comparison of average major and trace elements content of the two generations of white mica from Backofen (BO1), Erzengel (EE2) and Gabe Gottes (GG1) greisen samples. The first generation contains more Fe, Mg, Mn, Ti, Li and, F whereas the second generation is enriched in Na, P, and Sn.

Compositional data of silicate minerals that are typical for the calc-silicate skarns and that are part of the prograde assemblage (garnet, amphibole, and pyroxene) is shown in Table 3. Garnet show different compositions depending on the lithology where it is present. Ca-rich almandine occurs in massive garnet skarn (e.g. sample HGS1), whereas Fe-rich grossular have been found at contacts between garnet and amphibole skarns (e.g. sample HAS2). It is noticeable that grossular contains up to ~0.12 wt% Sn, whereas the Sn concentration in almandine is below the detection limit of the electron microprobe. Fe-rich cummingtonite in the amphibole skarn has up to ~0.07 wt% Sn and Fe-rich augite in the pyroxene skarn shows up to ~0.45 wt% Sn.

Tourmaline crystals are common in greisen but occur also in some skarn samples. Greisen tourmaline is schorl whereas skarn tourmaline is foitite (Table 4). The main compositional difference between greisen and skarn tourmaline is the content of Na and, thus, the occupancy of the X-site. Schorl belongs to the alkali group of tourmaline, whereas foitite belongs to the X-site vacancy group (Hawthorne and Dirlam, 2011) (Fig. 8). It is also noticeable that, in both kinds of tourmaline, Sn concentrations are below the detection limit of microprobe analysis.

Table 3: Representative electron microprobe analyses of garnet, amphibole, and pyroxene from skarns from Hämmerlein

	HAS2 Grt	HGS1 Grt	HAS2 Am	CSV1 Px
SiO_2	38.08	37.64	29.47	38.61
TiO_2	0.06	0.11	0.02	0.09
Al_2O_3	16.94	20.90	15.28	10.31
FeO	10.55	27.82	20.25	32.36
MgO	0.21	1.17	19.04	1.08
CaO	28.55	9.71	0.08	10.98
K_2O	0.02	bdl	0.04	1.70
Na_2O	bdl	0.03	0.01	1.16
Cr_2O_3	bdl	0.02	0.02	bdl
MnO	4.54	1.99	2.22	0.73
SnO_2	0.12	bdl	0.07	0.45
Total	99.07	99.40	86.50	97.47
Si	3	3	4.8	1.6
Al iv	-	-	2.9	0.4
Fe^{3+}	-	-	2.6	-
Fe^{2+}	0.3	1.9	bdl	0.4
Mn	0.3	0.1	bdl	bdl
Mg	bdl	0.1	bdl	bdl
Ca	2.4	0.8	bdl	0.5
Na	-	-	-	0.1
Total	3.0	2.9	2.6	1.0
Mg	-	-	4.6	bdl
Mn	-	-	0.3	-
Ti	bdl	bdl	bdl	bdl
Al	1.6	2.0	bdl	0.2
Cr	bdl	bdl	bdl	bdl
Fe^{3+}	0.4	bdl	0.1	0.3
Fe^{2+}	-	-	-	0.5
Total	2.0	2.0	5.0	1.0
Classified as	Grs	Alm	Cum	Aug

Fe^{2+} and Fe^{3+} calculated after Brady and Perkins (2015) for garnet and pyroxene, after Leake et al. (1997) for amphibole. Analytical data in wt %; mineral formula calculation results are given in apfu. Bdl: below detection limit. Alm: almandine, Am; amphibole, Aug: augite, Cum: cummingtonite, Grs: grossular, Grt: garnet, Px: pyroxene. Additional analyses are given in the Electronic supplementary material 1.

Table 4: Representative electron microprobe analyses of tourmalines from greisen and skarns from Hämmerlein

	Greisen			Skarn
	GG3	JG1	JG2	HAS1
B_2O_3	10.26	10.34	10.32	9.34
SiO_2	34.39	35.70	35.40	27.99
TiO_2	0.63	0.09	0.01	0.04
Al_2O_3	32.17	29.74	31.53	19.44
FeO	17.16	15.88	17.79	28.58
MgO	0.55	3.57	0.86	11.24
CaO	0.07	0.81	0.44	0.09
K_2O	0.07	0.03	0.03	0.51
Na_2O	2.42	2.16	2.09	0.03
BaO	0.08	0.08	0.08	0.07
MnO	0.17	0.06	0.06	0.13
Cl	bdl	0.01	0.01	0.01
F	1.14	0.30	0.44	bdl
Li_2O	0.12	bdl	0.07	bdl
H_2O	3.00	3.42	3.35	3.22
Total	102.23	102.19	102.48	100.69
B	3	3	3	3
Si	5.83	6	5.96	5.21
Al (T)	0.17	bdl	0.04	0.79
Al (Z)	6	5.89	6	3.47
Mg (Z)	bdl	0.11	bdl	2.53
Fe^{2+}	2.43	2.23	2.51	2.45
Ti	0.08	0.01	bdl	0.01
Al (Y)	0.25	bdl	0.22	bdl
Mn	0.02	0.01	0.01	0.02
Mg	0.14	0.78	0.22	0.65
Li	0.08	bdl	0.05	bdl
Total Y	3	3.03	3	3.13
Na	0.80	0.70	0.68	0.01
Ca	0.01	0.15	0.08	0.02
[]	0.17	0.14	0.23	0.85
K	0.02	0.01	0.01	0.12
Total X	1	1	1	1
OH (V)	3	3	3	3
OH (W)	0.39	0.84	0.76	1
F (W)	0.61	0.16	0.23	bdl
Classified as	Schorl	Schorl	Schorl	Foitite

B_2O_3, Li_2O and H_2O calculated after Selway and Xiong (2015). Analytical data in wt %; mineral formula calculation results are given in apfu. Bdl: below detection limit. Additional analyses are given in the Electronic supplementary material 1.

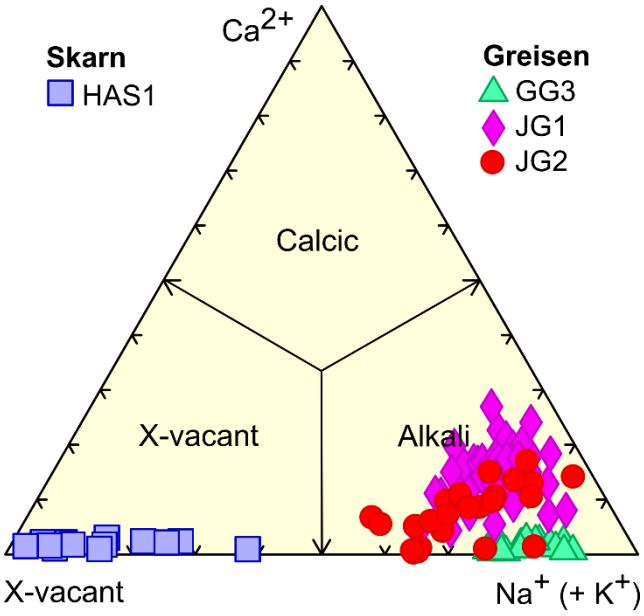

Figure 8: Classification diagram for tourmaline based on the occupancy of the X site. Tourmaline from greisen samples GG3, JG1, and JG2 are part of the alkali group whereas tourmaline from the skarn HAS1 is distinctive by very low Ca-occupancy. This tourmaline falls in the field of X-vacant tourmaline and defines a broad range from the X-vacant compositions toward variable X-occupancy by Na and K. (Diagram modified after Hawthorne and Dirlam, 2011).

2.5.2. Theriak-Domino modelling

The skarn type changes on the meter scale and locally even on the centimeter scale (Lefebvre et al., 2017). The sequence of skarn type is very variable on the scale of the mine. The close spatial coexistence of the different skarn types implies that they formed together under similar pressure and temperature conditions. The various calc-silicate skarn types of Hämmerlein have similar whole rock compositions (Electronic supplementary material 2). Therefore, the contrasting mineralogical composition of the skarns reflects the presence of contrasting fluids and/or reactions. The fluid composition may be locally controlled by the consumption of carbonates that generates CO_2, which may increase XCO_2 of the fluid or induce phase separation (Diamond 2001). The mineral assemblages of the skarns have been modelled (Fig. 9) in terms of temperature and XCO_2 at 2 and 5 kbar, respectively, using the Theriak-Domino thermodynamic modelling software of de Capitani and Petrakakis (2010). The compositions used for the modelling are the average skarn composition (see Electronic supplementary material 2) for the silicate skarns and the composition of an individual sample for the magnetite skarn. The pressure of 2 kbar roughly corresponds to the emplacement depth of the Eibenstock granite (Förster et al., 1999) and, therefore, the depth of the skarnified wall rocks at the time of the granite emplacement. Thus a pressure of 2 kbar would correspond to a situation of contact metamorphism with skarn formation triggered by fluids and heat from the granite. The pressure of 5 kbar roughly corresponds to the metamorphic conditions reached by the host-rocks of the skarn during the Variscan orogeny at c. 340 Ma (Rötzler et al., 1998), i.e., clearly before the emplacement of the granite.

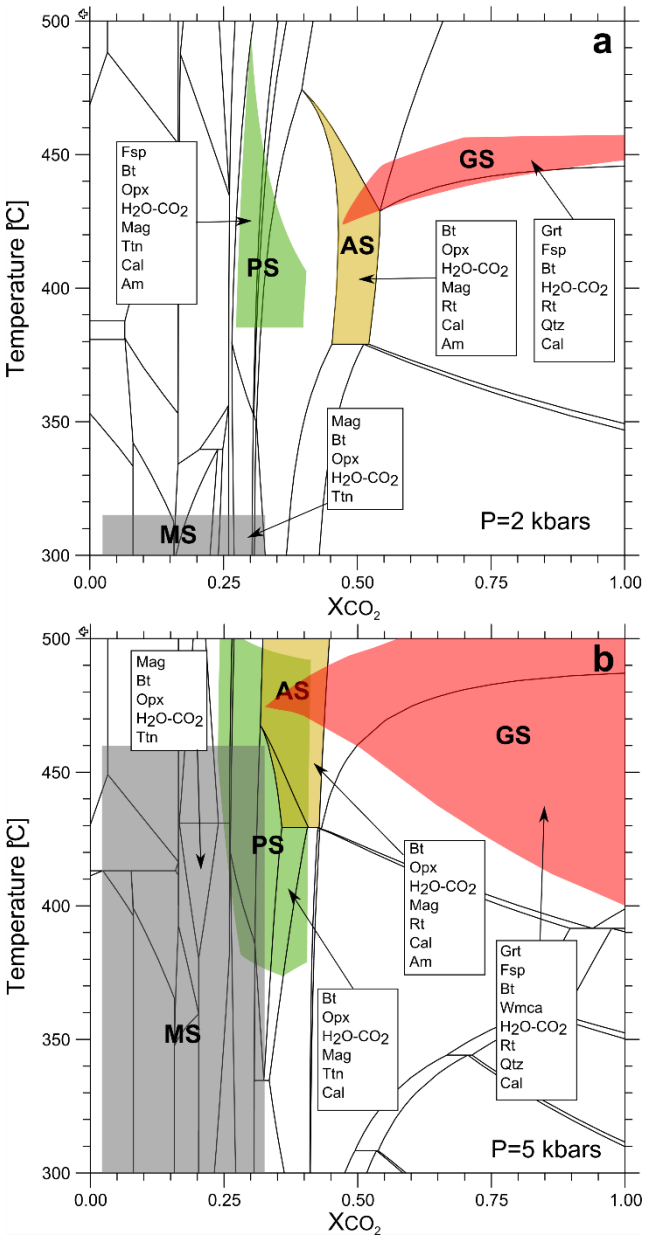

Figure 9: Simplified T-P-XCO_2 modeling of the stability ranges of the various skarn assemblages at 2 kbar (a) and 5 kbar (b), respectively. Independent of pressure, the major difference among the various skarn assemblages is XCO_2, which increases systematically from magnetite skarn to pyroxene, amphibole, and garnet skarn. For 5 kbar, the various skarn types are stable in the same temperature range, whereas at 2 kbar, the magnetite skarn is stable at lower temperature. Individual modeling parameters for each skarn unit is available in the Electronic supplementary material 2 and 3. Am: amphibole, Bt: biotite, Cal: calcite, Fsp: feldspar, Grt: garnet, Mag: magnetite, Opx: orthopyroxene, Qtz: quartz, Rt: rutile, Ttn: titanite, Wmca: white mica.

Figure 9 shows the stability fields of the various skarn types for 2 and 5 kbar, respectively. The various skarn mineral assemblages include biotite, rutile or titanite, and calcite. The various skarns differ by the nature of the main calc-silicate minerals, i.e., garnet, amphibole, and pyroxene. The magnetite skarn assemblage is dominated by magnetite with minor biotite, pyroxene, and titanite. The most distinctive differences of the various stability fields are the contrasting ranges of XCO_2. At 5 kbar (Fig. 9b), the stability fields of the various skarns are relatively large and overlap, the garnet skarn mineral assemblage is stable at high XCO_2, whereas the amphibole, pyroxene, and magnetite skarns are stable at systematically lower XCO_2. The various stability fields have an overlapping temperature range at 400-450°C. At 2 kbar (Fig. 9a), the stability fields of the various skarns are narrower than at 5 kbar and extend to lower temperatures. Garnet and magnetite skarns have clearly contrasting temperature ranges. Amphibole and pyroxene skarns, compared to garnet skarn, have broader temperature ranges that overlap with those of garnet skarn.

2.5.3. Rb-Sr age determination

Three groups of Rb-Sr multimineral ages have been determined for the skarn and greisen samples (Fig. 10). The youngest age of ~290 Ma was obtained for the greisen sample GG1. The other six dated greisen samples yield ages around 320 Ma, whereas the two samples from the Hämmerlein skarn deposit yield ages around 340 Ma.

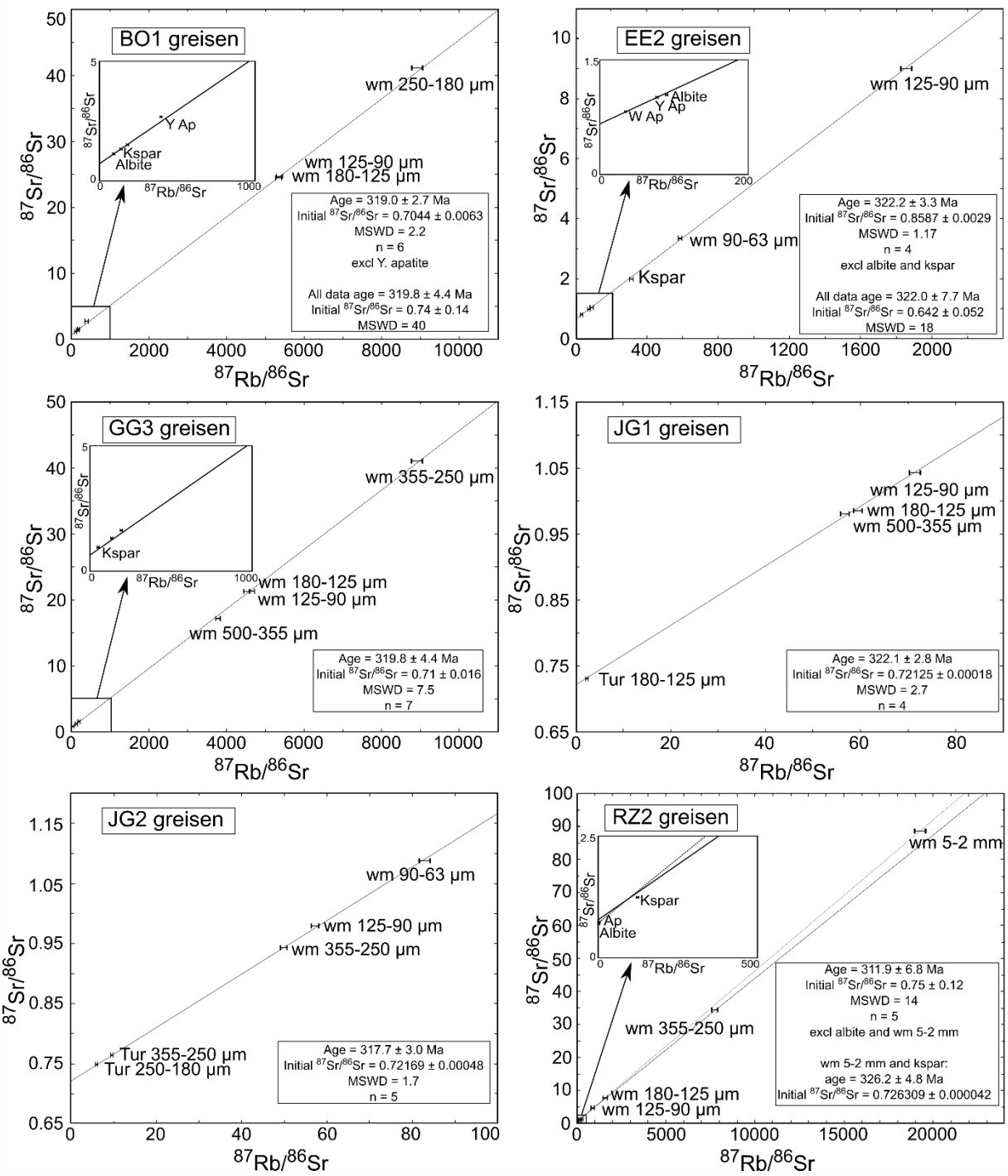

Figure 10: Rb-Sr mineral data for greisen mineralization associated with the Eibenstock granite and skarns from Hämmerlein. Analytical data: see Table 5. Ap: apatite, Kspar: K-feldspar, Tur: tourmaline, W Ap: white apatite, Wm: white mica, Y Ap: yellow apatite.

For the greisen sample GG1, three size fractions (250-180 µm, 180-125 µm, and 125-90 µm) of white mica, the whole rock fraction, and one apatite fraction were analyzed. Two mica fractions (250-180 µm and 180-125 µm) and apatite together define an isochron age of 294.8 ± 3.1 Ma (n = 3, MSWD = 3.0) with an initial $^{87}Sr/^{86}Sr$ at 0.714604 ± 0.000042 (Fig. 10, Table 5). The whole rock and one white mica fraction plot slightly above the regression line and, therefore, they are excluded from the calculation.

Note, using all samples to constrain calculate isochron parameters does not affect the age significantly, but increases considerably the uncertainty of age and of the initial Sr isotopic composition (Fig. 10).

The six other samples of greisen consistently yield Rb-Sr multimineral ages around 320 Ma (Fig. 10, Table 5). Greisen sample BO1 yields an isochron age of 319 ± 2.7 Ma (n = 6, MSWD = 2.2) with initial $^{87}Sr/^{86}Sr$ of 0.7044 ± 0.0063. The isochron is defined by three muscovite fractions (250-180 µm, 180-125 µm, and 125-90 µm) and one fraction each of white apatite, K-feldspar, and albite. Yellow apatite was not included in the regression. Its inclusion would not significantly affect the age information, but only deteriorate precision (see Fig. 10 for greisen sample EE2).

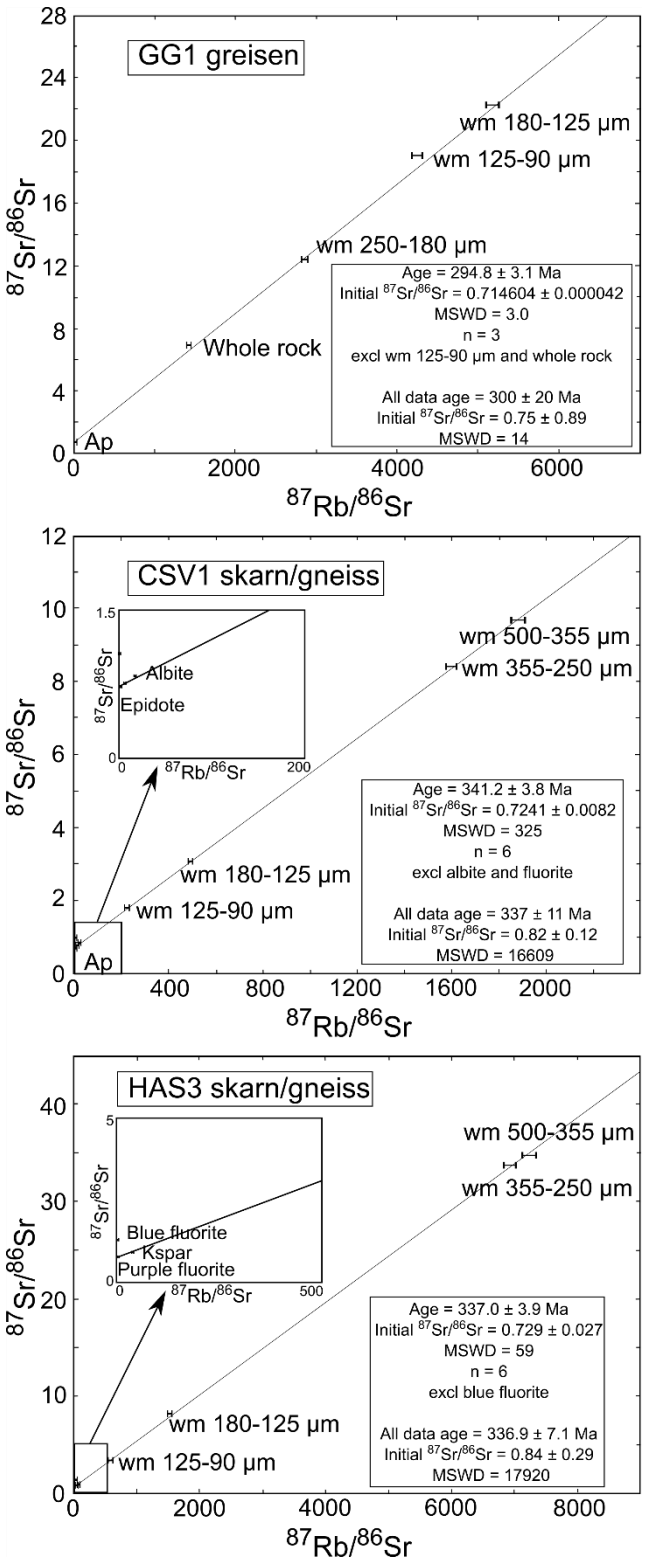

Figure 10 continued

For greisen sample EE2, two muscovite (125-90 µm and 90-63 µm) and two apatite (yellow and white) fractions define an isochron with an age of 322.2 ± 3.3 Ma (n = 4, MSWD = 1.17) and an initial $^{87}Sr/^{86}Sr$ of 0.8587 ± 0.0029. Note, this initial Sr isotopic composition is significantly higher than initial $^{87}Sr/^{86}Sr$ for different types of Eibenstock granite (up to 0.713; Velichkin et al., 1994). Albite and K-feldspar have been omitted from the calculation of the isochron, as they plot below the isochron and would shift the apparent initial Sr isotopic composition to an unreasonably low value of 0.642 ± 0.052 (Fig. 10). We hypothesize that this effect is caused by crystallizational overprint of feldspar, potentially, by upper crustal fluids or by weathering.

The Rb-Sr age of sample GG3 is determined by an isochron constrained by four muscovite fractions (500-355 µm, 355-250 µm, 180-125 µm, and 125-90 µm), two apatite fractions (yellow and white apatite), and one K-feldspar fraction, to be 319.8 ± 4.4 Ma (n = 7, MSWD = 7.5) with a poorly constrained initial $^{87}Sr/^{86}Sr$ ratio of 0.71 ± 0.16 (Fig. 10). The excess scatter (indicated by the elevated MSWD) cannot be assigned to one particular mineral fraction. In any case, the large range in $^{87}Rb/^{86}Sr$ values spanned by the four white mica samples renders the slope of the isochron nearly insensitive to potential secondary alterations of the low-$^{87}Rb/^{86}Sr$ mineral fractions.

Metasomatized phyllite sample JG1 is unusual among the here dated greisen samples as it has the smallest range in $^{87}Sr/^{86}Sr$ with a maximum $^{87}Sr/^{86}Sr$ as low as 1.04240 (Table 5). The slope of the isochron is constrained by three grain size fractions of muscovite (500-355 µm, 180-125 µm, and 125-90 µm) and one tourmaline fraction. The isochron yields an age of 322.1 ± 2.8 Ma (n = 4, MSWD = 2.7) with an initial $^{87}Sr/^{86}Sr$ of 0.72125 ± 0.00018 (Fig. 10). A second sample from the same metasomatized phyllite, sample JG2, yields a five-point isochron that is defined by three muscovite fractions (355-250 µm, 125-90 µm, and 90-63 µm) and two tourmaline fractions (355-250 µm and 250-180 µm). The isochron corresponds to an age of 317.7 ± 3.0 Ma (n = 5, MSWD = 1.7) and yields an initial $^{87}Sr/^{86}Sr$ of 0.72169 ± 0.00048 (Fig. 10). The ages and initial $^{87}Sr/^{86}Sr$ values of these two greisen samples overlap within respective uncertainties.

Table 5: Rb/Sr analytical data of Hämmerlein skarns, and of greisen associated with the Eibenstock granite

Sample	Material	Rb (ppm)	Sr (ppm)	$^{87}Rb/^{86}Sr$	$^{87}Sr/^{86}Sr$	$^{87}Sr/^{86}Sr$ $2\sigma_m$ (%)
Skarn/gneiss samples						
CSV1 (Hämmerlein) (341.2 ± 3.8 Ma (excl. albite, apatite and fluorite); MSWD = 325, Sr_i = 0.7241 ± 0.0082)						
MLP06	wm 500-355 µm	2094	6.04	1883	9.68243	0.0012
MLP07	wm 355-250 µm	2033	6.45	1599	8.41746	0.0018
MLP08	wm 180-125 µm	1990	14.3	494	3.07608	0.0010
MLP09	wm 125-90 µm	1834	26.4	222	1.78948	0.0011
MLP10	Fluorite	19.6	1109	0.0529	1.05602	0.0021
MLP11	Epidote	423	860	1.43	0.72624	0.0046
MLP12	Ap	114	2666	0.126	0.93551	0.0019
MLP13	Albite	206	35.4	17.1	0.83217	0.0014
MLP14	Kspar	410	195	6.11	0.75788	0.0010
HAS3 (Hämmerlein) (337.0 ± 3.9 Ma (excl. blue fluorite); MSWD = 59, Sr_i = 0.729 ± 0.027)						
MLP34	wm 500-355 µm	2014	3.50	7226	34.839	0.0040
MLP35	wm 355-250 µm	2024	3.57	6930	33.7152	0.0012
MLP36	wm 180-125 µm	1986	6.21	1609	8.25514	0.0006
MLP37	wm 125-90 µm	1780	11.3	578	3.45693	0.0008
MLP39	Kspar	1189	92.1	38.0	0.89841	0.0016
MLP40	Purple fluorite	81.5	125	1.89	0.75044	0.0061
MLP41	Blue fluorite	23.4	738	0.0969	1.27200	0.0036
Greisen samples						
BO1 (Backofen/Sosa) (319.0 ± 2.7 Ma (excl. Y. apatite); MSWD = 2.2, Sr_i = 0.7044 ± 0.0063)						
MLP57	wm 250-180 µm	3881	6.23	8905	40.9793	0.0020
MLP58	wm 180-125 µm	3852	6.94	5354	24.5610	0.0010
MLP59	wm 125-90 µm	3595	6.49	5336	24.5019	0.0009
MLP60	Albite	350	11.7	89.8	1.11015	0.0013
MLP61	Kspar	1082	24.2	137	1.31150	0.0028
MLP62	Y Ap	712	6.23	394	2.67194	0.0020
MLP63	W Ap	164	2.85	179	1.49377	0.0040
EE2 (Erzengel/Sosa) (322.2 ± 3.3 Ma (excl. albite and kspar); MSWD = 1.17, Sr_i = 0.6587 ± 0.0029)						
MLP16	wm 125-90 µm	3277	9.27	1851	8.9844	0.0040
MLP17	wm 90-63 µm	2698	16.7	587	3.32459	0.0014
MLP18	Kspar	827	8.66	311	1.98703	0.0012
MLP19	Albite	38.4	1.27	90.0	1.04228	0.0036
MLP65	Y Ap	370	14.3	76.9	1.00298	0.0020
MLP66	W Ap	72.5	6.13	34.5	0.81505	0.0040

Sample	Material	Rb (ppm)	Sr (ppm)	$^{87}Rb/^{86}Sr$	$^{87}Sr/^{86}Sr$	$^{87}Sr/^{86}Sr$ 2σm (%)
GG1 (Gabe Gottes/Dönitzgrund) (294.8 ± 3.1 Ma (excl. wm 125-90 µm and whole rock); MSWD = 3.0, Sr_i = 0.714604 ± 0.000042)						
MLP01	wm 180-125 µm	2564	4.46	5176	22.2708	0.0019
MLP02	wm 250-180 µm	1799	3.91	2854	12.3836	0.0022
MLP03	wm 125-90 µm	2259	4.30	4248	19.0493	0.0020
MLP04	Ap	59.1	535	0.320	0.71592	0.0040
MLP64	whole rock >500 µm	1082	3.52	1426	6.8970	0.0060
GG3 (Gabe Gottes/Dönitzgrund) (319.8 ± 4.4 Ma; MSWD = 7.5, Sr_i = 0.71 ± 0.16)						
MLP42	wm 500-355 µm	2487	5.02	3736	17.1464	0.0006
MLP43	wm 355-250 µm	2541	4.08	8917	41.0440	0.0012
MLP44	wm 180-125 µm	2560	4.85	4603	21.2957	0.0010
MLP45	wm 125-90 µm	2537	4.82	4589	21.2927	0.0022
MLP46	Kspar	968	56.0	51.2	0.95391	0.0011
MLP47	W Ap	151	3.44	134	1.3156	0.0077
MLP48	Y Ap	1057	17.1	194	1.62713	0.0040
JG1 (Jugel NW) (322.1 ± 2.8 Ma; MSWD = 2.7, Sr_i = 0.72125 ± 0.00018)						
MLP22	wm 500-355 µm	1713	89.8	56.7	0.98019	0.0013
MLP23	wm 180-125 µm	1697	84.9	59.4	0.98621	0.0020
MLP24	wm 125-90 µm	1563	65.4	71.3	1.04240	0.0014
MLP27	Tur 180-125 µm	144	185	2.26	0.73147	0.0016
JG2 (Jugel NW) (317.7 ± 3.0 Ma; MSWD = 1.7, Sr_i = 0.72169 ± 0.00048)						
MLP28	wm 355-250 µm	1167	69.3	49.8	0.94236	0.0012
MLP30	wm 125-90 µm	1172	60.8	57.2	0.97975	0.0020
MLP31	wm 90-63 µm	1256	45.4	82.9	1.08731	0.0012
MLP32	Tur 355-250 µm	327	99.2	9.60	0.76441	0.0011
MLP33	Tur 250-180 µm	244	119	5.98	0.74830	0.0011
RZ2 (Roßzeche/nördlich Carlsfeld) (2311.9 ± 6.8 Ma (excl. wm 5-2 mm and albite); MSWD = 14, Sr_i = 0.75 ± 0.12)						
MLP49	wm 5-2 mm	4007	5.78	19277	88.766	0.0020
MLP50	wm 355-250 µm	3919	6.28	7739	34.3233	0.0020
MLP51	wm 180-125 µm	3697	11.3	1604	7.7957	0.0020
MLP52	wm 125-90 µm	3533	15.8	900	4.74661	0.0005
MLP53	Albite	29.5	410	0.208	0.71726	0.0052
MLP54	Kspar	297	7.38	122	1.23730	0.0014
MLP55	Ap	16.0	597	0.0775	0.72510	0.0014

Ap: apatite, Kspar: K-feldspar, Tur: tourmaline, W Ap: white apatite, Wm: white mica, Y Ap: yellow apatite

Two gneiss samples with skarn have been dated (Fig. 10, Table 5). Sample CSV1 yields an age of 341.2 ± 3.8 Ma (n = 6, MSWD = 325) with an initial $^{87}Sr/^{86}Sr$ of 0.7241 ± 0.0082 (Fig. 10). The calculation is based on four white mica grain size fractions (500-355 µm, 355-250 µm, 180-125 µm, and 125-90 µm), one K-feldspar fraction, and one epidote fraction. The albite and fluorite fractions plot considerably

above the regression line and, therefore, have not been included into the calculation. The fluorite fraction has a low $^{87}Rb/^{86}Sr$ of 0.0529 and, therefore, its radiogenic $^{87}Sr/^{86}Sr$ (1.0561) (Fig. 10, Table 5) implies that this texturally late fluorite crystallized from a fluid with higher $^{87}Sr/^{86}Sr$ than the fluid that formed the skarn silicates used for isotopic dating.

The Rb-Sr age of the sample HAS3 was determined using four muscovite fractions (500-355 µm, 355-250 µm, 180-125 µm, and 125-90 µm), K-feldspar, and purple fluorite. Regression yields an age of 337.0 ± 3.9 Ma (n = 6, MSWD = 59) with an initial $^{87}Sr/^{86}Sr$ of 0.729 ± 0.027 (Fig. 10). The blue fluorite plots far above the regression line and was not used to calculate the age. The abnormally high Sr isotopic signature of this fluorite requires, as in sample CSV1, post-crystallizational influx of high-$^{87}Sr/^{86}Sr$ fluorite precipitating fluids. The high strain induced layering and the metamorphism of both the gneiss and the skarn are related to the same ductile event (Fig. 3). Therefore, the age obtained for white mica, which likely belong to the gneiss, also yields the age of the skarn.

2.5.4. Pb isotopic composition of skarn minerals of the Hämmerlein deposit

The Pb isotopic compositions of skarn silicates and sulfides are listed in Table 6 and plotted in Fig. 11. The data fall into two groups: one group includes samples with relatively unradiogenic Pb isotopic composition ($^{206}Pb/^{204}Pb_{meas}$: 18.36 – 19.1) and the other group has relatively radiogenic Pb isotopic composition ($^{206}Pb/^{204}Pb_{meas}$: 20.9 – 33.2). The difference between the two groups that do not form a continuous trend is most obvious in the $^{206}Pb/^{204}Pb$ vs. $^{238}U/^{204}Pb$ diagram (Fig. 11b). Minerals that formed during the regional Variscan metamorphism, maintained a closed U-Pb system, and had similar initial Pb isotopic compositions should fall on a straight line whose slope corresponds to an age of 340 Ma and whose intercept corresponds to the common initial Pb isotopic composition. All mineral samples of the first group fall on such a line, whereas all samples of the second group plot above this line (Fig. 11b). Minerals of the first group are derived from the garnet, pyroxene, and magnetite skarns and include garnet, sulfides, feldspar, and amphibole. There are also two amphibole and three apatite samples from the amphibole skarn that plot on this trend. Most minerals of this low-$^{206}Pb/^{204}Pb$ group form a tight cluster in the $^{206}Pb/^{204}Pb$-$^{207}Pb/^{204}Pb$ and $^{206}Pb/^{204}Pb$-$^{208}Pb/^{204}Pb$ diagrams (Figs. 11a and 11c).

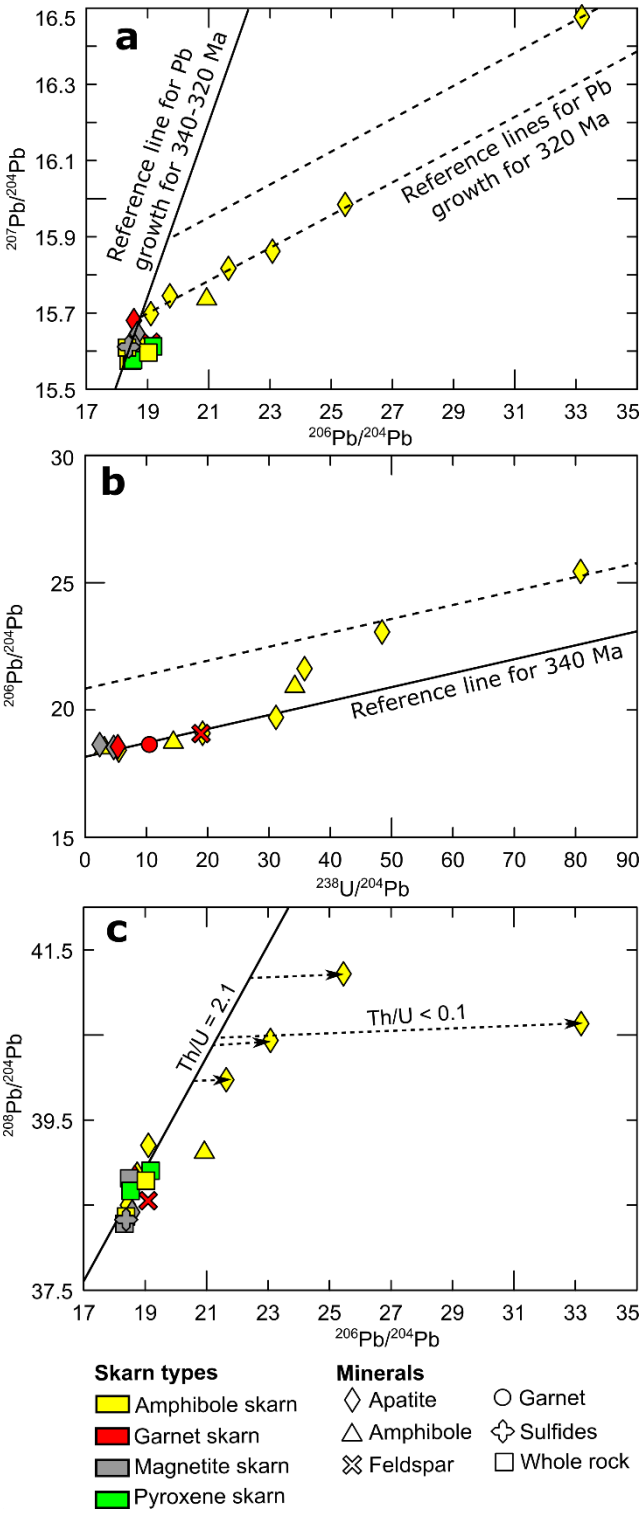

Figure 11: $^{207}Pb/^{204}Pb$ vs $^{206}Pb/^{204}Pb$ (a), $^{206}Pb/^{204}Pb$ vs $^{238}U/^{204}Pb$ (b), and $^{208}Pb/^{204}Pb$ vs $^{206}Pb/^{204}Pb$ (c) diagrams for skarn samples from the Hämmerlein deposit. Minerals data: see Table 6, whole rocks data: unpublished data.

Minerals of the second high-$^{206}Pb/^{204}Pb$ group all come from the amphibole skarn and include one amphibole and three apatite samples (Fig. 11). Initial $^{206}Pb/^{204}Pb$ values calculated for the ages of 340 and 320 Ma, respectively are very radiogenic for these minerals. Furthermore, the various samples have different calculated initial $^{206}Pb/^{204}Pb$ values (Fig. 11b). In the $^{206}Pb/^{204}Pb$-$^{207}Pb/^{204}Pb$ diagram (Fig. 11a), these samples also show high $^{207}Pb/^{204}Pb$, which implies that their Pb either comes from a different source or has a poly-stage development. Such a poly-stage development also is indicated by the Sr isotopic composition of fluorite and apatite form amphibole skarn that have anomalously radiogenic initial $^{87}Sr/^{86}Sr$ values and fall far above the Rb-Sr isochron. For a simple two-stage Pb-growth for skarn formation during regional metamorphism at 340 Ma and disturbance during emplacement of the Eibenstock granite at c. 320 Ma, the offset in the $^{206}Pb/^{204}Pb$ vs. $^{238}U/^{204}Pb$ diagram and the scatter in the $^{206}Pb/^{204}Pb$-$^{207}Pb/^{204}Pb$ and $^{206}Pb/^{204}Pb$-$^{208}Pb/^{204}Pb$ diagrams is best explained by Pb growth from 340 to 320 Ma with a high μ ($^{238}U/^{204}Pb$), followed by Pb growth from 320 Ma to present with a lower μ value. Note, the age of c. 340 Ma is implied by the Rb-Sr isochron obtained for minerals from the same sample. In contrast, the age of c. 320 Ma is not closely constrained by the data. The various minerals that fall on the trend with the low initial $^{206}Pb/^{204}Pb$ in the $^{206}Pb/^{204}Pb$ vs. $^{238}U/^{204}Pb$ diagram did not see such a high-μ stage. Instead, these samples always had a low-μ (even in case they had seen the same two stage development). There are two possible scenarios for such a two-stage Pb growth: (i) In a first stage that lasted from 340 to c. 320 Ma, apatite and amphibole would have high $^{238}U/^{204}Pb$ and, thus, develop

markedly higher $^{206}Pb/^{204}Pb$ and $^{207}Pb/^{204}Pb$ values that the other skarn minerals. During a second event at c. 320 Ma, apatite and amphibole would lose U (and Th). (ii) Apatite formed at c. 320 Ma and incorporated Pb that was derived from a source that had evolved in a high-μ environment. Such a late addition of radiogenic lead also would explain the restricted variation of $^{208}Pb/^{204}Pb$ at very variable $^{206}Pb/^{204}Pb$, as Th is considerably less mobile in medium and low temperature fluids than U and Pb and, thus, was not available for incorporation (schematically indicated by the dashed trend lines for Th/U < 0.1 in Fig. 11c).

Table 6: U/Pb analytical data of Hämmerlein skarns

Sample No.	Material	U (ppm)	Pb (ppm)	$^{206}Pb/^{204}Pb$	$^{207}Pb/^{204}Pb$	$^{208}Pb/^{204}Pb$	$^{238}U/^{204}Pb$
ASb (Amphibole skarn)							
ASb-1	Apatite >125 µm	12	2.2	33.192	16.480	40.641	430
ASb-2	Apatite 125-100 µm	30	43	23.068	15.864	40.442	48.6
ASb-3	Apatite <100 µm	45	40	25.448	15.987	41.225	81.3
ASb-5	Amphibole	0.80	17	18.504	15.634	38.422	2.97
HAS1 (Amphibole skarn)							
HAS1-1	Apatite	0.56	6.7	18.427	15.605	38.505	5.34
HAS1-3	Amphibole	2.2	9.9	18.725	15.632	38.876	14.3
HAS3 (Amphibole skarn)							
HAS3-1	Apatite >125 µm	0.27	0.93	19.091	15.700	39.208	19.1
HAS3-2	Apatite 125-100 µm	3.2	6.1	21.629	15.819	39.980	35.9
HAS3-3	Apatite <100 µm	1.5	3.0	19.714	15.747	34.612	31.2
HAS3-4	Amphibole	0.72	1.4	20.916	15.738	39.122	34.3
HGS2 (Garnet skarn)							
HGS2-1	Apatite	0.25	3.5	18.534	15.682	38.726	4.51
HGS2-2	Feldspar	0.89	3.0	19.080	15.625	38.556	18.9
HGS2-3	Garnet	0.41	2.4	18.623	15.333	36.356	10.5
HMS1 (Magnetite skarn)							
HMS1-1	Apatite >125 µm	0.059	1.7	18.647	15.648	38.831	2.21
HMS1-2	Apatite <125 µm	0.39	4.7	18.562	15.616	38.421	5.20
HMS1-3	Feldspar	0.022	1.2	18.877	15.874	39.125	1.15
HMS1-4	Sulfides	0.0087	872	18.365	15.613	38.334	<0.001

2.6. Discussion

2.6.1. Age of skarn formation

The Rb-Sr age determination on two gneiss samples with skarn (CSV1 and HAS3) yields ages at 341.2 ± 3.8 Ma and 337.0 ± 3.9 Ma, respectively. The structural observations indicate that both the dated gneisses and the skarn in contact with the gneisses are pervasively foliated and thus reflect ductile conditions. As the metamorphic rocks of the Erzgebirge had cooled below the ductile-brittle transition long before 330 Ma, it is clear that the skarn formation is older than 330 Ma. Decarbonation is driven by the influx of aqueous fluids (e.g., Heinrich 2007). Aqueous fluids become available during prograde metamorphism by the dehydration of hydrous minerals rather than during post-peak cooling. Therefore, it is quite possible that the age of the skarn is close to the Rb-Sr age of the gneisses. Besides, simple thermodynamic modelling using Theriak-Domino and the whole rock composition of the various skarn types demonstrates that the stable mineral assemblages may be obtained at pressures of 5 kbar, which

corresponds to peak conditions of regional metamorphism in the area at 340 Ma and is coherent with the Rb-Sr age of the skarn/gneiss. The prograde skarn assemblages formed at this time at ~5 kbar at ambient temperature of ~450°C, and contrasting XCO_2 (Fig. 9) corresponding to the four skarn types. However, the same minerals assemblages are also stable at lower pressure (Fig. 9a). This means that the skarn assemblages could not be destabilized at the pressure conditions prevailing during the emplacement of the Eibenstock granite (2 kbar) and that the calc-silicates assemblages may not be affected by major retrogression. Locally, strong chloritization as well as apatite formation affects the primary skarn assemblage. The age of this retrograde mineral assemblage is not known. It may represent retrogression after peak metamorphic conditions, retrogression caused by the Eibenstock granite intrusion, or retrogression related to even younger disturbances. The anomalously radiogenic Sr isotopic composition of apatite and fluorite and the Pb isotopic composition of apatite and amphibole, however, indicate that there must have elapsed a significant period of time after the formation of the skarn and its retrogression. Thus, chloritization with associated cassiterite and the formation of apatite and fluorite are not related to the 340 Ma metamorphism.

2.6.2. Age of greisen mineralization, age and source of tin additions in greisen and skarn

Late stages of the Eibenstock and related granites (e.g. Kirchberg, Pobershau, Satzung) are major sources of Sn mineralization, as demonstrated by the abundance of Sn-rich greisen, some of which have been dated here (Table 5, Fig. 10). The dated greisen samples yield Rb-Sr isotopic ages ranging from 322.2 ± 3.3 Ma to 311.9 ± 6.8 Ma, which is essentially identical to the U-Pb zircon age range of the granite (314 ± 6 Ma, Tichomirowa et al., 2016). There is only one greisen sample that yields a distinctly younger age (294.8 ± 3.1 Ma; Fig. 10), which indicates that some of the greisen have been possibly overprinted during later events.

Cassiterite is the major Sn mineral in the greisen. It is texturally clearly related to the greisen formation and not to a later event. This is also corroborated by the enhanced Sn contents of greisen silicates. Typically, Sn contents of white mica range between 0.03 and 0.36 wt % (Electronic supplementary material 1). This implies that late-magmatic fluids available at the time of emplacement of the Eibenstock and related granites transported Sn, and, therefore, Sn has been introduced into the greisen by fluids released from these granites. Furthermore, this also implies that these fluids may have introduced Sn into the skarn.

If all tin in the Hämmerlein skarn mineralization was derived from the Eibenstock granite, older skarn minerals should not have elevated Sn contents. Instead, only secondary skarn minerals that formed during the same event as secondary fluorite and chlorite should have elevated Sn contents. Primary 340 Ma old skarn minerals in the Hämmerlein deposit, however, do have elevated Sn contents. For instance, grossular from the garnet skarn has 0.10 to 0.88 wt% Sn (Electronic supplementary material 1). Similarly, cummingtonite from the amphibole skarn has 0.03 to 0.49 wt% Sn, and augite from the

pyroxene skarn has 0.45 to 0.77 wt% Sn (Electronic supplementary material 1). This implies that Sn was available for incorporation at 340 Ma and must have been introduced into the skarn in the process of Variscan regional metamorphism, i.e., c. 20 Ma before the emplacement of the Eibenstock and related granites. During this early event of Sn mobilization, Sn did not form early stage cassiterite, but was incorporated into skarn minerals. The later alteration of some of these skarn minerals may have released Sn that was then precipitated as cassiterite. Such a formation of secondary ore minerals during the alteration of biotite to chlorite has been described by Zhao et al. (2005) and Wang et al. (2013). For the Hämmerlein skarn, the amount of chlorite is relatively small. Thus, the release of Sn during the consumption of biotite, or muscovite, or garnet to form chlorite seems insufficient to explain the observed amount of cassiterite. Thus, the Hämmerlein skarn experienced two phases of Sn accumulation, one during regional metamorphism and one during the emplacement of the Eibenstock and related granites. During the first event of Sn addition, the devolatilizing sedimentary rocks beneath the later skarn seem to represent the Sn source, whereas during the second event Sn was brought along by late magmatic fluids emanating from the Eibenstock granite and resulting in the superimposition of tin mineralization on the previous skarn, just in the same way as in the Huanggangliang Fe-Sn skarn in Inner Mongolia (Wang et al., 2001).

At Hämmerlein, cassiterite is paragenetic with secondary chlorite, fluorite, tourmaline, and locally also with a second generation of fine-grained ferroan poly-lithionite, i.e., a texturally late generation, with overprint-related minerals that have not been used to constrain the Rb-Sr ages. Actually, the Rb-Sr isotope systematics of the few analyzed secondary minerals clearly show anomalously high $^{87}Sr/^{86}Sr$ values. It is unclear from textural observations whether these secondary minerals formed in a retrograde phase during regional metamorphism, i.e., whether they are temporally close to the dated peak assemblage, or formed during a second, unrelated and distinctly younger event, in connection to the emplacement of the Eibenstock granite at c. 320 Ma.

Among the analyzed secondary minerals, fluorite from the pyroxene skarn (sample CSV1) and blue fluorite and apatite from the amphibole skarn (sample HAS3) have particularly high $^{87}Sr/^{86}Sr$ ratios and very low $^{87}Rb/^{86}Sr$ ratios. To highlight the contrast of Sr isotopic signatures between these two fluorite and the apatite samples and the other minerals used to date the skarn, $^{87}Sr/^{86}Sr$ isotopic ratio of all mineral fractions have been recalculated from the measured value to their initial value at 341.2 ± 3.8 Ma for the pyroxene skarn (Fig. 12a) and at 337.0 ± 3.9 Ma for the amphibole skarn (Fig. 12b). The reduced isochron diagrams with initial $^{87}Sr/^{86}Sr$ vs $^{87}Rb/^{86}Sr$ show that all mineral fractions are, considering the uncertainty intervals, on the initial isochron with a $^{87}Sr/^{86}Sr$ of 0.724 for the pyroxene skarn and 0.729 for the amphibole skarn, except the fluorite fraction ($^{87}Sr/^{86}Sr_{341.2\ Ma}$ = 1.0558) and apatite ($^{87}Sr/^{86}Sr_{337.0\ Ma}$ = 0.93492) of the pyroxene skarn and blue fluorite ($^{87}Sr/^{86}Sr_{337.0\ Ma}$ = 1.2715) of the amphibole skarn. Thus, these minerals have acquired their radiogenic Sr isotopic compositions at a time different from the time of skarn formation. Using the initial $^{87}Sr/^{86}Sr$ of the isotopic compositions of skarn samples

CSV1 and HAS3 and the initial $^{87}Sr/^{86}Sr$ of the Eibenstock granite (all below 0.73) as estimates of the Sr isotopic composition available for redistribution at the time of the skarn formation and as estimates of the Sr released from the granite, respectively, it is obvious that fluorite and apatite received Sr from a different source. One possible source includes high $^{87}Rb/^{86}Sr$ minerals that had developed high $^{87}Sr/^{86}Sr$ at the time they were destabilized during fluorite formation. For instance, biotite and muscovite were consumed during the formation of chlorite. Biotite and muscovite (Fig. 12) have very high $^{87}Rb/^{86}Sr$ ratios, and thus may develop markedly radiogenic $^{87}Sr/^{86}Sr$ ratios within a short period of only a few million years. The minimum duration of time elapsed between the time of biotite formation and biotite alteration can be roughly estimated using the following assumptions: (i) biotite is the dominant source for the Sr in fluorite and apatite; (ii) the highest $^{87}Rb/^{86}Sr$ among skarn minerals is a good estimate for the $^{87}Rb/^{86}Sr$ of the mineral that serves as Sr source for the Sr in fluorite and apatite; (iii) the initial $^{87}Sr/^{86}Sr$ of the skarn assemblage represents a good estimate of the initial $^{87}Sr/^{86}Sr$ of biotite. Using 0.7241 as $^{87}Sr/^{86}Sr$ initial for the skarn, 1.056 for the fluorite, and 1900 as $^{87}Rb/^{86}Sr$ estimated for the biotite, the gap between skarn formation and fluorite crystallization is estimated to be about 20 million years. Additions of Sr derived from minerals with lower $^{87}Rb/^{86}Sr$ actually would require a longer gap between the formation of the skarn and the formation of secondary fluorite and apatite. A shorter duration, however, would be obtained if the Sr source for Sr in fluorite had an even higher $^{87}Rb/^{86}Sr$ than assumed for the above estimate. For instance, to obtain a gap of only 2 Ma, fluorite would have to have a $^{87}Rb/^{86}Sr$ ratio as high as 40 000, which is very unlikely even for mineralized skarn systems. For instance, the highest $^{87}Rb/^{86}Sr$ among the here dated mica fractions from greisen samples is c. 19 300 (Table 5, Fig. 10) and greisen represent a system that generally develops a much higher $^{87}Rb/^{86}Sr$ than skarns. Therefore, fluorite, apatite, and texturally related minerals (albite, chlorite, tourmaline, secondary muscovite, and cassiterite) are not related to the process of formation of the skarn, but instead are related to a second unrelated event of retrogression. This second event could well be the emplacement of the Eibenstock granite at c. 320 Ma. Such a two-stage process of skarn and mineralization formation also is known from the Big Bell gold skarn (Australia) that shows a pre-granite skarn with one mineralization before the granite intrusion, and another mineralization after the granite intrusion (Mueller et al., 1996; Mueller et al., 2000).

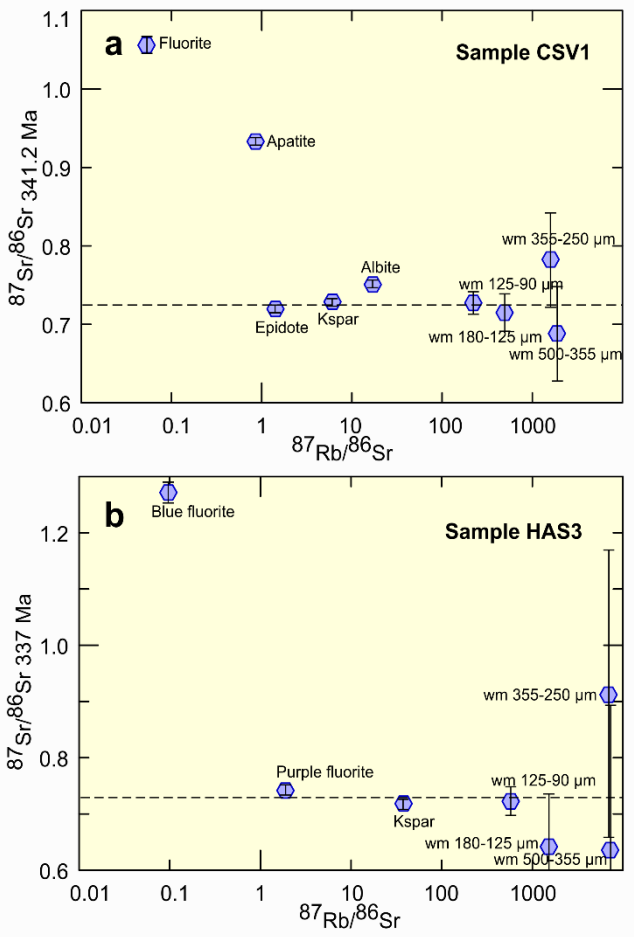

Figure 12: Rb-Sr reduced isochron diagrams of the pyroxene skarn (sample CSV1) and the amphibole skarn (sample HAS3). Samples that do not fall within uncertainties on the dashed lines (reduced isochrones) are in isotopic disequilibrium with the mineral assemblage which defines the age. Note the extremely radiogenic Sr isotopic composition of fluorite in sample CSV1 and of blue fluorite in sample HAS3. Such high ratios require a Sr source that has a very high $^{87}Sr/^{86}Sr$ and that aged for some time. Pyroxene and amphibole skarn Rb-Sr mineral data have been recalculated to the age of initial assemblage formation, i.e. 341.2 and 337.0 Ma, respectively.

A two-stage Pb growth also highlights two stages for skarn formation. The two stages have to be separated in time to explain the observed isotopic compositions. Similar as for Sr in apatite and fluorite, the two stages could be (i) the development between the regional metamorphism and the emplacement of the granites and (ii) post-granite Pb development. During the first stage between c. 340 and c. 320 Ma, apatite and amphibole with high $^{238}U/^{204}Pb$ developed higher $^{206}Pb/^{204}Pb$ and $^{207}Pb/^{204}Pb$ than the other minerals of the skarn. For the second stage at c. 320 Ma, the fluid derived from the Eibenstock and related granites induced either the loss of U and Th from apatite and amphibole or the incorporation of radiogenic Pb by apatite and amphibole.

2.6.3. Hämmerlein – a skarn with two events of Sn mineralization

Isotopic dating of the mineral assemblage of the amphibole skarn (Fig. 10) and the anomalous Sr and Pb isotopic composition of retrograde minerals associated with cassiterite (Figs. 11 and 12) in combination with the enhanced Sn contents in skarn minerals demonstrate that there are two stages of Sn introduction into the Hämmerlein skarn deposit. Tin related to the first stage is economically irrelevant as it is bound to silicate minerals and does not form a phase of its own. In contrast, Sn related to the second stage is mostly bound to cassiterite and, therefore, economically interesting.

The first tin enrichment corresponds to the tin-bearing calc-silicate minerals that crystallized during the skarn formation. Therefore, these minerals are directly associated with the c. 340 Ma regional metamorphism which affected the Cambro-Ordovician volcanosedimentary rocks. One likely scenario for the first tin enrichment is, upon heating (up to 400-450°C) during the Variscan metamorphism, the Cambro-Ordovician volcanosedimentary rocks may have released fluids, which were able to mobilize Sn from the sedimentary rocks and to form Sn(II) chloride complexes (Schmidt 2018). Those complexes

reacted with the carbonate layers within the sedimentary units, increasing XCO_2 of the fluid (Schmidt 2018). In units containing more carbonates, XCO_2 was higher, stabilizing garnet skarn. Amphibole and pyroxene skarns formed at lower XCO_2, possibly reflecting either a lower carbonate content or that the actually reacting rocks already had partially been decarbonated. The release of CO_2 due to fluid-rock interaction destabilized Sn-complexes in the fluid (Schmidt 2018). Sn was incorporated into garnet, amphibole, and pyroxene by substituting for Fe^{2+} (McIver and Mihálik, 1975), Mg^{2+} or Ca^{2+} (De Vore 1955), or as SnO_4^{4-} that may substitute for SiO_4^{4-} (Dadák and Novák, 1965), resulting in Sn-rich skarn silicates.

Cassiterite in the skarn, which formed during a second stage mineralization, occurs mostly in the amphibole skarn, typically in association with chlorite, and in the greisen, forming cassiterite-chlorite-fluorite-tourmaline assemblages. The systematic cassiterite-chlorite association both in skarn and greisen may indicate that chloritization of biotite and amphibole is the likely cause of destabilization of Sn complexes in the hydrothermal fluid. The acidic fluids derived from the Eibenstock granite altered biotite and to a lesser extent amphibole. Formation of chlorite at the expense of biotite releases Fe and Sr. The latter is distinctive by its highly radiogenic composition (because of the high $^{87}Rb/^{86}Sr$ of the precursor biotite) and eventually becomes incorporated into newly formed fluorite with remarkably high initial $^{87}Sr/^{86}Sr$ ratios (Fig. 12). Iron released in the skarn and greisen mineralization may form complexes with Cl ($FeCl_2$ or $FeCl_3$) and, thus, compete with Sn for Cl as ligand. As the formation of Fe-chlorides is energetically more favorable than that of Sn-chlorides (Sukhoruchkin and Soroko, 2009a; 2009b) and there is much more Fe in the system than Sn, Cl-ligands are mostly bound to Fe, which eventually implies that Sn precipitates as cassiterite in skarn and greisen. Biotite could also have released Sn into the system as described by Johan et al. (2012). This retraction of Cl-ligands could have caused an oversaturation of tin in the fluid, which would have resulted in the precipitation of cassiterite.

3. Chapter 3: Two stages of skarn formation in the Hämmerlein tin-skarn deposit, western Erzgebirge, Germany

Abstract

The Hämmerlein Sn-skarn deposit of the western Erzgebirge is hosted in early Palaeozoic schists and gneisses and is closely associated with one of the most voluminous granite intrusions of the Erzgebirge, the Eibenstock granite. The main valuable ore mineral in Hämmerlein is cassiterite which is disseminated in the four types of skarn occurring in the deposit, i.e., garnet, amphibole, pyroxene, and magnetite skarn. There are two scenarios for deposit formation: (1) formation of the skarn during the regional metamorphism at 340 Ma followed by mineralization during granite emplacement at 320 Ma and (2) skarn formation and mineralization directly related to the granite intrusion. Theriak-Domino thermodynamic P-T-XCO_2 modelling shows that both scenarios are possible for the formation of the skarn series, but as the Rb-Sr muscovite-based age of skarn samples is 340 Ma, the first scenario is the relevant one. The skarn mineral assemblages formed during regional metamorphism, whereas cassiterite mineralization is related to younger granite emplacement and is associated with chloritization of biotite and precipitation of fluorite. These reactions changed the fluid composition and induced cassiterite mineralization.

Keywords

Sn-skarn, Rb-Sr dating, P-T-XCO_2 modelling, Erzgebirge, fluid evolution

Published as

Lefebvre MG, Romer RL, Glodny J, Roscher M (2017) Two stages of skarn formation in the Hämmerlein tin-skarn deposit, western Erzgebirge, Germany. 14th SGA Biennial Meeting 4:1305–1308

3.1. Introduction

The Hämmerlein Sn-skarn deposit is located in the western Erzgebirge and is hosted in gneisses and schists with intercalated marbles. The host rocks dominantly consist of early Paleozoic rocks that have been subducted during the Variscan orogeny and reached peak metamorphic conditions at c. 340 Ma (Rötzler at al., 1998; Kroner and Romer, 2013). The metamorphic nappes have been intruded later by a wide range of geochemically contrasting granites, some of which with important tin mineralization (Förster et al., 1999). The S-type Eibenstock granite, which covers an area of 25 by 22 km, is the most voluminous granite of the Erzgebirge. It has given rise to a series of greisen-type and skarn-type Sn-W mineralizations, including the Hämmerlein Sn-skarn deposit (Schuppan and Hiller, 2012).

In the Hämmerlein deposit, cassiterite is the most valuable ore mineral. On a small scale it is irregularly distributed within the skarns subunits and in the mica schist wall-rocks. On a large scale however, its occurrence is structurally controlled. In the skarns, cassiterite generally is fine-grained and dominantly occurs in amphibole skarn. In contrast, local cassiterite occurrences in the mica schists are typically

coarse-grained. In addition to Sn, the Hämmerlein skarn also contains two types of In mineralization. Indium is markedly enriched in a discontinuous sphalerite layer beneath the magnetite skarn, and In-sphalerite exsolutions occur in chalcopyrite lenses in the magnetite skarn.

There are two Variscan events during which fluids were available to induce skarn formation: (1) regional metamorphism at c. 340 Ma and (2) fluid escape from the Eibenstock granite, which intruded at around 320-325 Ma (Kempe et al., 2004; Romer et al., 2007). As the introduction of Sn is apparently related to the emplacement of the Eibenstock granite, as also indicated by the numerous tin greisen mineralizations related to this granite, there are two scenarios for the skarn formation: (1) the skarns crystallized at 340 Ma when metamorphic fluids produced by dehydration of the shales induced the formation of the zoned skarns. Tin was introduced later by magmatic fluids that reacted with remaining carbonates from the protolith and/or altered the existing mineral assemblage of the skarn. In this case, there were two separate skarn-forming events. (2) No fluids were available to induce skarn formation during regional metamorphism at 340 Ma and the skarn was formed by a magmatic fluid that also introduced the metals into the skarn. In this case, the skarn mineralization would reflect one single event.

We present P-T models based on the chemistry of skarn samples. Rb-Sr mineral data have been used to determine the chronology of skarn formation, and to distinguish between the two mineralizations scenarios.

3.2. Samples

There are four skarn types at Hämmerlein that at the sample location form a profile (Fig. 13) from bottom to the top of the skarn unit: garnet skarn, amphibole skarn, pyroxene skarn and magnetite skarn. The brownish-red garnet skarn is composed of phenocrysts of almandine or grossular in a feldspar-quartz-muscovite matrix. Biotite is largely altered to chlorite. The amphibole skarn is greyish-green and shows a feldspar-quartz matrix with clusters of altered grunerite surrounding calcite. Some foitite (tourmaline) crystals occur disseminated in the matrix. The light brown pyroxene skarn is similar to the amphibole skarn except for the presence of augite lenses (surrounded by quartz) instead of grunerite and the absence of tourmaline. Late veins of calcite crosscut the matrix and the augite lenses. Rare sulfides and oxides, including pyrite, arsenopyrite, and magnetite, occur as disseminated crystals in the various calc-silicate skarns. In the magnetite skarn, magnetite is strongly altered to hematite. In addition, there are irregular patches of pyrite and chalcopyrite with exsolutions of In-sphalerite in the chalcopyrite. Minor arsenopyrite and Bi-Cu minerals occur disseminated in the magnetite matrix.

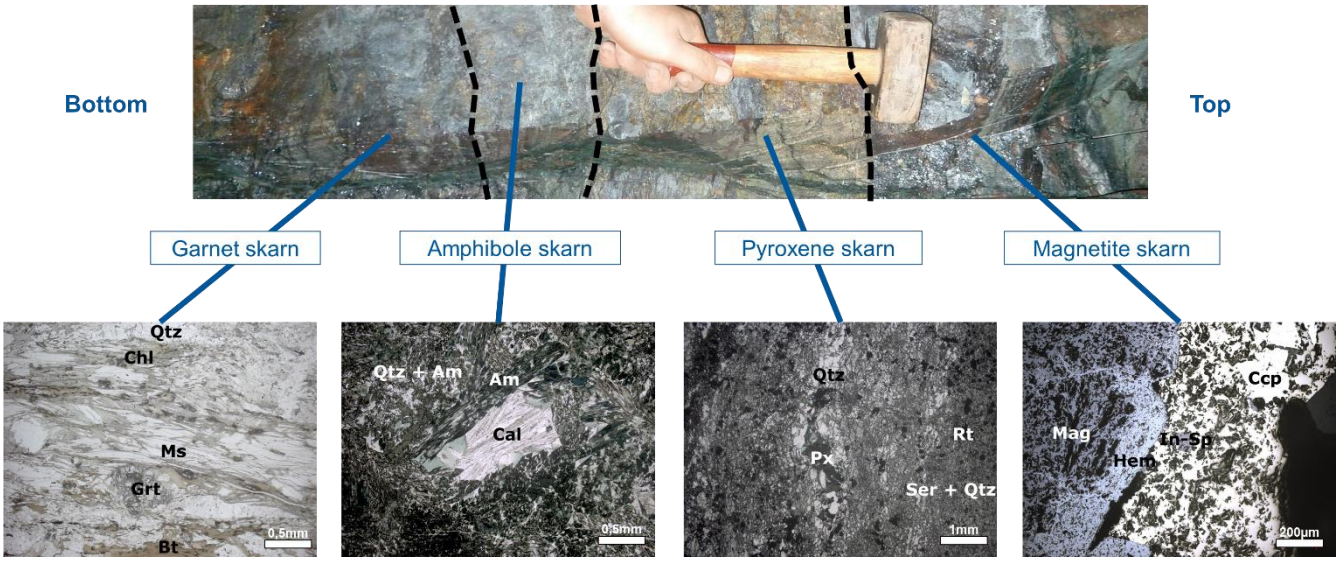

Figure 13: Hämmerlein skarn profile (Am: amphibole, Bt: biotite, Cal: calcite, Ccp: chalcopyrite, Chl: chlorite, Grt: garnet, Hem: hematite, In-Sp: In-sphalerite, Mag: magnetite, Ms: muscovite, Px: pyroxene, Qtz: quartz, Rt: rutile, Ser: sericite)

The distribution of Sn within the different skarn units is heterogeneous. Sn enrichment occurs between grunerite and magnetite-hematite assemblages and within the amphibole skarn. Typically, cassiterite grains are small (~10 µm) and occur disseminated in a quartz-chlorite matrix. Only at the contact between amphibole and magnetite skarns, cassiterite crystals may locally be coarse grained (up to 10 mm).

3.3. Whole rock composition of the various skarn units

Despite their contrasted mineralogy, the major element chemistry of the various skarn systems, obtained by XRF analysis, is quite homogeneous averaging around 35.9% SiO_2, 0.6% TiO, 15.3% Al_2O_3, 18.7% Fe_2O_3, 1.3% MnO, 4.3% MgO, 17.6% CaO, 1.2% Na_2O and 1.6% K_2O. All silicate skarns produced from decarbonation of the protolith have high Mg and Ca contents. Furthermore, the skarns have high Fe and K contents and are enriched, to different extents, in Cu, As, In and Sn. The REE pattern of the skarns is flat and shows a positive Eu anomaly (Fig. 14). Differences among skarns are related to element concentrations, i.e., to variable dilution by phases with low REE contents. The REE patterns of skarns markedly differ from the one of mica schists and gneisses that also have a flat REE pattern but without Eu anomaly. Mineralized and barren rocks show similar REE pattern, indicating the REE were essentially immobile during skarn formation and, thus, were inherited from the protolith.

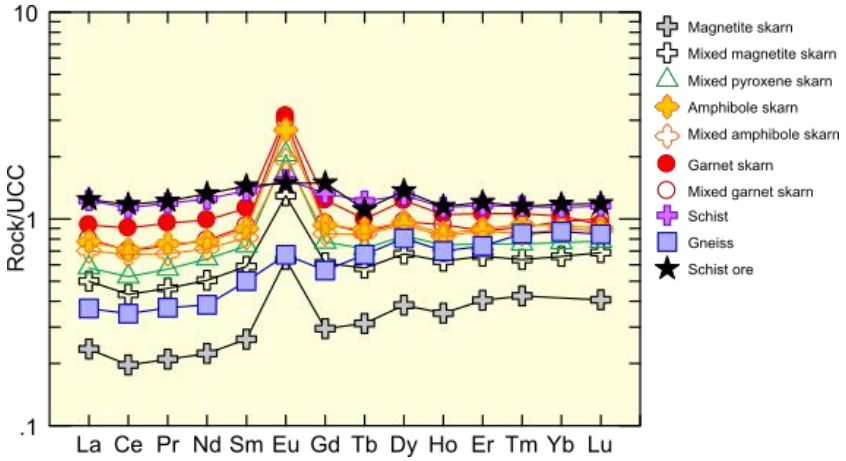

Figure 14: REE patterns of skarns, gneiss and schists from Hämmerlein deposit normalized to Upper Continental Crust (UCC) REE composition from Taylor and McLennan (1985).

Trace element concentrations are highly variable among different skarn types, largely reflecting the ability of the various skarn minerals to incorporate different groups of trace elements.

3.4. P-T-XCO_2 models

The similarity of the whole rock composition of different skarn types implies that the mineralogical variability is controlled by P, T, and the fluid composition, most importantly XCO_2, which is modified by consumption of carbonates and possibly by phase separation. Using the average chemical composition of the skarns (except for the magnetite skarn that had been calculated with the actual composition), we modelled the mineral assemblage of the skarns for 5 kbar (regional metamorphism) and 2 kbar (contact metamorphism) in terms of temperature and XCO_2 (Fig. 15) using the Theriak-Domino thermodynamic modelling software package of de Capitani and Petrakakis (2010).

At 2 kbar, the stability fields of the various skarn mineral assemblages differ in temperature and XCO_2 range. The garnet skarn is stable at high temperature and high XCO_2 (Fig. 15). The other skarn types show stability fields at systematically lower XCO_2 from amphibole and pyroxene to magnetite skarn (Fig. 15). Amphibole and pyroxene skarns are stable at the same temperature as the garnet skarn, but they can also be stable at lower temperature. The magnetite skarn forms at even lower temperature. Note, the temperature of formation is modelled the same for the amphibole and pyroxene skarns because the only difference between their assemblages is the occurrence of amphibole versus pyroxene + calcite veins, which can be explained by contrasting XCO_2. If the skarn formed at 2 kbar, the temperature range would imply that the various types of skarn did not form from the same fluid at the same time and that there must have been heat input with the fluid. Later formed skarns (pyroxene and magnetite skarns) would have formed at lower XCO_2 when much of the wall rock carbonates had been consumed.

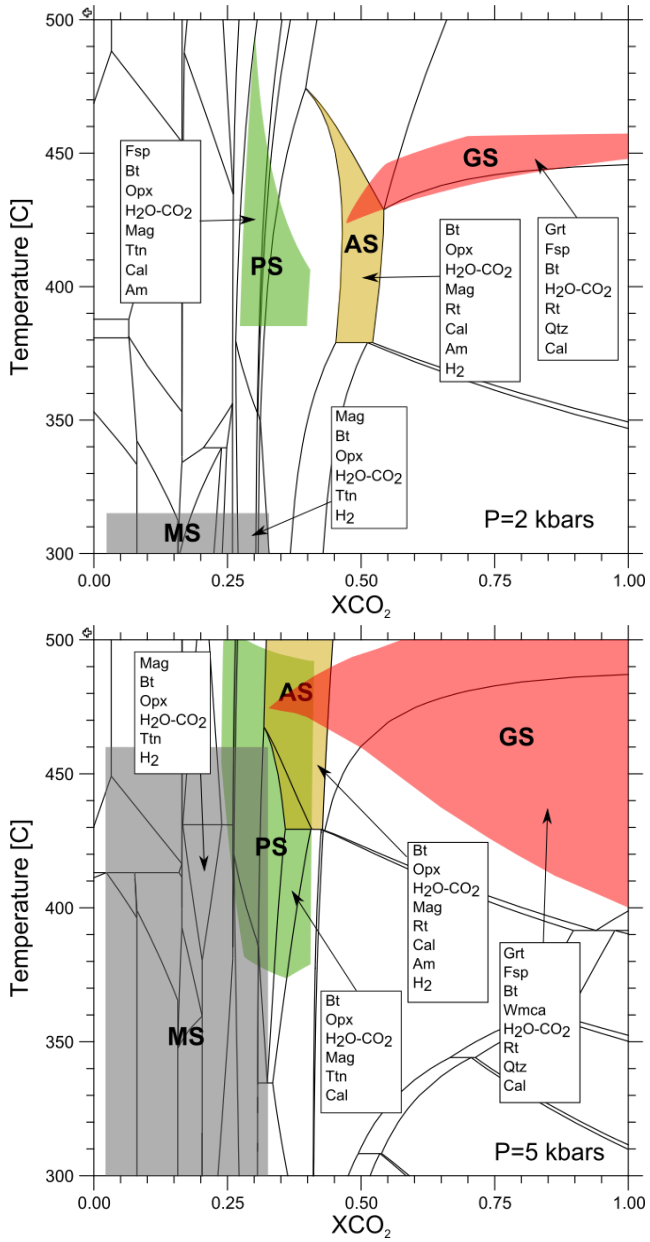

Figure 15: Theriak-Domino modelling of T and XCO_2 evolution of Hämmerlein skarns at 2 kbar (up) and 5 kbar (down) (Am: amphibole, Bt: biotite, Cal: calcite, Fsp: feldspar, Grt: garnet, Mag: magnetite, Opx: orthopyroxene, Qtz: quartz, Rt: rutile, Ttn: titanite, Wmca: white mica).

At 5 kbar, the stability fields of the various skarn types are larger and shifted to higher temperatures. For the temperature range of 400-450°C all skarns types are stable, although at different XCO_2 (Fig. 15). This implies that at higher pressure, the various skarn assemblages may be produced by variation in XCO_2 alone and the skarn mineral assemblage also may have formed during regional metamorphism, when an ambient temperature of c. 450°C at 5 kbar was reached. The fluid source to form the skarns was dehydration of silicate wall-rocks, whereas the variations in XCO_2 reflect decarbonation during skarn formation and metamorphism.

3.5. Rb-Sr ages and mineral data

Rb-Sr multi-mineral data have been determined for a calc-silicate associated to amphibole skarn (CSV1) and an amphibole (HAS3) skarn. Six mineral analyses define an age of 341.2 ± 3.8 (MSWD = 325) for skarn CSV1. Five mineral analyses define an age of 338.0 ± 5.0 Ma (MSWD = 77) for skarn HAS3. This implies that the skarn has formed during regional metamorphism rather than during granite emplacement. Reduced isochron diagrams (Fig. 16) show significant isotopic heterogeneity in the samples, which is also reflected in the high MSWD values. The isotopic heterogeneity is most obvious for albite and fluorite of sample CSV1 and for blue fluorite of sample HAS3 that have highly radiogenic initial $^{87}Sr/^{86}Sr$ values (Fig. 16). Textural evidence shows that fluorite along with chlorite formed later than white mica. The Sr isotopes support this observation as they imply that fluorite and, to some degree, also albite obtained their Sr from a different reservoir than white mica. To develop a Sr isotopic composition as radiogenic as observed in fluorite, the Sr source needs a very high $^{87}Rb/^{86}Sr$ ratio for quite some time. It should be noted that the white mica did not record the younger

crystallization event giving rise to fluorite, albite, and chlorite. Instead, white mica dates the regional metamorphism at 340 Ma.

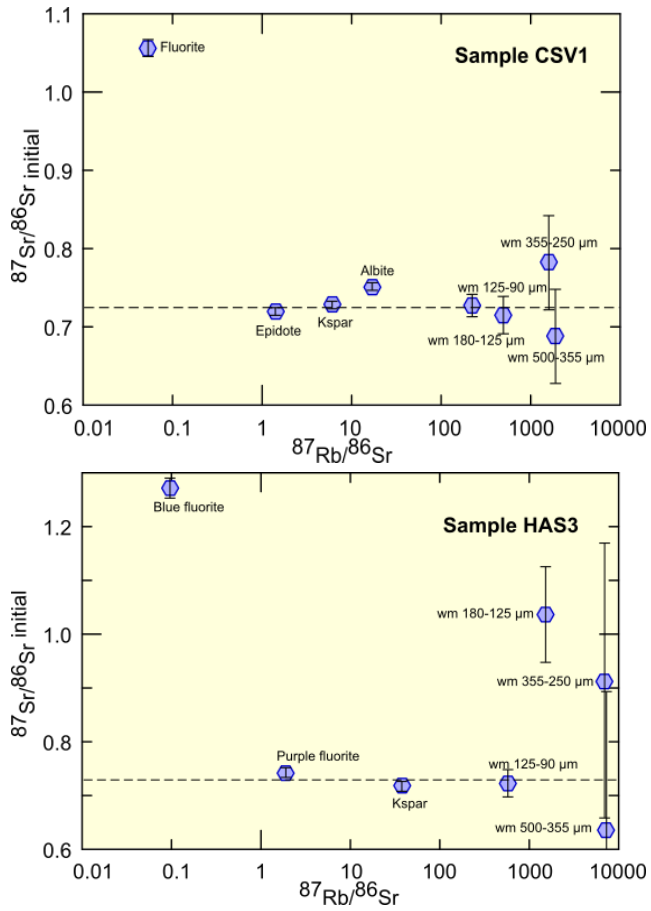

Figure 16: Rb-Sr reduced isochron diagrams of the samples CSV1 (up) and HAS3 (down).

3.6. Discussion

The muscovite-based Rb-Sr ages of the skarn samples demonstrate that the skarn formed at around 340 Ma. This age is identical to the age of regional metamorphism of the host-rocks of the skarns. Thus, the skarn formation is likely to have been induced by fluids derived from the metamorphism of the silicate wall rocks. Textural evidence shows that one generation of fluorite is related to a later event, during which albite and chlorite crystallized. Chlorite formed at the expense of biotite, which is present only as rare relics. Chlorite also forms pseudomorphs after amphibole. Cassiterite in the skarns always occurs together with chlorite. Therefore, cassiterite crystallization may be related to chloritization of biotite and alteration of amphibole. The fluid that induced chloritization may have transported Sn along with F. The destruction of biotite released the radiogenic Sr incorporated in fluorite and albite. The dissolution of biotite and/or the precipitation of fluorite may have changed the ability of the fluid to complex and transport Sn, thus, eventually leading to the precipitation of cassiterite. The martitization of magnetite can also be in part responsible for the precipitation of cassiterite.

The source of the fluid inducing the precipitation of fluorite and cassiterite and the chloritization of biotite in the skarn is not related to the regional metamorphism at 340 Ma, but is likely related to the intrusion of the Eibenstock granite because of the following reasons: (i) cassiterite, chlorite, and fluorite are texturally related and (ii) the Sr isotopic data show that one generation of fluorite was formed later than 340 Ma as it is out of equilibrium with the skarn assemblages.

Thus, Sn mineralization in the Hämmerlein skarn is the result of two separate events, i.e. (i) the formation of a zoned skarn during regional metamorphism at 340 Ma and, (ii) the local retrogression of the original skarn assemblage by granite-derived fluids that introduced Sn, In, and F and that led to chloritization and deposition of cassiterite and fluorite. The dated muscovite formed during regional

metamorphism and did not record the partial retrogression by this late fluid. Our study demonstrates that dating of skarn minerals in poly-stage skarns not necessarily provides the age of skarn mineralization.

4. Chapter 4: Skarn formation and tin enrichment during regional metamorphism: the Hämmerlein polymetallic skarn deposit

Abstract

The Hämmerlein Sn-rich polymetallic skarn deposit (Erzgebirge, Germany), which is hosted by Variscan schists and gneisses, includes garnet, amphibole, pyroxene, and magnetite skarns that formed during regional metamorphism at ~340 Ma. The skarn deposit was overprinted during the intrusion of the ca. 320 Ma Eibenstock granite. Tin was introduced into the system during regional metamorphism at 340 Ma (Sn mostly hosted in silicate minerals) and after the intrusion of the Eibenstock granite at c. 320 Ma (Sn hosted in cassiterite). The emplacement of late stage magmatic pulses of the Eibenstock granite also resulted in the formation of cassiterite-quartz veins in the schists hosting the Hämmerlein skarns and at some distance in the formation of several cassiterite greisen.

Major, trace, and rare earth element data of the skarn units and their hosts rocks demonstrate that skarns formed from impure carbonates with variable proportions of silicate minerals. Depending on the original modal compositions of the skarns and their host rocks, the mineralizing fluid selectively added and removed elements, which resulted for the skarns and the schist ore in a general enrichment in Sn, In, Cu, and W and a noticeable depletion in Al and Sr. The Sr, Nd, and Pb isotopic composition of the skarns, schists, and gneisses resembles those of the metamorphic rocks of the Erzgebirge rather than those of the granites, possibly indicating that the geochemical signature of granite-derived fluids had been severely altered during fluid-rock interaction before these fluids reached the skarns, schists, and gneisses. Similarly, the Li and B isotopic composition of the skarn samples reflects the likely range of possible source rocks for metamorphic fluids, rather than the composition of the granite-derived fluid. In contrast, the Li and B signature of greisen samples shows a variable mixture of material derived from the granite and the metasedimentary rocks, respectively.

Our data show that a first Sn enrichment took place when the Paleozoic sedimentary rocks were affected by regional metamorphism at ca. 340 Ma. Fluids derived from these siliciclastic sedimentary protoliths mobilized and transported Sn and possibly W and Fe. These fluids reacted with the impure carbonates, resulting in decarbonation and the formation of calc-silicate minerals and biotite in the various skarn types. The changing fluid composition as well as the incorporation of Fe in skarn silicates and formation of Fe-oxides resulted in the incorporation of Sn into silicate minerals. During or after the emplacement of the Eibenstock granite, the original skarn was to a variable extent retrogressed and Sn was released from Sn-bearing calc-silicates and biotite. During this event additional Sn was added to the skarn and the hosting schists. Released Sn and newly added Sn precipitated as cassiterite.

Keywords

Hämmerlein, Erzgebirge, Tin, Skarn, Greisen, Lithium, Boron

Published as

Lefebvre MG, Romer RL, Glodny J, Roscher M (submitted) Skarn formation and tin enrichment during regional metamorphism: the Hämmerlein polymetallic skarn deposit.

4.1. Introduction

Skarn deposits occur on every continent in rocks dated from Precambrian to the Pliocene. Typically, the formation of skarn is induced by aqueous fluids emanating from a granitic intrusion that is emplaced in carbonates and carbonate-rich siliciclastic sedimentary rocks that experience contact metamorphism. Inflow of aqueous fluids results in the wall rocks of the intrusion in the formation of Ca- and Mg-silicates at the expense of precursor carbonates and the development of a zoned metamorphic aureole with garnet in the proximal and pyroxene in the distal zone. Furthermore, aqueous magmatic fluids induce pervasive alteration of this aureole and may introduce significant amounts of Si, Al, and Fe into the contact metamorphic aureole. Decarbonation releases CO_2 that eventually (depending on pressure) results in the unmixing of fluids into a saline H_2O-rich fluid and a low-salinity H_2O-CO_2 fluid. This phase separation may induce precipitation of ore elements contained in the magmatic fluids, as would cooling of the fluid and mixing with meteoric fluids. Cooling of the magmatic fluids and inflow of meteoric water into the system eventually result in the retrogression of the high-temperature skarn. For instance, garnet may be replaced and/or altered to epidote, biotite, chlorite, calcite, plagioclase, and quartz. Pyroxene may be replaced by tremolite and talc. Ore minerals may occur as disseminated crystals and veins that cut across the prograde assemblages and may show evidence for multiple metal redistribution (Lentz, 1998; Meinert et al., 2005; Robb, 2005).

The Hämmerlein polymetallic skarn deposit in the western Erzgebirge does not fit well into this general model, most importantly as the skarn and associated mineralization seem to be the results of several processes. The various skarn mineral assemblages formed during Variscan metamorphism at c. 340 Ma (Lefebvre et al., 2019), i.e., about 15 to 20 Ma before the emplacement of the Eibenstock and spatially related granites (Fig. 17). Silicate minerals that formed during this first event show enhanced Sn contents (up to 0.9 wt% SnO_2 in garnet, Lefebvre et al., 2019). Thus, Sn was mobile during regional metamorphism and became concentrated in the skarn. Most Sn available at that time seems to have been incorporated into calc-silicate minerals. The second event affecting the Hämmerlein skarn is related to the emplacement of the post-kinematic granites that resulted in significant chloritization of biotite and other silicates in the skarn. Tin released from tin-bearing silicates during chloritization precipitated as cassiterite (SnO_2) along with minor fluorite and apatite. The evidence that chloritization is related to a second event comes from the anomalous radiogenic initial Sr isotopic composition of apatite and fluorite ($^{87}Sr/^{86}Sr_i > 1.0$; Lefebvre et al., 2019). Strontium with such radiogenic compositions requires a high-Rb/Sr environment and time and may be released from aged biotite during chloritization (Lefebvre et al., 2019). There are several greisen mineralization related to the emplacement of the Eibenstock granite.

Thus, it is quite possible that the emplacement of the Eibenstock granite also introduced significant amounts of Sn and other elements into the Hämmerlein skarn mineralization.

In this paper, we characterize the chemical changes that were brought about by (i) metamorphic fluids that induced the formation of the skarns and (ii) magmatic fluids that eventually resulted in the retrogression of the original skarn assemblage. Apart from the enhanced contents of the ore elements Sn, W, Zn, and In, the skarns also show enhanced contents in F, Mn, Li, F, and B. We use the chemical and Li, B, Sr, Nd, and Pb isotopic composition of unmineralized shales and carbonates as a proxy for the protolith composition of the mineralized skarns and mica-schists, respectively, and the Li and B isotopic composition of the greisen as a proxy for the composition of late-magmatic fluids. We demonstrate that both the skarn and its host rocks by and large kept the elemental signature of their protolith. The isotopic signature of skarns, schists, and gneisses differs distinctly from the one of the granites, but resembles the one of the metamorphic rocks of the area.

4.2. Geological setting

4.2.1. Regional pre-Varsican and Variscan development of peri-Gondwana

The Variscan orogenic belt formed during the closure of the Rheic Ocean between Gondwana and Laurussia (Franke, 1989; Matte, 1986). The orogeny started at c. 400 Ma with the collision of the leading parts of the Armorican Spur, i.e., Armorica and the Teplá-Barrandian Unit, with Laurussia and culminated at c. 340 Ma, when crustal rocks that had reached UHP and UHT metamorphic conditions during intra-continental subduction began to exhume rapidly. Variscan intra-continental subduction took place in zones where continental crust had been thinned during the opening of the Rheic Ocean. Slices of subducted material, representing former peri-Gondwana crust, were emplaced after peak metamorphism, into the middle and upper crust, forming high-strain belts (Kroner and Romer, 2013). The Erzgebirge is part of the Allochthonous Domain of the Saxo-Thuringian Zone (Kroner et al., 2007) and represents a stack of nappes with medium to ultra-high pressure metamorphic rocks that have been rapidly exhumed after reaching Variscan peak metamorphic conditions at 340 Ma (Rötzler and Plessen, 2010). Along crustal scale shear zones between the Autochthonous and Allochthonous domains of the Saxo-Thuringian Zone, granitic intrusions (e.g., Berbersdorf [von Quadt, 1993], Meissen ([Wenzel and von Quadt, 1993]) were emplaced at the same time as the metamorphic nappes (Förster and Romer, 2010; Wenzel et al., 1997). After the metamorphic nappes were emplaced in the Erzgebirge, they became intruded by a wide range of geochemically contrasting post-kinematic granites, some of them with important Sn mineralization (Förster et al., 1999).

The former Gondwana margin was composed of a Cadomian basement and its sedimentary cover. The Cadomian basement represents the remnant of a magmatic arc that locally shows abundant and voluminous Cambrian granodiorite intrusions (Linnemann et al., 2004). During the late Cambrian to early Ordovician opening of the Rheic Ocean, peri-Gondwana became stretched and (thick) crustal

blocks that are characterized by voluminous Cambrian granodiorites became surrounded by zones of thinned continental crust. Examples of such blocks include the Teplá-Barrandian Unit, Lusatia, Armorica, and the Central Iberian Zone (Kroner and Romer, 2013). These blocks did not experience significant reworking during the Variscan orogeny. The zones of thinned continental crust developed into sedimentary basins with voluminous late Cambrian to early Ordovician sedimentary rocks that largely represent redeposited Cambrian sedimentary material that originally had been deposited on uplifted peri-Gondwana. Intercalated within the sedimentary rocks are volcanic rocks and locally early Ordovician magmatic complexes (Tichomirowa and Leonhardt, 2010). The Cadomian basement, its volcanosedimentary cover, and the Ordovician magmatic complexes had different rheological behavior during the Variscan orogeny:

(1) The Cadomian basement and the Ordovician volcanic complexes were subducted to medium-pressure conditions and form now gneiss domes in the Erzgebirge. In the eastern Erzgebirge, the Freiberger Gneiss Dome (Tichomirowa et al., 2012) with its granodioritic orthogneisses of the former Cadomian basement represents the tectonostratigraphically lowermost unit (Mingram, 1998). In the central Erzgebirge, the medium pressure units of the Reitzenhain Gneiss Dome (Tichomirowa et al., 2012) are sandwiched between volcanosedimentary nappes that reached higher grade metamorphism during the Variscan orogeny. The protoliths of the gneisses in the Reitzenhain Gneiss Dome are former Ordovician volcanic complexes (c. 490 Ma; Tichomirova and Leonhardt, 2010).

(2) The volcanosedimentary cover rocks are dominated by greywackes, pelites, conglomerates, rhyolites, metabasites, and marbles. During the Variscan orogeny, these rocks locally reached high and ultra-high pressure metamorphic conditions (Rötzler and Plessen, 2010). The metamorphic nappes of the Erzgebirge are dominated by lithologies that have the same chemical signatures as the pre-Silurian sedimentary rocks of the Schwarzburg area (Mingram, 1996; 1998). The corresponding chemical composition of metamorphic rocks of the Erzgebirge and sedimentary rocks of the Schwarzburg area originally was used to infer (i) that the metamorphic rocks of the Erzgebirge represent former peri-Gondwana shelf and (ii) that the same type of shelf sediments experienced a wide range of different Variscan metamorphic histories (Rötzler and Plessen, 2010). The Schwarzburg area is dominated by early Ordovician sedimentary rocks (Mingram, 1998), which are characterized by a distinct depletion in Ca, Na, and Sr relative to Al and K, which is typical for siliciclastic rocks that experience intense chemical alteration during weathering (decomposition of feldspar; Mingram, 1998). In the metamorphic nappes of the Erzgebirge, the same chemical signature (Ca, Na, and Sr depletion) is found in most metasedimentary rocks of the metamorphic nappes.

4.2.2. Post-kinematic granites

Post-kinematic granites in the Erzgebirge region mostly fall in two age groups: (i) 325-318 Ma old granites (e.g., Eibenstock, Kirchberg) that represent crustal melts and inherited their geochemical

variability from the lithologically and geochemically heterogeneous Variscan metamorphic nappes (Förster et al., 1999; Förster and Romer, 2010) and (ii) 305-280 Ma old intrusions and volcanic complexes (e.g., Gottesberg, Halle Volcanic Complex) with variable input of mantle-derived material. This younger magmatism is bound to extensional structures of the Central Europe Extensional Province that formed with the reorganization of the regional stress field after the Variscan orogeny (Kroner and Romer, 2013; Kroner et al., 2016). According to Förster et al. (1999), most Sn and W mineralization is related to 325-318 Ma old granites, that formed by melting of Sn and W-rich micaceous metapelites mixed with quartzo-feldspathic rocks (Breiter, 2012).

The 325 to 318 Ma old post-kinematic granites of the Erzgebirge are distinguished into three chemically distinct groups: (i) low-F granites (e.g., Kirchberg granite), (ii) low-F two-mica granites (e.g., Fichtelgebirge granite), and (iii) high-F, high-P2O5 Li-mica granites (e.g., Eibenstock granite) (Förster et al., 1999; Förster and Romer, 2010). The Eibenstock-Nejdek plutonic complex (Breiter, 1993) is the largest exposed granitic body (35 by 32 km large) of the Erzgebirge (Fig. 17). It intruded medium and low grade metamorphic units (paragneisses and schists) of the Erzgebirge (Förster et al., 1999). The Eibenstock granite forms the northern part of the plutonic complex and is a typical representative of the high-F, high-P2O5 Li-mica granites. It is coarse-grained and shows mainly an equigranular texture with local quartz and K-feldspar phenocrysts. There are no distinct chemical differences between the equigranular and phenocrystic granite types (Förster et al., 1999). There is Sn and W mineralization in association with the granite (Förster et al., 1999).

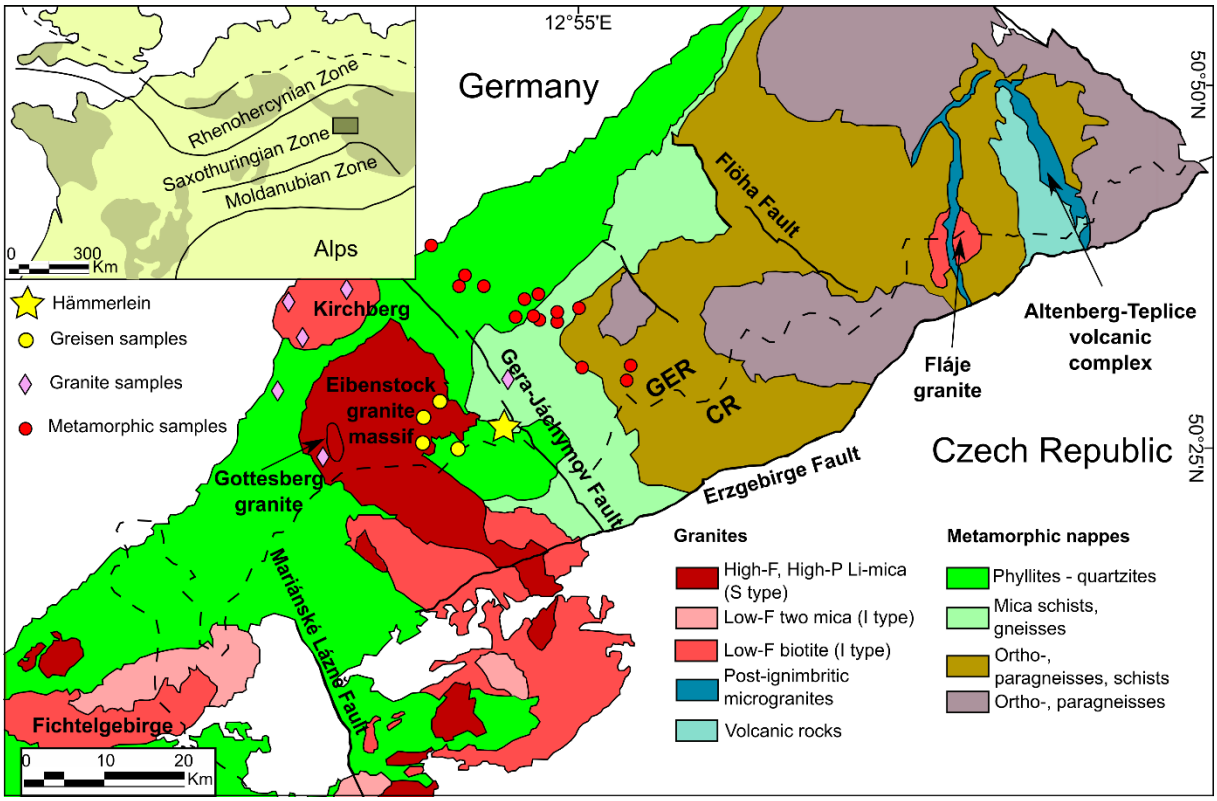

Figure 17: Simplified geological map of the Erzgebirge-Vogtland-Fichtelgebirge area showing the location of the Hämmerlein polymetallic skarn deposit and the location of greisen samples associated with the Eibenstock granite. Locations of granite (pink diamonds, Romer et al. 2014b) and metamorphic rocks (red dots, Romer and Meixner, 2014) used for geochemical comparison are also plotted on the map.

The Eibenstock granite is a Si-rich, peraluminous, reduced granite derived from crustal protoliths (initial $^{87}Sr/^{86}Sr$ ranges from 0.711 to 0.713, Velichkin et al., 1994). Breiter et al. (1999) suggested that the Paleozoic metamorphic units (mica schists and gneisses) were involved in the formation of the granite. There are several stages of intrusions that have ages between ~320 Ma (Förster et al., 1999; Kempe et al., 2004) for the main phase and ~310 Ma (Tichomirowa et al., 2016) for late stage intrusions.

4.2.3. The Hämmerlein polymetallic skarn

The Hämmerlein polymetallic skarn deposit in the western Erzgebirge was discovered and prospected during the second half of the 20th century mainly for Sn, but also for Zn and In. The current resources of the Hämmerlein deposit have been estimated at 101 500 t Sn with a cut-off grade of 0.2 wt% Sn. Zinc and In contents are estimated at 200 200 t and 2 149 t respectively (Anglo Saxony Mining, 2015). The Hämmerlein polymetallic skarn is hosted in Variscan schists and gneisses that reached peak metamorphic conditions at 340 Ma (Rötzler et al., 1998; Willner et al., 1997). The protoliths of the schists and gneisses are Cambro-Ordovician sedimentary rocks of the peri-Gondwana shelf with intercalated carbonates, marls, and felsic and mafic volcanic rocks (Shapenko and Šmidel, 1991). Variscan metamorphism transformed these protoliths into skarns, gneisses, amphibolites, and graphite-rich schists (Schuppan and Hiller, 2012). The age of the skarn is c. 340 Ma (Lefebvre et al., 2019), i.e.,

the skarn formed during regional metamorphism of the host rocks. To the west of the Hämmerlein skarn deposit, the nappe pile was intruded by the about 320 Ma old Eibenstock granite.

There are three types of mineralization in the Hämmerlein deposit: (i) strata-bound Sn and sulfide mineralization (mainly sphalerite) within the skarn and cassiterite within quartz-feldspar veinlets in mica schists, (ii) magnetite mineralization within the skarn, and (iii) post-Variscan uranium-bearing veins (Schuppan and Hiller, 2012). Tin mineralization occurs in the skarn (Schuppan and Hiller, 2012) and to a lesser extent in mica schists that may contain Sn-rich biotite with up to 0.1% Sn (Malyshev et al., 1997; Malyshev and Korzhanovskaya, 1989). Tin mineralization in the various skarns typically is closely associated with secondary minerals such as fluorite, apatite, and chlorite. Cassiterite (10 µm – 1 cm) occurs in the skarn occurs mainly together with these secondary minerals. In the mica schists, cassiterite is also relatively coarse (0.1-1 mm) and in places occurs as palisade-cassiterite in thin quartz-feldspar veinlets in a 5-10° angle to the schistosity.

There are four types of skarn: garnet skarn, amphibole skarn, pyroxene skarn, and magnetite skarn. The succession of the various skarn types within the deposit differs locally. The various types of calc-silicate skarn are microcrystalline and show similar mineralogy. They are mainly composed of calc-silicate minerals (garnet, amphibole, or pyroxene) and quartz. Chlorite forms as a secondary phase from the alteration of amphibole and biotite. Apatite is systematically associated with this secondary chlorite. Cassiterite mainly occurs in the amphibole skarn as coarse aggregates (up to 10 mm) at the contact between amphibole and magnetite skarn, and as fine (~10 µm) disseminated crystals in the amphibole-quartz assemblage. The fourth type of skarn is mainly composed of massive magnetite with up to 5 cm large patches of chalcopyrite with In-rich sphalerite.

The age of cassiterite is not known. There are two lines of evidence, however, that indicate there are two events of Sn mobilization, i.e., one at c. 340 Ma and one at c. 320 Ma (Lefebvre et al., 2019). Primary calc-silicate minerals such as garnet, amphibole, and pyroxene have high concentrations of Sn (up to 0.9% SnO_2; Lefebvre et al., 2019). These minerals are part of the prograde c. 340 Ma skarn assemblage (Rb-Sr multi-mineral isochron, Lefebvre et al., 2019). Thus, Sn had been available in elevated amounts during regional metamorphism. As there is no evidence for granitic magmatism of this age in the Erzgebirge, this implies that Sn was mobilized and transported by metamorphic fluids during prograde metamorphism. The secondary minerals apatite and fluorite have anomalous radiogenic Sr isotopic compositions that demonstrate that these secondary minerals are not related to post-peak retrogression of the 340 Ma mineral assemblage, but are related to a second event that is 20 or more million years younger. The retrogression released Sn found together with the secondary minerals chlorite, apatite, and fluorite (Lefebvre et al., 2019). It is quite possible that the emplacement of the Eibenstock granite caused the retrogression and brought along additional Sn. The potential of the Eibenstock granite to supply Sn to the Hämmerlein skarn is shown by the various greisen Sn mineralization directly related to this granite (Fig. 17).

Zinc mineralization is related to the skarn, but uncorrelated to the younger Sn mineralization. The Zn mineralization occurs in 5-10 cm thick subhorizontal massive sphalerite veins in garnet and magnetite skarn units. Moreover, small lenses of Fe-rich sphalerite-chalcopyrite-pyrite assemblages form veinlets that crosscut both the skarn and the massive sphalerite veins (Bauer et al., 2017). Indium is strongly enriched in two different types of rock, i.e., in the Fe-rich sphalerite-chalcopyrite-pyrite veinlets and in the magnetite skarn. Sulfide blebs of several centimeter diameter in the magnetite skarn consist of pyrite, chalcopyrite, and Fe-rich sphalerite, which may be associated with roquesite. Up to 5 wt% In occur in Fe-rich sphalerite. In contrast, extreme In enrichment (up to ~20 wt%) occurs in sphalerite grains of the veinlets. These differences in In concentration have been explained by two stages of In enrichment (Bauer et al., 2017): (i) Indium concentration up to 5 wt% is interpreted to be related to the formation of the Fe-rich sphalerite-chalcopyrite-pyrite assemblage. (ii) The extreme In enrichment is related to the decomposition of In-bearing chalcopyrite during a secondary hydrothermal overprint.

The Hämmerlein deposit is located to the west of the Gera-Jàchymov zone, which is a major NW-SE striking fault that has been recurrently reactivated. Along the fault, there occurs major hydrothermal U mineralization. The oldest mineralization is c. 280 Ma (Förster, 1996). During later mineralization U was redistributed and Bi, Co, Ni, As, and Ag were introduced into the various mineralization (Ondruš et al., 2003). There are locally U anomalous fractures in the skarn, but workable U veins do not occur within the Hämmerlein skarn, but further to the SE (Schuppan and Hiller, 2012).

4.2.4. Greisen mineralization related to the Eibenstock granite

Sn-greisen mineralization is located close to or within the Eibenstock granite. Greisen mineralization is mainly concentrated along the granite margin, but also along SE-striking zones within the granite. Tin mineralization is rare outside the granite. The age of most greisen is ~320 Ma (Lefebvre et al., 2019), which implies that the greisen formed at the same time as the Eibenstock granite intrusion. Greisens are mainly composed of quartz and fine-grained muscovite. Some large crystals of polylithionite, strongly altered feldspar, and chloritized biotite may be remains from the granite protolith. Cassiterite forms up to ~250 µm large crystals together with fine-grained muscovite. In greisen alteration outside the granite, phyllite is metasomatized and the cassiterite-muscovite assemblage occurs with tourmaline and locally up to 200 µm large apatite. Mineralized veins also occur in association with the greisen and show coarse-grained cassiterite together with arsenopyrite, löllingite, sericite, topaz, wolframite, and minor fluorite and pyrite (Rojík 2005).

4.3. Material and methods

Whole rock chemical data have been obtained for 224 samples (ALS minerals, Rosia Montana, Romania). Major elements concentrations have been determined following the geochemical procedure ME-ICP61a (ALS minerals, 2009a) using Inductively Coupled Plasma – Atomic Emission Spectroscopy

(ICP-AES). Trace and rare earth elements concentrations have been measured following the procedure ME-MS81 (ALS minerals, 2009b) using inductively coupled plasma – mass spectroscopy (ICP-MS).

For a set of 13 whole rock samples that also was used for isotope analysis, major, trace, and rare earth elements were determined at Deutsches GeoForschungsZentrum (Potsdam, Germany). For X-ray Fluorescence Spectroscopy (XRF) using a PANalytical AXIOS Advanced instrument, samples were powdered (grain size <62 μm), melted, quenched into glass disks, and analyzed with an end-window Rh X-ray tube SST-mAX with 4kW output. Trace elements were determined using an Element 2XR High-Resolution Inductively Coupled Plasma – Mass Spectrometer (HR-ICP-MS) after the preparation procedure described by Dyar et al. (2001). The REE content of these whole rock samples was determined using the dissolution and separation procedure described by Zuleger and Erzinger (1988) and using Inductively Coupled Plasma – Optical Emission Spectroscopy (ICP-OES). For In-rich samples, trace element contents were also determined by LA-ICP-MS at Friedrich-Alexander University (Erlangen-Nürnberg, Germany), using fused discs and the protocol described in Doroshkevich et al. (2017).

Strontium and Nd isotope analyses were carried out on 13 whole rock samples at Deutsches GeoForschungsZentrum (Potsdam, Germany). Sr was separated using cation exchange resin (Bio Rad AG50 W-X8, 100-200 mesh, 3.8 ml resin volume) in 2.5N HCl medium. After Sr was collected and Ba was washed out using 2.5N HNO_3, REE were eluted from the cation exchange column using 6N HCl. Nd was purified using cation exchange (HDEHP-coated Teflon, 2 ml resin volume) in 0.18N HCl medium. For isotope analysis, Sr and Nd were loaded on single Ta-Filaments and double Re-filaments, respectively, and their isotopic composition was determined on a TRITON multicollector thermal ionization mass spectrometer (TIMS) using dynamic multi-collection. Strontium reference material NBS 987 and Nd reference material La Jolla gave $^{87}Sr/^{86}Sr = 0.710258 \pm 8$ (2σ, n=11) and $^{143}Nd/^{144}Nd = 0.511858 \pm 8$ (2σ, n=10), respectively.

The Pb isotopic composition was determined on concentrates of apatite, amphibole, feldspar, garnet, and sulfides. Lead was separated using HCl-HBr ion-exchange procedure (Bio Rad AG1-X8, 100-200 mesh, 0.5 ml resin volume) described by Romer and Hahne (2010). Pb was loaded together with silica gel and H_3PO_4 on single Re-filaments and analyzed at 1200-1260°C using a Triton TIMS operated in static multi-collection mode. The isotopic ratios were corrected for mass bias by 0.1 %/a.m.u. as determined by the repeated analysis of Pb reference material NBS 981.

The B and Li isotopic composition was determined for 13 whole rock samples and 16 mineral concentrates (white mica, feldspar, and tourmaline). For B isotope analysis, the samples were decomposed by alkaline fusion at 950°C using K_2CO_3 as flux and purified using a two-step ion exchange procedure modified after Tonarini et al. (1997) and Kasemann et al. (2001). Each sample series included one or two reference samples and a blank. For Li isotope analyses, samples were digested in HF. Lithium was separated using 1N HNO_3 in 80% methanol as carrier medium and Bio Rad AG 50 W-X8 (200-400

mesh), following a procedure slightly modified after Tomascak et al. (1999). A second separation step using HCl in methanol was used to remove Na (Jeffcoate et al., 2004). The contents and isotopic compositions of Li and B were determined using a MC-ICP-MS Neptune (ThermoFisher Scientific, TFS). For isotope analysis, the Li and B contents of the analyzed solutions were adjusted to 25 ppb and isotope ratios were determined using the standard-sample-standard bracketing method. For each sample, at least six values in total were determined in two or more separate analytical sessions. For instrument settings see Romer and Meixner (2014). The obtained δ^{7}Li and δ^{11}B values are reported relative to reference materials NIST 8545 and NBS 951, respectively.

4.4. Results

4.4.1. Whole rocks chemistry

During the regional metamorphism at 340 Ma, the siliceous protoliths of Hämmerlein rocks, including mainly shales and sandstones with local felsic and mafic volcanic rocks, were metamorphosed to mica schists, gneisses, and amphibolites, respectively. In the studied part of the mineralization there are no amphibolites. Carbonates and impure carbonates (e.g. marls) were altered to skarns. To highlight the chemical changes related to the formation of Sn mineralization in the schists and skarns, we normalize all data in major, trace, and rare earth elements diagrams to Upper Continental Crust (UCC; Taylor and McLennan, 1995). For such a normalization, silicate rocks that have not been altered by metamorphic or hydrothermal fluids should yield flat pattern. Deviations from the flat pattern reflect addition or loss of those elements that show peaks or valleys, respectively. As skarns formed variably impure carbonate protoliths, we normalize their composition also to UCC. UCC-normalized average carbonate (Bolhar and van Kronendonk 2007; Huang et al., 2011) is shown for comparison in all relevant diagrams (Figs. 18, 19 and 20).

Table 7: Representative major, trace, and rare earth elements data of whole rock samples of skarns and silicate wall rocks from Hämmerlein (the other analysis are shown in the Electronic supplementary material 4)

Sample (wt%)	Garnet skarn	Amphibole skarn	Pyroxene skarn	Magnetite skarn	Gneiss	Schist	Schist ore
SiO_2	58.4	54.2	47.6	37.9	74.4	74.0	81.5
Al_2O_3	10.7	12.3	8.01	4.35	9.31	8.84	5.78
Fe_2O_3	13.6	15.7	23.9	52.0	5.85	6.13	4.63
MnO	0.38	0.58	0.64	0.40	0.17	0.08	0.02
MgO	3.28	2.70	3.23	2.64	1.14	2.02	1.39
CaO	8.91	10.4	14.9	1.79	2.83	1.96	0.34
Na_2O	2.22	1.86	0.66	0.15	3.65	2.48	1.37
K_2O	1.81	1.57	0.72	0.60	2.17	3.73	4.22
TiO_2	0.50	0.52	0.15	0.10	0.30	0.60	0.60
P_2O_5	0.16	0.12	0.20	0.09	0.22	0.15	0.15
Total (ppm)	100	99.9	100	100	100	100	100
V	69	96	25	20	41	113	111
Cr	70	70	40	20	50	100	90
Cu	20	160	40	240	30	40	310
Zn	390	890	1860	660	490	230	60
Ga	25	26	20	18	20	31	30
As	720	410	890	490	340	160	370
Rb	241	295	60	54	249	322	276
Sr	210	168	47	18	130	212	57
Y	20	24	17	12	20	27	27
Zr	137	133	60	53	106	136	187
Nb	9.8	12	7.4	3.1	12	14	11
Cd	55	40	10	205	25	20	20
In	11	38	50	49	15	0.65	3.4
Sn	1350	2060	4180	4380	1160	118	5700
Cs	24	44	8.2	51	28	104	90
Ba	253	264	124	40	342	639	647
Hf	4.1	3.8	1.8	1.6	3.4	3.8	5.9
Ta	0.90	1.1	1.5	0.70	1.8	1.0	0.9
W	11	16	16	10	8.0	3.0	12
Th	8.5	12	5.2	2.2	8.7	12	12
U	3.0	3.1	7.2	2.4	12	2.6	3.2
La	29	42	8.2	5.7	18	45	39
Ce	57	79	16	11	39	85	79
Pr	6.9	9.2	2.1	1.3	4.7	10	9.5
Nd	25	37	9.4	6.1	17	39	38
Sm	4.9	6.4	2.2	1.4	3.5	6.8	7.5
Eu	1.6	1.9	1.1	0.84	0.63	1.4	1.4
Gd	4.1	5.0	2.3	1.8	3.2	5.5	6.2
Tb	0.65	0.78	0.41	0.34	0.61	0.82	0.76
Dy	3.8	4.3	2.8	2.0	3.5	4.6	5.3
Ho	0.72	0.90	0.60	0.37	0.72	0.92	0.95
Er	2.0	2.7	1.6	1.3	2.2	2.5	3.0
Tm	0.34	0.32	0.27	0.12	0.34	0.37	0.44
Yb	2.0	2.3	1.9	1.3	2.3	2.6	2.9
Lu	0.29	0.41	0.28	0.19	0.32	0.38	0.41

There are two types of samples: (i) averaged exploration samples and (ii) individual samples used for isotope analyses. There are a few marked differences between the pattern of averaged samples (Figs 18a, 19a, and 20a) and those of individual samples (Figs 18b, 19b, and 20b) that mainly originate from different sampling strategies and sampling purposes. The individual samples were taken to get representative compositions of the various skarn types and, therefore, special care was taken to exclude heterogeneous material that represents mixtures or shows later overprint. In contrast, the samples used to determine average compositions are line samples used to estimate the average metal contents in the skarn and the assignment to one or another skarn type essentially refers to the dominant type and does not exclude mixtures. The most notable differences are: (i) some individual samples have markedly lower contents of some trace elements than the corresponding average sample. This largely reflects admixtures of variable amounts of material from the other skarn types. (ii) Individual skarn samples typically show Cu depletion relative to UCC, whereas the average samples generally show Cu enrichment. This is an artifact from the contrasting sampling strategies. For the individual samples, sections with blebs of late Cu-sulfides were excluded from analysis. Nonetheless, a comparison between the pattern of averaged samples and individual samples shows great similarity and implies that the samples used for isotope investigations are representative for the deposit.

The average major element compositions of rocks of the Hämmerlein deposit fall in two groups that are most distinct for the samples also used for isotope analysis: (1) mica schists and gneisses have relatively flat UCC-normalized major element pattern, the slightly lower Ca and Na contents possibly being a fingerprint of the intense chemical alteration that is typical for Early Ordovician sedimentary rocks of the former Gondwana margin, which are by volume the most important protoliths of the metamorphic nappes (e.g., Mingram, 1998; Romer and Hahne, 2010). The major element content of schist ore and its unmineralized equivalents differ mainly by lower (Al), Ca, Fe, Mg, Mn, and Na contents in the schist ore (Fig. 18a). (2) The major element compositions of the silicate-dominated skarn samples fall in a relatively narrow range, despite their contrasting abundances of garnet, amphibole, and pyroxene. This implies that very similar protolith developed into a wide range of mineralogically different skarn types. The contrasting mineral assemblage is largely due to equilibration of the peak-metamorphic assemblages with fluids of contrasting XCO_2 (cf. Lefebvre et al., 2019). The major element patterns of skarn rocks show a strong enrichment (from a factor 2 to 10) in Fe, Ca, and Mn and a slight depletion in Al, K, and Na compared to the upper continental crust (Taylor and McLennan, 1995). The magnetite skarn (Fig. 18) differs from all other skarn types by an extreme enrichment in Fe (and to a lesser extent Mn), which dilutes the contents of the other elements (Fig. 18).

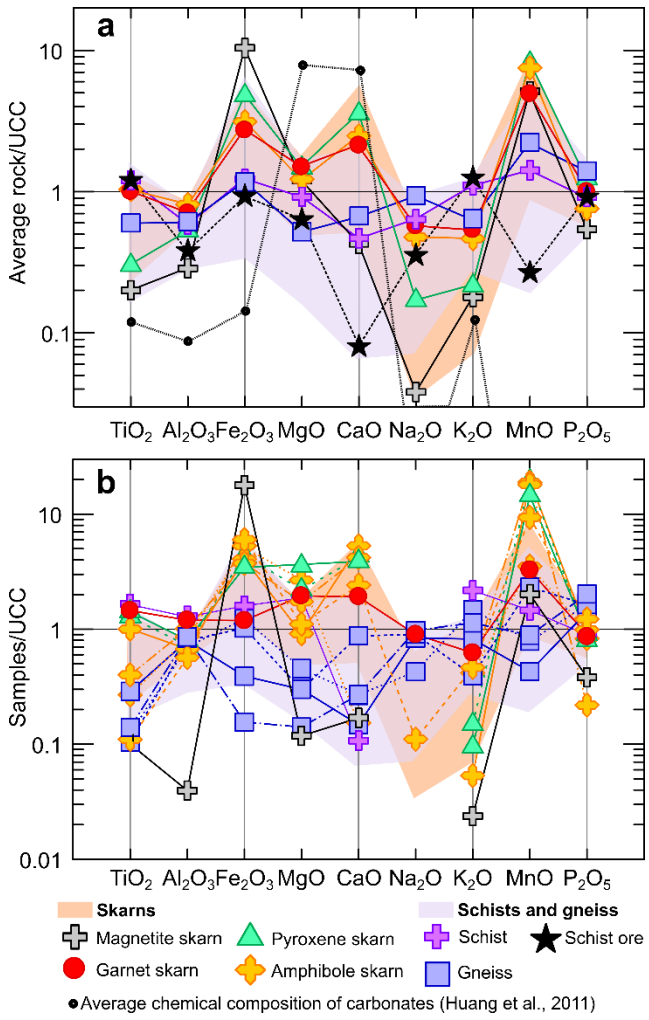

Figure 18: Major and trace element patterns of whole rocks from the Hämmerlein skarn normalized to the upper continental crust composition (Taylor and McLennan, 1995). (a) UCC-normalized pattern of average rocks are obtained from representative samples that do not show any lithological mixture (Table 7). The compositional ranges are shown for skarns (orange field) and schists and gneisses (purple field), respectively. The data for the fields (n = 224 samples) are shown in the Electronic Supplementary Material 4 and 5. (b) UCC-normalized pattern of individual skarn, schist, and gneiss samples correspond to those used for isotope analysis and are taken from Table 7 and the Electronic Supplementary Material 4 and 5. The major element pattern of "average carbonates" is shown for reference in both (a) and (b) (Huang et al., 2011).

The trace element pattern of the various schist and gneiss samples show relatively flat UCC-normalized pattern, except for Sr, which is variably depleted and may represent a protolith signature similar to the Ca and Na depletion (Figs. 18 and 19). The schists and gneisses are slightly enriched in Cu, Zn, and W, and strongly enriched in As, Cd, In, and Sn (Fig. 19). Furthermore, the mineralized schists have higher contents of Cu, In, Sn, and W and lower contents of Zn and Sr than the barren schists (Fig. 19a). The trace element pattern of the silicate skarns shows a general similarity with the one of the schists and shows – except for Sr and Y –distinctly higher trace element contents. As carbonates have markedly lower contents of most trace elements than most siliciclastic sedimentary rocks (Sr being a notable exception), the similarity of the skarn pattern with those of the schists indicates that the protoliths of the skarns were impure carbonate rocks, such as marls or argillaceous carbonates, rather than pure carbonates. The UCC normalized skarn samples form a relatively homogenous group with moderate depletions in Sr and Ba, moderate enrichment in Cu, Zn, Cs, and W, and strong enrichment in As, Cd, In, and Sn relative to UCC (Fig. 19a). The pyroxene skarn and in particular the magnetite skarn have generally lower contents in most trace elements than the other skarn types. At least for the magnetite skarn, these lower trace element contents may reflects the higher dilution by magnetite that does not incorporate these elements to a significant extent. The UCC-normalized trace element pattern of schist and gneiss samples and skarn samples are similar, except for Zn (not enriched in the schist ore) as well as In and Sn that are distinctly lower in the unmineralized mica schists. Schist, gneiss, and skarns are all enriched in trace elements (except for Sr and Y) relative to average carbonates.

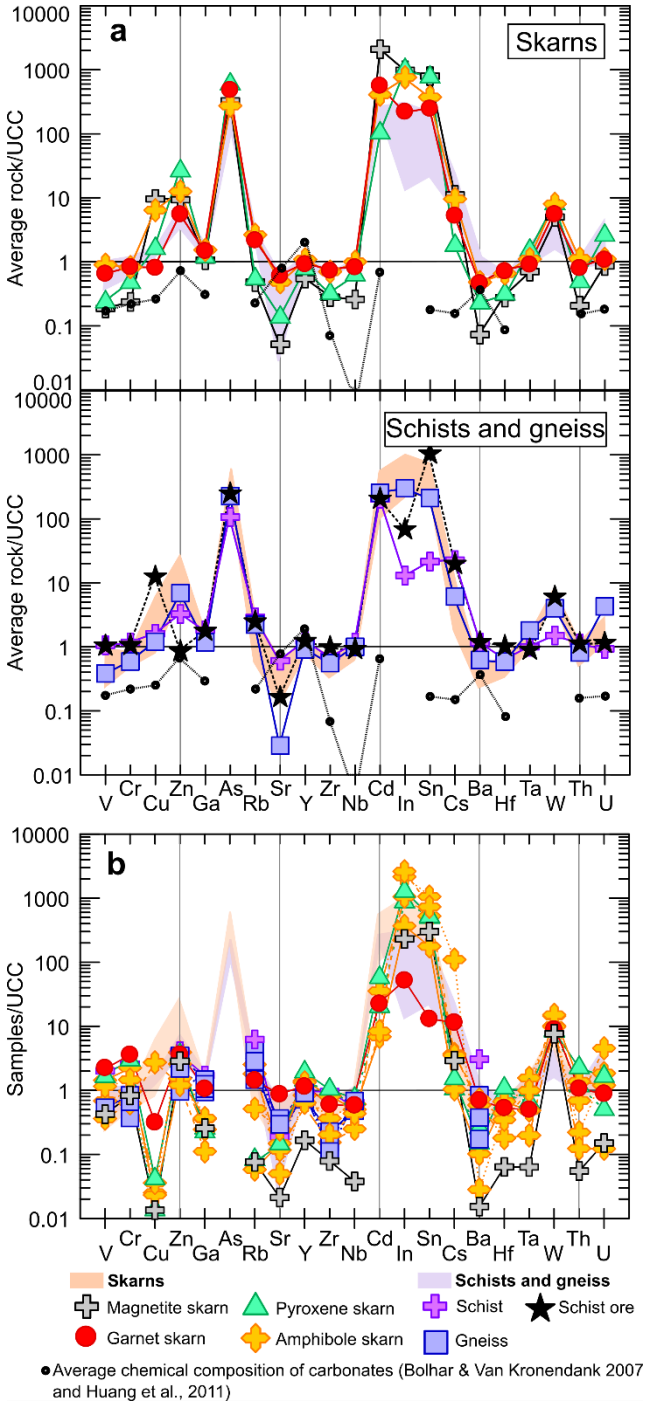

Figure 19: Trace element patterns of whole rocks of Hämmerlein normalized to the upper continental crust (Taylor and McLennan, 1995). (a) average rocks patterns are obtained from representative samples that do not show mixed lithologies (Table 7). Data of the 224 samples are given in the Electronic Supplementary Material 4 and 5. The purple field (upper part) represents the schists and gneisses, and the orange field (lower part) represents the compositional range of skarns. The trace elements pattern of "average carbonates" is given for reference (Bolhar and van Kronendank, 2007; Huang et al., 2011). (b) sample patterns of individual skarns, schist, and gneiss correspond to samples that were used for isotope analysis (Table 7 and the Electronic Supplementary Material 4 and 5).

Mineralized and unmineralized schist samples and the gneiss sample have regular UCC-normalized REE pattern without Eu anomaly. The mineralized schist has slightly lower LREE and slightly higher HREE contents than the unmineralized schist. The gneiss has overall lower REE than mineralized and unmineralized schist samples, whereby the difference is more pronounced for LREE than for HREE (Fig. 20). The UCC-normalized REE patterns of the skarn samples shows a variable depletion of the LREE, a distinct positive Eu anomaly, and a flat HREE pattern (Fig. 20). The magnetite and pyroxene skarns have the lowest REE contents and, therefore, these samples show the most pronounced "spoon" pattern for the LREE, with Ce being more depleted than La, and the most pronounced positive Eu anomaly. For the garnet and amphibole skarns, which have distinctly higher REE contents, the "spoon" pattern of the LREE is less pronounced (Fig. 20). The comparison between the average composition of carbonates and skarns shows that their patterns have a similar shape, with a depletion in LREE and a positive Eu anomaly. Pattern with a marked LREE depletion relative to HREE (with or without a Eu anomaly) is typical for hydrothermal mineralization (Möller et al., 1982; Schwinn and Markl, 2005). These similarities are more obvious for average magnetite and pyroxene skarns (Fig. 20a) and for an individual amphibole skarn (Fig. 20b), as these rocks have low REE contents and, therefore, their REE concentration is more readily changed by

hydrothermal additions. Garnet and amphibole skarns that are more enriched in REE (similar to the UCC) also show a flatter pattern. The difference between magnetite and pyroxene skarns and the garnet and amphibole skarns may be that the protolith carbonates of the former were less diluted by silicate minerals.

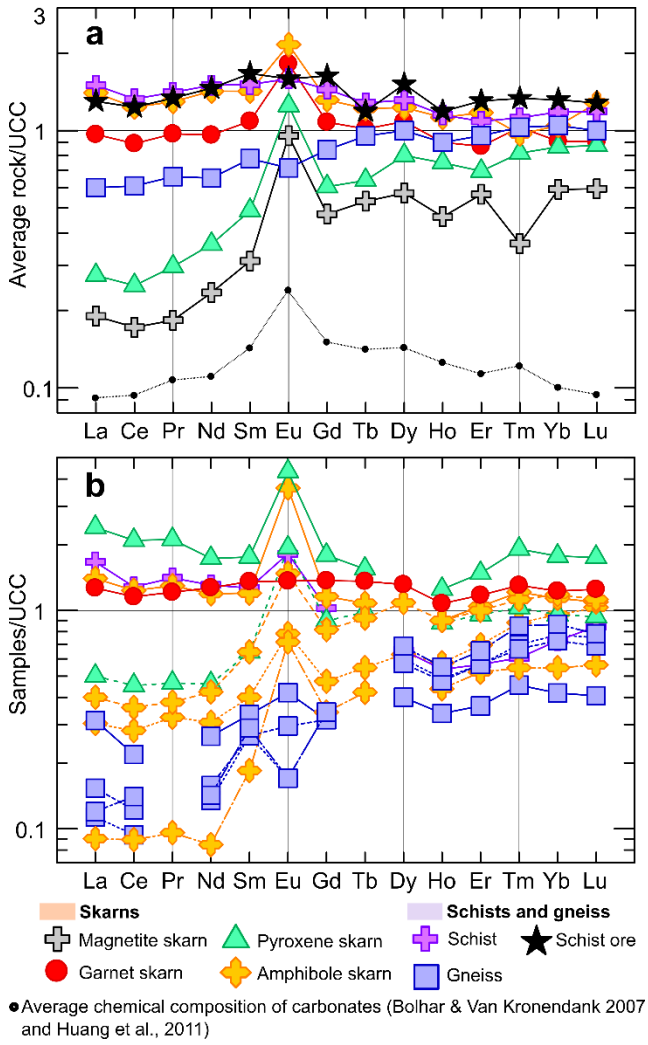

Figure 20: Rare earth element pattern of whole rock samples from the Hämmerlein skarn. The patterns are normalized to the composition of upper continental crust (Taylor and McLennan 1995). (a) average rocks patterns are obtained from samples that do not show admixtures of other lithologies and are derived from the central part of individual skarn lithologies (Table 7). REE pattern of "average carbonates" is shown for reference (Bolhar and van Kronendank, 2007; Huang et al., 2011). (b) UCC-normalized pattern of individual skarns, schist, and gneiss samples are from those samples that were used for isotope analysis. Note the generally flat pattern without positive Eu anomaly of schist and gneiss samples and the slight LREE depletion with positive La and Eu anomalies in the skarn samples. The Ho and Tm contents of the magnetite skarn sample are near the detection limit, therefore the anomalies are considered to be artifacts.

4.4.2. Nd and Sr isotopic composition

The Nd and Sr isotopic compositions of schist, gneiss, and skarn samples fall in the same field as rocks of the regional metamorphic nappes (and their sedimentary equivalents from the Schwarzburg area) and have distinctly less radiogenic Nd isotopic compositions and more radiogenic Sr isotopic compositions than the Eibenstock and other granites of the western Erzgebirge (Fig. 21). The extremely radiogenic measured Sr isotopic compositions of some samples reflects the high Rb/Sr of these samples that is due to low Sr contents rather than high Rb contents (cf. Fig. 19). It is important to note, however, that the high measured $^{87}Sr/^{86}Sr$ values are not due to in situ growth alone, but some samples had high $^{87}Sr/^{86}Sr$ already at the time of Variscan metamorphism and skarn formation (Table 8). Recalculated to 340 Ma, $^{87}Sr/^{86}Sr$ values of metamorphic rocks range between 0.7119 and 0.7922 and εNd_{340} ranges between –11.8 and –5.7 (Table 8). Among Paleozoic sedimentary rocks of the peri-Gondwana shelf, i.e., the rocks that contribute largely to the metamorphic nappes of the Erzgebirge (Mingram, 1998; Rötzler and Plessen, 2010), only those of the early Ordovician Frauenbach Group of the Schwarzburg area have $^{87}Sr/^{86}Sr$ values above 0.74. Two samples, i.e., one amphibole skarn and the magnetite skarn, show marked overcorrection of in situ Sr growth resulting in unreasonably low

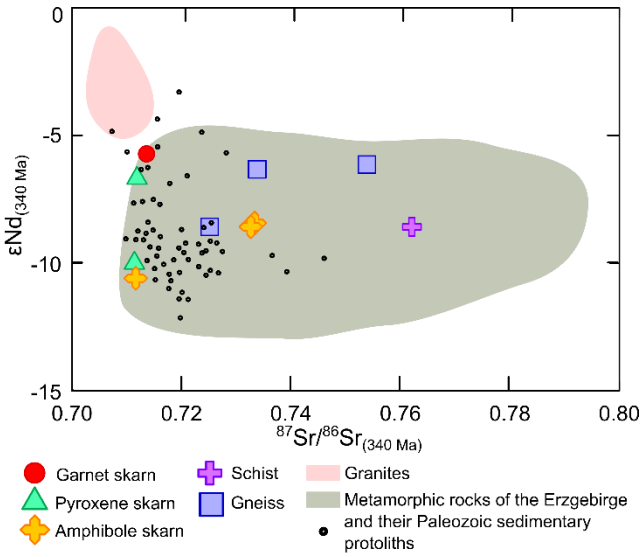

apparent $^{87}Sr/^{86}Sr_{340}$ values. Thus, there must have been Sr loss or Rb addition in some samples after Variscan peak-metamorphism during one or several later events, like the magmatic pulses of the Eibenstock granite intrusion or later tectonic reactivations of fault zones, such as the nearby Gera-Jáchymov Zone (Schuppan and Hiller, 2012).

Figure 21: εNd vs $^{87}Sr/^{86}Sr$ diagram for skarn, schist, and gneiss samples from the Hämmerlein deposit. Reference fields for granites and metamorphic rocks (including their sedimentary protolith analogues from the Schwarzburg area) base on Romer et al. (2014a, 2014b) and Romer and Meixner (2014).

4.4.3. Pb isotopic composition of skarn minerals

Different terrestrial reservoirs (e.g., mantle, upper crust, lower crust) have contrasting average Pb development, as the chemical elements of the parent and daughter nuclides are separated by a wide range of geochemical processes. The average development of these reservoirs has been modeled by Zartman and Doe (1981). The Pb isotopic composition of amphibole, pyroxene (Fig. 22a), and magnetite skarn (Fig. 22b) whole rock samples (Table 8) fall between the growth curves of upper crustal and orogenic Pb. This implies that the Pb of these rocks was derived from ancient crustal rocks or from sediments that are derived from ancient crustal rock, as for instance the Paleozoic sedimentary rocks of the Central European peri-Gondwana shelf that recycle material derived from the late Archean and early Paleoproterozoic West African Craton (Romer and Kroner, 2015). There is no mantle contribution to the Pb isotopic composition of the skarns and schists. In the $^{206}Pb/^{204}Pb$ vs. $^{208}Pb/^{204}Pb$ diagram, the major part of whole rock samples plot offset from the upper crust (UC) curve toward the lower crust (LC) curve (Fig. 22a). There are two explanations for this offset: (i) The crustal Pb sources include recycled ancient lower crust; (ii) intense chemical alteration with the decomposition of feldspar results in the preferential loss of U, eventually leading to the retarded growth of uranogenic Pb and the accelerated growth of thorogenic Pb. The early Ordovician sedimentary rocks of the former peri-Gondwana shelf, which also dominate the metamorphic rocks of the Erzgebirge, have experienced such an alteration and show enhanced $^{208}Pb/^{204}Pb$ ratios, as illustrated for the sedimentary rocks of the Frauenbach Group (Schwarzburg area; Romer and Hahne, 2010; Romer et al., 2014b).

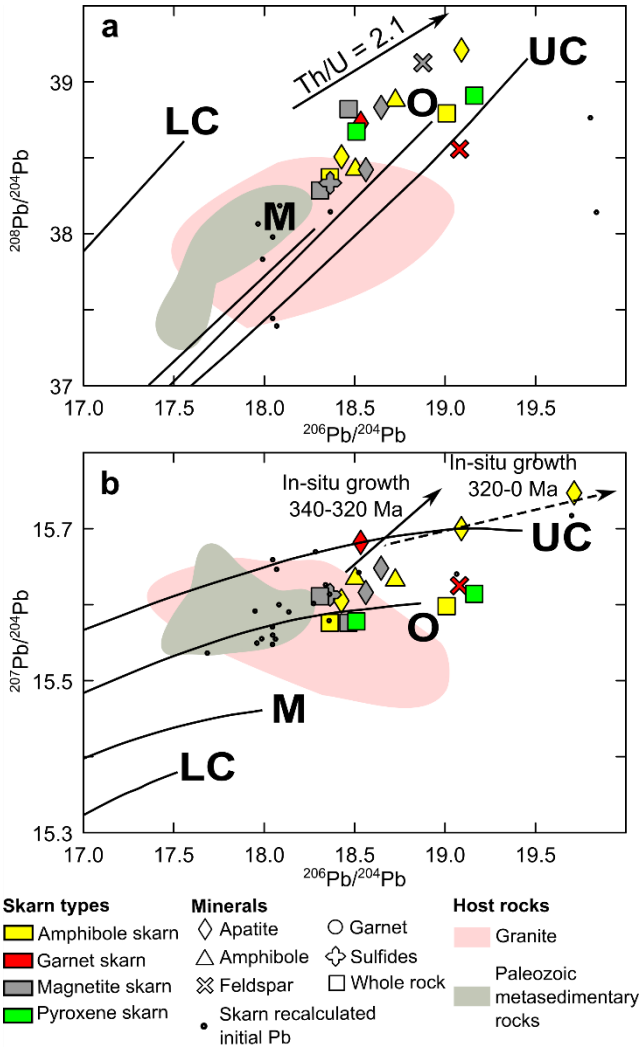

Figure 22: (a) $^{208}Pb/^{204}Pb$ vs $^{206}Pb/^{204}Pb$ and (b) $^{207}Pb/^{204}Pb$ vs $^{206}Pb/^{204}Pb$ diagrams for skarn samples from the Hämmerlein deposit. Data sources: Table 8 for whole rock data, Lefebvre et al. (2019) for mineral data. Reference curves for average lead growth are taken from Zartman and Doe (1981): LC = lower crust; UC = upper crust; M = mantle; O =orogenic Pb. The reference fields for metamorphic rocks and granites base on Bielicki and Tischendorff (1991), Förster and Romer (2010), Romer et al. (2014a, 2014b), and Romer and Meixner (2014).

The initial Pb isotopic composition of the whole rock samples from the Hämmerlein skarn falls within the compositional range of the late-Variscan granites and Paleozoic metasedimentary rocks that form the Variscan nappes of the Erzgebirge. The fields of the granites and the metasedimentary rocks broadly overlap as the granites formed from the melting of metasedimentary rocks (Förster and Romer, 2010) and therefore inherited the Pb isotopic composition of the metasedimentary rocks.

Data obtained from Hämmerlein samples (Table 8 for whole rock samples and Lefebvre et al., 2019 for mineral fractions) fall in two groups. One group including primary skarn minerals that formed during regional metamorphism (Lefebvre et al., 2019) shows relatively unradiogenic Pb signatures ($^{206}Pb/^{204}Pb_{meas}$: 18.31 - 19.71). The second group includes secondary apatite and amphibole from the amphibole skarn with more radiogenic compositions ($^{206}Pb/^{204}Pb_{meas}$: 20.92 – 25.45). The first group shows $^{207}Pb/^{204}Pb$ ratios between 15.33 and 15.87, whereas the second group shows higher ratios which range from 15.68 to 16.48. Both groups show $^{208}Pb/^{204}Pb$ ratios in the same range (from 38.28 to 41.22).

Table 8: Whole rock Sr, Nd, Pb, Li, and B data for skarns, schist, and gneiss from the Hämmerlein deposit

Sample	Rock	$^{87}Sr/^{86}Sr$[a]	$^{87}Sr/^{86}Sr_{340}$[b]	$^{143}Nd/^{144}Nd$[a]	εNd[b]	$^{206}Pb/^{204}Pb$[c]	$^{207}Pb/^{204}Pb$[c]	$^{208}Pb/^{204}Pb$[c]	$^{206}Pb/^{204}Pb_{340}$[d]	$^{207}Pb/^{204}Pb_{340}$[d]	$^{208}Pb/^{204}Pb_{340}$[d]	δ^7Li[e] ± 2SE	Li (ppm)	$\delta^{11}B$[e] ± 2SE	B (ppm)
CSV1-01	Gneiss	0.751700 ± 4	0.7339	0.512273 ± 6	-6.3	25.365	15.943	38.606	22.63	15.80	38.14	-3.40 ± 0.08	39	-11.95 ± 0.15	16.3
CSV1-02	Amphibole skarn	0.744594 ± 9	0.7334	0.512123 ± 5	-8.4	21.246	15.728	38.436	17.99	15.55	37.82	0.29 ± 0.09	120	-8.28 ± 0.14	12.7
CSV2-01	Gneiss	0.796129 ± 8	0.7534	0.512358 ± 5	-6.2	24.704	15.900	38.537	21.99	15.76	38.08	-3.78 ± 0.09	13	-15.11 ± 0.15	10.2
HAS1-01	Amphibole skarn	0.720806 ± 7	*0.667*	0.512105 ± 7	-11.8	18.363	15.576	38.371	18.05	15.56	37.98	-3.33 ± 0.13	109	-19.10 ± 0.34	8.4
HAS1-02	Pyroxene skarn	0.718226 ± 10	0.71176	0.511923 ± 2	-10.0	19.162	15.614	38.908	*17.69*	*15.54*	*36.42*	-4.35 ± 0.17	119	-7.40 ± 0.14	8.5
HAS3-01	Gneiss	1.036798 ± 7	0.90308	0.512349 ± 6	-6.1	29.794	16.186	38.834	26.89	16.03	38.34	-4.6 ± 0.1	40	-7.80 ± 0.12	7.5
HAS3-02	Amphibole skarn	0.856793 ± 14	0.7327	0.512069 ± 6	-8.5	22.516	15.800	38.756	18.36	15.58	38.14	-7.88 ± 0.13	158	6.86 ± 0.22	17.5
HGS1-01	Garnet skarn	0.720791 ± 6	0.71369	0.511908 ± 6	-5.7	18.466	15.576	38.820	17.96	15.55	38.07	-3.49 ± 0.15	77	-9.87 ± 0.12	22.1
HMS1	Magnetite skarn	0.729678 ± 8	*0.666*	0.512181 ± 6	-6.4	18.308	15.611	38.285	18.08	15.60	38.18	10.6 ± 0.1	22	-19.55 ± 0.18	25.2
HPS1-01	Pyroxene skarn	0.717772 ± 8	0.71172	0.511983 ± 2	-6.7	18.510	15.578	38.672	18.07	15.55	37.39	-1.88 ± 0.11	101	-7.95 ± 0.12	8.2
HPS1-02	Amphibole skarn	0.716873 ± 6	0.71168	0.511893 ± 4	-10.6	19.009	15.598	38.792	18.05	15.55	37.43	5.26 ± 0.12	57	-5.51 ± 0.20	9.1
SG1-01	Gneiss	0.764762 ± 8	0.7258	0.512055 ± 10	-8.5	22.464	15.794	38.592	19.83	15.65	38.15	-1.86 ± 0.19	271	-14.28 ± 0.22	15.3
SG1-02	Schist	0.907762 ± 25	0.7622	0.511985 ± 3	-8.6	20.317	15.676	39.396	19.80	15.65	38.77	-1.49 ± 0.18	52	-15.29 ± 0.10	46.9

[a] $^{87}Sr/^{86}Sr$ and $^{143}Nd/^{144}Nd$ are normalized to $^{86}Sr/^{88}Sr = 0.1194$ and $^{146}Nd/^{144}Nd = 0.7219$, respectively. Both Sr and Nd were analyzed on a TRITON multicollector thermal ionization mass spectrometer using dynamic multi-collection. Uncertainties are given at 2σm level.

[b] $^{87}Sr/^{86}Sr_{340}$ and εNd were calculated for the samples age (340 Ma) using $\lambda^{87}Rb = 1.3972 \pm 0.0045E\text{-}11$ y-1 (Villa et al., 2015) and $\lambda^{147}Sm = 6.539 \pm 0.061E\text{-}12$ y-1 (Begemann et al., 2001). Geologically unreasonably low calculated values (reflecting secondary disturbance of the parent-to-daughter ratio) are given in italics.

[c] Lead isotope data are recalculated for mass discrimination with 0.1%/AMU with a reproducibility at 2σ.

[d] Lead isotope data were recalculated for the sample age (340 Ma), using the contents of U, Pb, and Th (Electronic supplementary material 4) and the constants recommended by the IUGS $\lambda^{232}Th = 4.9475E\text{-}11$ y-1, $\lambda^{235}U = 9.848E\text{-}10$ y-1, and $\lambda^{238}U = 1.55125E\text{-}10$ y-1. Geologically unreasonably low calculated values are given in italics.

[e] Lithium and boron isotopes were analyzed on a MC-ICP-MS Neptune (ThermoFisher Scientific, TFS) using the standard-sample-standard bracketing method. Lithium and boron isotope ratios are expressed in the delta notation relative to NIST 8545 and NBS 951, respectively.

4.4.4. Li and B isotopic composition of skarns, gneiss, schist, and greisen

Li and B isotopic composition and concentration of skarns, gneiss, schist, and greisen are reported in Tables 8 and 9 and plotted in Fig. 23. The B and Li isotopic signature and concentration of granites and metamorphic units of the Erzgebirge (and the sedimentary rocks of the Schwarzburg area [Romer and Meixner, 2014]) are shown for comparison in Fig. 23. The metamorphic (metasedimentary) rocks and granites of the western Erzgebirge show relatively light Li isotopic compositions with δ^7Li values ranging from -5.9 to 1.4 and from -1.9 to -0.3 (Romer et al., 2014a; 2014b), respectively, whereby the lowest δ^7Li values are observed for rocks of higher metamorphic grade (Romer and Meixner, 2014). The δ^7Li ranges of granites and metamorphic rocks broadly overlap, with generally markedly higher Li contents for the non-mineralized granites (Fig. 23a). The Eibenstock granitic rocks have relatively high Li contents and plot at the high-Li end of the granite field (Fig. 23a). The Paleozoic sedimentary rocks of the Schwarzburg area have a much broader range in δ7Li and Li concentration than their metamorphic equivalents (Fig. 23a; Romer and Meixner, 2014) with excursions to high Li contents or to high δ^7Li values. These high δ^7Li values are due to authigenic marine minerals and seawater Li adsorbed to clay minerals and is only observed in samples with overall low Li contents (Romer et al., 2014a). This signature is lost already at relatively low-grade metamorphism (Romer and Meixner, 2014). The gneisses, mica schists, and ore schists from the Hämmerlein deposit fall all in the field defined by the metamorphic rocks of the Erzgebirge (Fig. 23a). The skarn samples show a similar compositional range as the Paleozoic sedimentary rocks (δ^7Li ≈ -8 to 11; Li ≈ 20 to 160 ppm) with a general correlation from high δ^7Li at low Li contents to low δ^7Li at high Li contents.

The Li isotopic composition of all skarn samples reflect a mix between Li derived from silicate and carbonate minerals. Because clay minerals have higher Li contents than calcite, the average δ^7Li values of skarn samples typically fall in the range of the metamorphic host-rocks that are dominated by former shales. Only few samples show higher values. Magnetite and amphibole skarn samples show the highest δ^7Li values that are displaced from the compositional field of the host-rocks toward the Li isotopic composition expected for authigenic minerals or carbonates that had formed in seawater. These observations are in agreement with the low REE contents and REE pattern of skarn samples. Most skarns have flat UCC-normalized REE pattern as their REE budget is dominated by originally present silicate minerals. Magnetite and a few amphibole skarn samples, however, have UCC-normalized REE pattern that approaches the composition of average carbonates (Fig. 20b). Thus, high δ^7Li values seem to be restricted to skarns that are derived from relatively pure carbonates and possibly were not changed significantly during later metamorphism or granite emplacement.

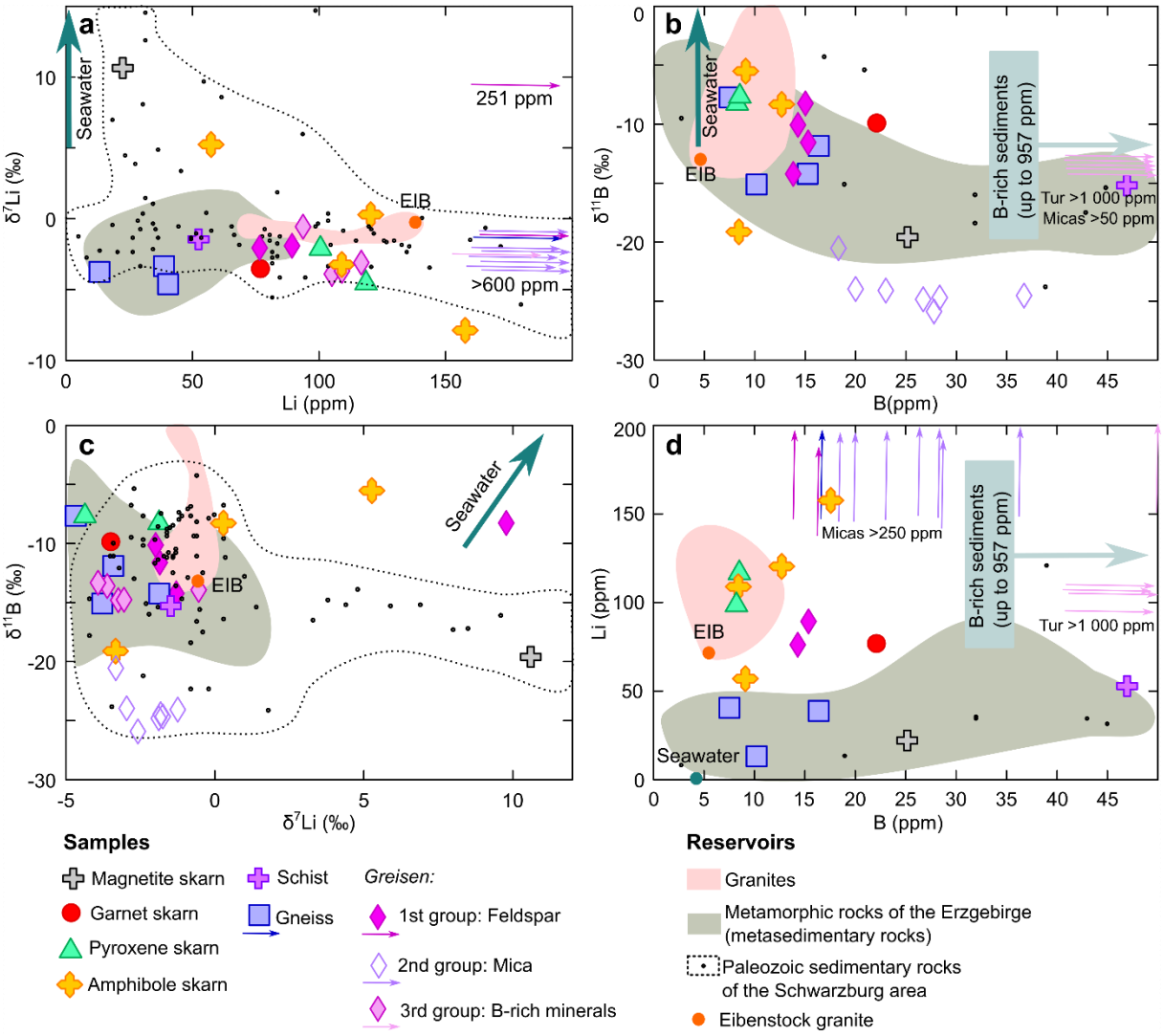

Figure 23: (a) δ^7Li vs Li concentration, (b) δ^{11}B vs B concentration, (c) δ^{11}B vs δ^7Li, and (d) Li concentration vs B concentration diagrams for skarn mineralization at Hämmerlein and greisen mineralization associated with the Eibenstock granite. Note, samples with particularly high Li or B contents are indicated by arrows. Reference fields (granites, metamorphic rocks of the Erzgebirge, and Paleozoic sediments) base on Romer et al. (2014a, 2014b) and Romer and Meixner (2014). The contents and isotopic compositions of Li and B of the Eibenstock granite (EIB) and seawater (representing average carbonates) are shown for reference.

The greisen samples that are spatially closely related to the Eibenstock granite fall in a relatively narrow range with slightly lower δ^7Li and Li concentrations than the Eibenstock granite (Fig. 23a). Feldspar, white mica, and tourmaline show very little variation in δ^7Li and the difference among different greisen commonly is larger than the variation among different minerals from the same location. The various greisen minerals have very different Li contents that typically are below 100 ppm for feldspar and tourmaline and above (500) 1000 ppm for white mica (Table 9). One feldspar sample, however, is unusual as it has relatively high Li contents and a δ^7Li value that is more than 10 δ-units heavier than white mica from the same hand specimen (Table 9).

The B isotopic composition and B concentration of skarn samples from the Hämmerlein deposit and the greisen related to the Eibenstock granite are shown together with granites and metamorphic rocks of the Erzgebirge and Paleozoic sedimentary rocks of the Schwarzburg area (Fig. 23b). The metamorphic rocks and their sedimentary protoliths broadly encompass the same range ($\delta^{11}B \approx$ -25 to -4 and B ≈ 1 - 950 ppm), whereas the granites of the western Erzgebirge show low B contents between 5 and 15 ppm at a relatively large $\delta^{11}B$ range between –14 and 0 that shows significant overlap with the metamorphic and sedimentary protoliths. Gneisses as well as mineralized and unmineralized schists fall in the compositional field of the metamorphic rocks of the Erzgebirge. Skarn samples show scattered signatures. They mainly show $\delta^{11}B$ values above -10 ‰ and plot in the compositional field of granites of the Erzgebirge. There are a few samples that deviate from the bulk of samples. For instance, garnet skarn has a higher B concentration (22.1 ppm) and one amphibole skarn and the magnetite skarn samples show lighter B signatures (~ -19 ‰) that are closer to the compositional field of metamorphic rocks. The contrasting content of B in the various skarn types is controlled by the mineralogy of the samples, which depends on the protoliths. The light B signatures of magnetite and some amphibole skarns may reflect the initial signature of the sedimentary protolith without important additions of material with higher $\delta^{11}B$ values. Therefore, the variation in the B composition may reflect both initial differences and contrasting relative addition during later processes.

The B isotopic compositions of greisen minerals fall in three groups: (1) feldspar has similar $\delta^{11}B$ values as the granites, although the B contents of feldspar, which may incorporate B in its structure (Eugster and McIver 1959, Sheppard and Gude 1973, Stamatakis 1989), are slightly higher (Fig. 23b). (2) The second group includes white mica from greisens with $\delta^{11}B$ below -20.5 and B concentration between 15 and 40 ppm. (3) The third group includes B-rich minerals, such as tourmaline (>20000 ppm B) and white mica from metasomatized phyllite with a B concentration above 50 ppm. B-rich mineral fractions show similar $\delta^{11}B$ values (from -14.8 to -13.4) that correspond to the one of the Eibenstock granite (Fig. 23b).

The combined B and Li isotopic compositions of skarn samples from the Hämmerlein deposits, greisen samples related to the Eibenstock granite, and reference reservoirs are plotted in Fig. 23c. Granites of the Erzgebirge show a relatively wide $\delta^{11}B$ range, from -14 to 0, and a narrow $\delta^{7}Li$ around -1. The metamorphosed sedimentary rocks dominating the nappes of the Erzgebirge show a $\delta^{7}Li$ range between -5 and 1 and a $\delta^{11}B$ range between -20 and -7. Corresponding sedimentary protoliths of these metamorphic rocks plot roughly in the same field, even though some of them have heavier Li isotopic compositions. Gneisses and schists near the Hämmerlein deposit fall in the field of the metamorphic and Paleozoic sedimentary rocks. Most skarn samples have $\delta^{11}B$ between -20 and 5 and $\delta^{7}Li$ below or slightly above 0. The magnetite skarn shows a heavier Li isotopic composition (above 10; Fig. 23). Note that the Li and B isotopic composition of one amphibole skarn sample (HPS1-02, Table 8) differs from all skarn samples and reference reservoirs by having heavy $\delta^{7}Li$ (slightly above 5) and relatively heavy $\delta^{11}B$ (around -5).

Table 9: Isotopic composition of Sr, Li, and B of minerals from greisen associated with the Eibenstock granite

Sample	Description	Age (Ma)[a]	$^{87}Sr/^{86}Sr$[b]	$^{87}Sr/^{86}Sr_{(t)}$[c]	$\delta^{7}Li$[d] ± 2SE	Li (ppm)	$\delta^{11}B$[d] ± 2SE	B (ppm)
BO1-01	Wm 125 - 90 µm	319	24.5019 ± 9	*0.667*	-1.83 ± 0.05	6200	-24.50 ± 0.55	36.7
BO1-02	Feldspar	319	1.31150 ± 28	0.7000	-1.87 ± 0.12	89	-10.53 ± 0.25	15.4
EE2	Feldspar	322	1.98703 ± 12	*0.584*	-1.30 ± 0.12	1250	-14.17 ± 0.25	13.8
GG1	Wm 125 - 90 µm	295	19.0493 ± 20	1.503	-2.58 ± 0.09	687	-25.91 ± 1.04	27.8
GG3-01	Wm 500 - 355 µm	320	17.1464 ± 6	*0.163*	-3.36 ± 0.06	1150	-20.56 ± 1.55	18.3
GG3-02	Wm 180 - 125 µm	320	21.2957 ± 10	*0.450*	-2.97 ± 0.09	1040	-23.95 ± 0.83	20.0
GG3-03	Feldspar	320	0.95391 ± 11	0.7244	-1.99 ± 0.07	77	-10.08 ± 0.20	14.3
JG1-01	Wm 125 - 90 µm	322	1.04240 ± 13	0.7207	-3.24 ± 0.09	663	-14.69 ± 0.14	60.3
JG1-02	Tur 250 - 180 µm	322	0.74830 ± 11	0.7217	-3.6 ± 0.1	109	-13.61 ± 0.09	>25000
JG1-03	Tur 180 - 125 µm	322	0.73147 ± 16	0.7212	-3.92 ± 0.14	105	-13.38 ± 0.10	>27000
JG2-01	Wm 90 - 63 µm	318	1.08731 ± 12	0.7180	-3.1 ± 0.1	117	-14.76 ± 0.09	749
JG2-02	Tourmaline	318	0.76441 ± 11	0.7217	-0.53 ± 0.09	94	-13.89 ± 0.09	>20000
RZ2-01	Wm 5 - 2 mm	312	88.766 ± 20	4.549	-1.24 ± 0.11	4200	-24.10 ± 0.76	23.0
RZ2-02	Wm 180 - 125 µm	312	7.7957 ± 20	0.7886	-1.9 ± 0.1	2300	-24.83 ± 0.44	26.7
RZ2-03	Wm 125 - 90 µm	312	4.74661 ± 5	0.81617	-1.77 ± 0.06	2100	-24.68 ± 0.35	28.3
RZ2-04	Feldspar	312	1.23730 ± 14	0.7026	9.78 ± 0.14	251	-8.23 ± 0.08	15.0

Wm = white mica, Tur = tourmaline

[a] Ages of samples are taken from Lefebvre et al., 2019.

[b] $^{87}Sr/^{86}Sr$ are normalized to $^{86}Sr/^{88}Sr = 0.1194$. Sr was analyzed on a TRITON multicollector thermal ionization mass spectrometer using dynamic multi-collection. Uncertainties are given at 2σm level.

[c] $^{87}Sr/^{86}Sr_t$ were calculated for the samples age using $\lambda^{87}Rb = 1.3972 \pm 0.0045E\text{-}11$ y-1 (Villa et al., 2015). Geologically unreasonably $^{87}Sr/^{86}Sr_t$ low calculated values, maybe due to late alteration that induced a loss of Sr, are given in italics.

[d] Lithium and boron isotopes were analyzed on a MC-ICP-MS Neptune (ThermoFisher Scientific, TFS) using the standard-sample-standard bracketing method. Lithium and boron isotope ratios are expressed in the delta notation relative to NIST8545 and NBS 951, respectively.

Lithium and B are hosted in different minerals and, therefore, their budget is dominated by contributions from different minerals and their isotopic composition may be dominated by contributions from different sources. The major part of Li-rich white mica and two Li-rich feldspar fractions has Li concentrations above 250 ppm and B concentrations between 14 and 37 ppm. There are however, two feldspar samples that have markedly lower Li concentrations of ~80 ppm and B concentrations ~15 ppm. Tourmaline, which is the major host of B, typically have Li concentrations around 100 ppm.

4.5. Discussion

4.5.1. Modification of protolith chemistry during skarn formation

Disregarding those elements that have been highly mobile during hydrothermal processes related to the 340 Ma regional metamorphism and the emplacement of the c. 320 Ma Eibenstock granite, mineralized and unmineralized schists have the same geochemical fingerprint as most skarn types of the Hämmerlein deposit, i.e., they form relatively flat UCC-normalized pattern for major and trace elements (Figs. 18 and 19). As shales, which represent the protoliths of the metamorphic wall rocks of the Hämmerlein deposit, have much higher contents of most analyzed trace elements (except for Sr) than carbonate minerals, the variable dilution of argillaceous material with carbonate would reduce to total content of most trace elements, but would not significantly affect the trace element pattern. The variable contribution of carbonates is apparent in the Ca (Mg) and Sr contents that are strongly enhanced in rocks with carbonates and – most importantly – in the REE pattern (Fig. 20). The mineralized and unmineralized schists have flat UCC-normalized pattern without Eu anomaly. The similarity of these REE patterns implies that the addition of ore elements possibly was not linked to any significant addition of REE. In contrast, skarn samples all have variably strongly developed LREE depletion and positive Eu anomalies, similar to typical marine carbonates (Fig. 20). The skarn samples with the lowest overall REE contents possibly had the protolith with the lowest contributions of argillaceous material.

The schists had carbonate-free protoliths, whereas all skarns had carbonate-bearing or carbonate-dominated protoliths even though the chemical fingerprint of these rocks is dominated by argillaceous material. Note, the low Ca, Na, and Sr contents in unmineralized schist possibly represent a protolith signature. In the Paleozoic sedimentary rocks of the former peri-Gondwana shelf, this signature is only known from the voluminous units of the Frauenbach Group (Mingram 1998; Romer and Hahne, 2010). Thus, the geochemical fingerprint may indicate an early Ordovician age of the protolith.

At metamorphic conditions, quartz and calcite (and/or dolomite) react with each other in the presence of H_2O (Spear 1995), resulting in the formation of Ca-Mg-silicates and CO_2. Thus, the aqueous fluid mostly reacted with the carbonate-bearing rocks, but may have percolated through the carbonate-free rocks with little interaction. The decarbonation not only results in the formation of calc-silicate minerals, but also modifies the fluid composition and, thus, may affect the solubility of transported metals, eventually resulting in the local enrichment of dissolved metals.

Elements added to the skarn and the mineralized schist, or lost from them, at 340 Ma or c. 320 Ma include: (i) Fe and Mn which are variably enriched in all skarn samples and seem to have been lost to some extent from the mineralized schists (Fig. 18). As the skarn (including the magnetite skarn) formed during the regional metamorphism at 340 Ma, Fe and Mn are likely to have been introduced by metamorphic fluids during this event. It cannot be ruled out that Fe and Mn also were mobile to some extent during the emplacement of the Eibenstock granite as magnetite has been altered to variable extent during later events. The low content of Fe and Mn in Erzgebirge granites, however, strongly indicate that these rocks represent very unlikely sources for Fe and Mn. The low contents of Ca in schists are not well understood, but may indicate that the mineralized schists lost some of its already low Ca content to the fluid. It should be noted that the low K, Na, Ba, and Rb contents in some of the skarns do not reflect loss of these elements, but imply that the protolith of these skarns had been dominated by carbonates. (ii) Sn and W are both enriched in all skarn types as well as in schists and gneisses. Even if the Sn enrichment is definitely more important, Sn and W contents are correlated (electronic supplementary material 5) and thus may reflect the same enrichment process. Note, the enhanced contents of Sn and W, but also of In, Cs, As and Cd, in the schists do not imply that the protolith already had high contents. Instead, the reaction of Sn-W-bearing aqueous fluids with impure marbles during regional metamorphism induced the formation of Mg-Fe-rich calc-silicates (garnet, amphibole, and pyroxene). The release of CO_2 resulting from this reaction lead to the destabilization of Sn complexes (Schmidt, 2018) and possibly of W complexes. Sn, and maybe W, were then incorporated in newly formed skarn calc-silicates. (iii) As, Cu, Zn, and In are found in blebs in the magnetite skarn and in layers of massive sphalerite that occur at the vicinity of the magnetite skarn (Bauer et al., 2017). These blebs are later than the original skarn formation and reflect post-metamorphic redistribution (Bauer et al., 2017). The retrogression of the original skarn by fluids derived from the Eibenstock granite intrusion at c. 320 Ma, induced the alteration of primary skarn minerals and the formation of secondary minerals such as chlorite, apatite, fluorite, and cassiterite.

4.5.2. Isotopic composition of Li and B in greisen and skarn

As shown in Fig. 23c, greisen minerals can be divided in three groups with different signatures. One group comprises feldspar that has similar B and Li isotopic compositions as the Eibenstock granite. These feldspar samples are likely to have been part of the granite before greisenization. The second group of minerals from the greisen mostly includes muscovite. The Li and B isotopic composition of muscovite falls in the field of Paleozoic sedimentary rocks (Fig. 23c). The other white mica and tourmaline samples (from metasomatized phyllites JG1 and JG2) constitute the third group. Their signature resembles that of metamorphic rocks of the Erzgebirge.

The Li and B budget of the greisen minerals is dominated by material derived from the granite. In contrast, the Li and B budget of the skarn samples is dominated by the Paleozoic sedimentary rocks that form the host rocks of the skarns and that have been percolated by the fluids that induced skarn

formation. Contributions of Li and B from the granite may be minor and noticed in late mineral phases as the granite intruded 20 Ma after the skarn formation (Lefebvre et al., 2019). For instance, the magnetite skarn and one amphibole skarn sample have high δ^7Li values, possibly still reflecting the original signature of carbonates and authigenic minerals (Fig. 23a). In some skarn samples (amphibole skarn, Lefebvre et al., 2019), there is late tourmaline (foitite). This tourmaline indicates that boron was introduced to the skarn by granitic fluids. This granitic influence on the isotopic signature of the skarn is visible with some amphibole and pyroxene skarn samples (samples CSV1-02, HAS1-02, HPS1-01, and HPS1-02) (Figs. 23b and 23d). The contrasting presence of Li and B derived from the granite in the skarn samples does not necessarily imply that there was no Li in fluids released from the granites. Instead, it could imply that Li was largely scavenged from the fluid by silicate minerals before these fluids reached the skarn and, therefore, contributions of Li are subordinate, whereas contributions of B are at least locally more significant.

4.5.3. General model for the formation of the Hämmerlein polymetallic skarn deposit

Two stages have been determined for the formation of the Hämmerlein polymetallic skarn deposit. The first stage occurred at ~340 Ma during the regional metamorphism. Primary Sn-bearing calc-silicates are typical of this first stage. The second stage occurred at least 20 Ma after the regional metamorphism during a thermal event. The age of this second event is only indirectly inferred from the highly radiogenic Sr isotopic composition of the secondary minerals of the skarn (apatite and fluorite) assuming these minerals derived their Sr from altered biotite. The estimated minimum age gap corresponds to the time needed before biotite developed such radiogenic Sr (for discussion see Lefebvre et al. 2019). Cassiterite is the dominant Sn carrier in these secondary mineral assemblages. The Eibenstock granite intrusion is likely to be related to this second event.

The REE elements are relatively little mobile in aqueous fluids. Therefore mineralizing fluids typically do not change the REE contents in skarn systems significantly, implying that the REE signatures represent those of the host rocks/protolith (Lottermoser, 1992). This is in line with our Nd isotope data that correspond to the Nd isotopic composition of the metasedimentary host-rocks, rather than the granite (Fig. 21). The magnetite and some amphibole/pyroxene skarns have the lowest REE contents among the skarn samples and the UCC-normalized pattern shows a relative depletion of the LREE relative to HREE. These features are typical for marine carbonates (Fig. 20) and therefore, the protoliths of these skarn samples most likely consisted of carbonates with little or no contribution of detrital silicate minerals. Furthermore, such low LREE contents are typical for minerals that precipitated from hydrothermal fluids (Möller et al., 1982; Schwinn and Markl, 2005). As hydrothermal fluids induce decarbonation reactions when they alter carbonate units, complexes transporting REE may be destabilized. This may explain the strong depletion in LREE in magnetite and pyroxene skarns, as they seem to have been the units with the highest proportion of carbonates. Furthermore, depletion in LREE implies depletion in Sm and Nd. Because Nd from the hydrothermal fluid does not contribute

significantly to the Nd budget of the skarn and the Nd isotopic composition of the fluid may have exchanged with the metasedimentary host rocks of the skarn, the additions of hydrothermal Nd are isotopically non-distinctive even in the pyroxene and magnetite skarns. In contrast, garnet and most amphibole skarn samples have higher REE contents and a flat UCC-normalized REE pattern. This indicates that the carbonate protolith of these samples had distinctly higher contents of detrital silicates. In these samples, the REE budget is dominated by the silicate minerals. Thus, the carbonates are geochemically not very prominent except for the few elements that are strongly enriched in carbonate minerals (e.g., Ca, Mg, Sr). The carbonates, however, are extremely important to modify the fluid and change its potential to transport metals. With such reduced proportions of carbonates, compared to magnetite and pyroxene skarns, the garnet and amphibole skarns did not see any important decarbonation reactions.

The c. 340 Ma old skarns at Hämmerlein have Sn-rich skarn minerals (garnet, pyroxene, and amphibole). This implies that at least some Sn was introduced into the skarns before the intrusion of the Eibenstock granite. Furthermore, this implies that granite-derived fluids were not the only Sn source and there was an additional Sn source. The metamorphosed sedimentary rocks are a likely source for this "pre-granite" Sn. During prograde Variscan metamorphism, reaching peak metamorphic conditions at ca. 340 Ma, the sedimentary rocks lost water. Most of the water is lost already at low and intermediate metamorphic grade (e.g., Fyfe et al., 1978). The mobility of Sn in aqueous fluids increases with temperature and availability of suitable ligands, in particular Cl, which may be derived from trapped pore water at low temperature and from the decomposition of Cl-bearing minerals at higher temperature. During prograde metamorphism, Sn adsorbed on or incorporated in Fe-oxyhydroxides and clay minerals will be redistributed between fluid and newly formed minerals. It is unclear whether there are multiple stages of Sn redistribution and whether Sn redistribution within the sedimentary rocks already started during early stages of subduction. The only essential point for the Hämmerlein deposit is that Sn was transported at the time of skarn formation. The correlation between Sn and W indicates that W also was transported by skarn-forming fluids, as well as Fe as all skarns have high contents (Fe_2O_3 > 20 wt%). All these elements may derive from the metamorphic recrystallization of sedimentary rocks, which is in line with the observed Li, B, Sr, and Pb isotopic compositions (Nd is unlikely to have been leached and transported). The isotope data, however, are little distinctive, as the entire stack of metamorphic nappes is dominated by metasedimentary rocks (Figs. 21, 22, and 23). Some of the Saxo-Thuringian Paleozoic shales that are incorporated into the metamorphic nappes of the Erzgebirge are particularly enriched in Sn (Mingram, 1998; Romer and Kroner, 2015). These rocks would represent excellent sources for Sn mobilized during prograde metamorphism. The encounter of aqueous metamorphic fluids with the impure marbles induced decarbonation and formation of Fe-rich calc-silicate minerals that contain variable amounts of Sn. The precipitation of the metals (Fe, Mn, Sn, W) and the preferential incorporation of Sn into silicates rather than into oxides may be related to the change of composition of fluids, with or without phase separation, and possibly the change of redox conditions due to the addition

of tremendous amounts of Fe (Pabalan, 1986; Wilson and Eugster, 1990; Taylor and Wall, 1993; Mlynarczyk et al., 2003).

Fluids derived from the granite intrusion at 320 Ma formed greisen mineralization at the contact between granite and metamorphic rocks and within the metamorphic rocks and altered the skarns. Elements that have been redistributed during greisen formation are likely also to have been also in the fluids that retrogressed the skarns after the destabilization of Sn-bearing minerals. The greisens formed by circulation of hydrothermal fluids produced by the various intrusions of Eibenstock granite (Velichkin et al., 1994; Werner et al., 1997; Werner and Lippolt, 1998; Förster et al., 1999) and are dominated by the mineral assemblage quartz-cassiterite-polylithionite-chlorite-schorl-apatite. The Li and B isotopic composition of minerals of this newly formed greisen assemblage reflects mixed contributions from meta-sedimentary and granitic sources. As magmatic/hydrothermal fluids introduced Sn, F, B, and Li to the greisen, it is likely that similar fluids contributed the same elements also to the skarn mineralization.

The magmatic/hydrothermal fluids, from the Eibenstock granite, most likely carried Sn as Cl-complexes and percolated into the wall rocks to form greisens and to retrogress skarns. In the skarn this resulted in the alteration of the original mineral assemblage, in particular in the chloritization of biotite and amphibole. This alteration released Sn, F, Ca, Fe, and radiogenic Sr (Malyshev and Korzhanovskaya, 1989; Lefebvre et al., 2019). A change in oxidation state and pH of the fluid is necessary to destabilize Sn-Cl complexes and to precipitate cassiterite (Heinrich, 1990; Korges et al., 2018). The release of both O_2 and Fe during chloritization as well as the increase of pH due to the alteration of amphibole are likely to have induced cassiterite formation (Malyshev and Korzhanovskaya, 1989; Tarantola et al., 2009). Thus, changes of the fluid composition promoted the formation of secondary assemblages with cassiterite, chlorite, and apatite and fluorite with radiogenic Sr isotopic compositions.

The comparison between mineralized and barren rocks (Fig. 19a) shows that the first ones are also more enriched in Cu, W, and In. These elements were introduced into the skarn, maybe at the same time as Sn, by magmatic/hydrothermal fluids derived from the Eibenstock granite. Redistribution of Cu, Zn, W, and In by hydrothermal fluids may have resulted in In accumulation especially in Fe-rich sphalerite and In-rich chalcopyrite-pyrite blebs in the magnetite skarn. Later decomposition of In-bearing chalcopyrite in the magnetite skarn resulted in In enrichment in exsolved sphalerite with up to 20 wt% In (Bauer et al., 2017). This alteration may reflect a late-stage event or may be related to later, entirely unrelated events, such as the post-280 Ma U mineralization/remobilization along the Gera-Jáchymov structure (Förster, 1996).

4.6. Summary/Conclusions

The Sn mineralization in the Hämmerlein skarn formed in two steps, both characterized by specific chemical and isotopic signatures:

(1) During regional metamorphism at 340 Ma, different types of skarn (garnet, amphibole, pyroxene, magnetite) formed by interaction of carbonate bearing lithologies with aqueous metamorphic fluids. The prograde skarn minerals garnet, amphibole, and pyroxene have high Sn contents (up to 0.9 wt%) (Lefebvre et al., 2019), which implies that the metamorphic fluids that formed the skarn transported Sn and that Sn was incorporated in the newly formed silicate minerals of the skarn. These metamorphic fluids also transported W, Fe, and As. At 340 Ma, there was no granitic magmatism in the Erzgebirge and, therefore, Sn and other elements introduced into the skarn were derived from the surrounding metamorphic nappes. The Sr, Nd, and Pb isotopic compositions of the skarns and various skarn minerals resemble those of the metamorphic nappes and their early Paleozoic sedimentary protoliths, some of which have enhanced Sn contents.

(2) Hydrothermal fluids, produced by several pulses of Eibenstock granite at ca. 320 Ma, induced the alteration of granitic units and skarns. Greisen that formed from granitic units shows typical cassiterite-tourmaline-polylithionite assemblages, which attest that the Eibenstock granite was a source of Sn, Li, and B. These hydrothermal fluids also percolated into the skarn units, retrogressed them and enriched them in Sn. The alteration of calc-silicate minerals also released Sn that precipitated as cassiterite. This type of cassiterite is spatially and causally related to the chloritization of biotite and amphibole that increases fO_2 and pH, eventually resulting in the precipitation of cassiterite together with chlorite, fluorite, and apatite.

Even though the tin mineralization of the Hämmerlein skarn presents several features of traditional tin skarn models (Einaudi et al., 1981; Kwak, 1997), the example of the Hämmerlein skarn shows that it is possible to form Sn-rich skarns during regional metamorphism. Metamorphic fluids obviously have the potential to leach Sn from sedimentary rocks and induce the formation of skarns at the expense of carbonates. Tin is incorporated in these newly-formed skarn minerals. The resulting skarn is not economically interesting as Sn is hosted in silicate phases rather than in cassiterite. Later retrogression of Sn-bearing silicates, however, may release Sn and allow the formation of cassiterite. As a result of such late alterations, economically interesting Sn skarn may form in association with barren granites or without associated granite.

5. Conclusion

The Hämmerlein polymetallic skarn deposit presents features that are typical of skarns, and more specifically, Sn-skarn deposits. The deposit shows a stratiform geometry, following the sedimentary layers of the host rocks. It is also directly linked to the Eibenstock granite intrusion, which is an evolved S-type granite. Minerals occuring at Hämmerlein are also typical of Sn-skarns, with several calc-silicates such as garnet, pyroxene, and amphibole. The main Sn host is cassiterite. Another typical characteristic of Sn-skarns is the occurrence of greisens. In the case of Hämmerlein, a greisen alteration and Sn

mineralization developped near the Eibenstock granite due to the percolation of granitic fluids. All of these characteritics lead to the conclusion that, at first sight, the Hämmerlein skarn is a typical Sn-skarn.

Isotopic dating shows that the skarns formed at 340 Ma during the regional metamorphism, i.e. 20 Ma before the Eibenstock granite intrusion. The granite cannot be responsible for the skarn formation. Furthermore, the several isotopic data (Sr, Nd, Pb, Li, B) of the skarns do not ressemble the isotopic composition of the granite. However, skarns isotopic signatures correspond to those of metamorphic rocks of the Erzgebirge and their Paleozoic sedimentary protolith. These metasedimentary rocks were the source for Sn that was transported and incorporated in primary calc-silicate minerals of the skarns during regional metamorphism.

On the other hand, the greisen and its mineralization are clearly associated to the Eibenstock granite. The age of c. 320 Ma obtained for the greisen in chapter 2 is coherent with field observations. In the greisen, the mineralization occurs as typical cassiterite-fluorite-apatite-polylithionite assemblages. In the skarn, the typical mineralization assemblage, which represents a retrograde alteration of the original mineral assemblage, is the same as in the greisen, except for polylithionite that does not occur because of the low amount of Li available for its formation in the skarn. In chapter 2, we showed that this cassiterite-fluorite-apatite assemblage formed later than the skarn, and its age was estimated around 320 Ma. Thus, even if the Eibenstock granite is not the cause of skarn formation, it is likely that it is the main source of Sn for the mineralization. The alteration of skarn calc-silicates and biotite, by magmatic/hydrothermal fluids, however, may have released Sn that formed cassiterite in those seconday assemblages.

To summarize, the Hämmerlein deposit is an example of skarn that formed during regional metamorphism with a first Sn enrichment via that leached Sn from sediments. The economic mineralization is linked to a late granitic intrusion that altered Sn-bearing minerals, and added more Sn to the system. It shows that it is possible to form a Sn-rich skarn without any mineralizing granite. The regional metamorphism does not result in economically valuable skarn, as Sn is mostly incorporated in silicate minerals. However, if Sn-bearing skarn minerals are altered, by any fluids from any heat source, to release Sn and precipitate cassiterite, the skarn may become economically interesting. It may then be possible to find new Sn-skarn deposits that are not associated with any mineralizing granite, or even no granite at all. The only prerequisites are a first Sn enrichment and a secondary heat and fluids source.

Bibliography

ALS Minerals (2009a) Short Method ME-ICP61a Four Acid Near Total ICP Multi element Intermediate Grade. https://www.alsglobal.com/myals/downloads. Accessed 02 February 2018.

ALS Minerals (2009b) Short Method ME-MS81 Lithium Metaborate fusion ICP-MS Multi element. https://www.alsglobal.com/myals/downloads. Accessed 02 February 2018.

Anglo Saxony Mining (2015) Westerzgebirge Project Hämmerlein-Tellerhäuser: Long Section through Adit. http://www.anglosaxony.com/projects/germany/tellerhauser. Accessed 04 June 2018.

Bauer ME, Seifert T, Burisch M, Krause J, Richter N, Gutzmer J (2019) Indium-bearing sulfides from the Hämmerlein skarn deposit, Erzgebirge, Germany: evidence for late-stage diffusion indium into sphalerite. Mineralium Deposita 54:175–192.

Begemann F, Ludwig KR, Lugmair GW, Min K, Nyquist LE, Patchett PJ, Renne PR, Shih CY, Villa IM, Walker RJ (2001) Call for an improved set of decay constants for geochronological use. Geochimica et Cosmochimica Acta 65:111–121.

Bielicki, KH Tischendorf G (1991) Lead isotope and Pb-Pb model age determinations of ores from Central Europe and their metallogenetic interpretation. Contributions to Mineralogy and Petrology 106:440–461.

Bolhar R, Van Kranendonk MJ (2007) A non-marine depositional setting for northern Fortescue Group, Pilbara Craton, inferred from trace element geochemistry of stromatolitic carbonates. Precambrian Research 155:229–250.

Brady J, Perkins D (2015) Mineral Formulae Recalculation. SERC Carleton College. http://serc.carleton.edu/research_education/equilibria/mineralformulaerecalculation.html. Accessed 31 May 2017.

Breiter K (1993) The Nejdek pluton – discussion of granite evolution and Sn-W mineralization. Zeitschrift für Geologische Wissenschaften 21:2–36.

Breiter K (2012) Nearly contemporaneous evolution of the A- and S-type fractionated granites in the Krušné hory/Erzgebirge Mts., Central Europe. Lithos 151:105–121.

Breiter K, Förster HJ, Seltmann R (1999) Variscan silicic magmatism and related tin-tungsten mineralization in the Erzgebirge-Slavkoský les metallogenic province. Mineralium Deposita 34:505–521.

Burt DM (1982) Skarn deposits; historical bibliography through 1970. Economic Geology 77:755–763.

Chappell BW, White AJR (1974) Two contrasting granite types. Pacific Geology 8:173–174.

Chen J, Halls C, Stanley CJ (1992) Tin-bearing skarns of South China: Geological setting and mineralogy. Ore Geology Reviews 7:225–248.

Dadàk V, Novák F (1965) Tin-containing andradite from Plavno mine in the Krušné Hory Mts., Czechoslovakia. Mineralogical Magazine 35:379–385.

de Capitani C, Brown TH (1987) The computation of chemical equilibrium in complex systems containing non-ideal solutions. Geochimica et cosmochimica Acta 51:2639–2652.

de Capitani C, Petrakakis K (2010) The computation of equilibrium assemblage diagrams with Theriak/Domino software. American Mineralogist 95:1006–1016.

de Vore GW (1955) The Rate of Adsorption in the Fractionation and Distribution of Elements. The Journal of Geology 63:159–190.

Diamond LW (2001) Review of the systematics of CO_2-H_2O fluid inclusions. Lithos 55:69–99.

Dobson DC (1982) Geology and alteration of the Lost River tin-tungsten-fluorite deposit, Alaska. Economic Geology 77:1033–1052.

Doroshkevich AG, Veksler IV, Klemd R, Khromova EA, Izbrodin IA (2017) Trace-element composition of minerals and rocks in the Belaya Zima carbonatite complex (Russia): Implications for the mechanisms of magma evolution and carbonatite formation. Lithos 284:91–108.

Dyar MD, Wiedenbeck M, Robertson D, Cross LR, Delaney JS, Ferguson K, Francis CA, Grew ES, Guidotti CV, Hervig RL, Hughes JM, Husler J, Leeman W, McGuire AV, Rhede D, Rothe H, Paul RL, Richards I, Yates M (2001) Reference Minerals for the Microanalysis of Light Elements. Geostandards Newsletter 24:441–463.

Eadington PJ, Kinealy K (1983) Some aspects of the hydrothermal reactions of tin during skarn formation. Journal of the Geological Society of Australia 30:461–471.

Einaudi MT, Burt DM (1982) Introduction; terminology, classification, and composition of skarn deposits. Economic Geology 77:745–754.

Einaudi MT, Meinert LD, Newberry RJ (1981) Skarn deposits. Economic Geology 75:317–391.

Eugster HP, McIver NL (1959) Boron analogues of alkali feldspars and related silicates. Geological Society of America Bulletin, 70:1598–1599.

Eugster HP, Wilson GA (1985) Transport and deposition of ore-forming elements in hydrothermal systems associated with granites, in: Halls, C. (Ed), High heat production (HHP) granites, hydrothermal circulation and ore genesis. Institute of Mining and Metallurgy Conference, London, pp. 87–98.

Förster B (1996) U/Pb Datierung an Pechblenden der U-Lagerstätte Aue-Niederschlema (Erzgebirge). Ph.D. Thesis, University of Giessen, Germany.

Förster HJ (1998) Die variszischen Granite des Erzgebirge und ihre akzessorischen Minerale. Habilitation Thesis, Tech Univ Bergakademie Freiberg, Germany.

Förster HJ, Romer RL (2010) Carboniferous magmatism. In: Linnemann U, Romer RL (ed) Pre-Mesozoic Geology of Saxo-Thuringia – From the Cadomian Active Margin to the Variscan Orogen, 1st edn. Schweizerbart, Stuttgart, pp 287–308.

Förster HJ, Tischendorf G, Trumbull RB, Gottesmann B (1999) Late-Collisional Granites in the Variscan Erzgebirge, Germany. Journal of Petrology 40:1613–1645.

Franke W (1989) Tectonostratigraphic units in the Variscan belt of central Europe. Geological Society of America Special Paper 230:67–90.

Fyfe WS, Price NJ, Thompson AB (1978) Fluids in the earth's crust. Elsevier, Amsterdam, 383 p.

Glodny J, Bingen B, Austrheim H, Molina JF, Rusin A (2002) Precise eclogitization ages deduced from Rb/Sr mineral systematics: the Maksyutov complex, Southern Urals, Russia. Geochimica et Cosmochimica Acta 66:1221–1235.

Hawthorne FC, Dirlam DM (2011) Tourmaline the Indicator Mineral: From Atomic Arrangement to Viking Navigation. Elements 7:307–312.

Heinrich C (1990) The chemistry of hydrothermal tin(-tungsten) ore deposition. Economic Geology 85:457– 481.

Heinrich W (2007) Fluid Immiscibility in Metamorphic Rocks. Reviews in Mineralogy and Geochemistry 65:389–430.

Huang J, Chu X, Jiang G, Feng L, Chang H (2011) Hydrothermal origin of elevated iron, manganese and redox-sensitive trace elements in the c. 635 Ma Doushantuo cap carbonate. Journal of the Geological Society 168:805–816.

Jeffcoate AB, Elliot T, Thomas A, Bouman C (2004) Precise, small sample determination of lithium compositions of geological reference materials and modern seawater by MC-ICPMS. Geostandards Newsletter 28:1–12.

Johan Z, Strnad L, Johan V (2012) Evolution of the Cínovec (Zinnwald) granite cupola, Czech Republic: Composition of feldspars and micas, a clue to the origin of W, Sn mineralization. Canadian Mineralogist 50:1131–1148.

Kasemann SA, Meixner A, Rocholl A, Vennemann T, Rosner M, Wiedenbeck M (2001) Boron and oxygen isotope composition of certified reference materials NIST SRM 610/612 and certified reference material JB-2 and JR-2. Geostandard Newsletter 25:405–416.

Kemnitz H, Ehling BC, Elicki O, Franzke HJ, Geyer G, Linnemann U, Leonhardt D, Plessen B, Rötzler J, Rohrmüller J, Romer RL, Tichomirowa M, Zedler H (2017) Proterozoikum–Silur in der Stratigraphischen Tabelle von Deutschland 2016. Zeitschrift der Deutschen Gesellschaft für Geowissenschaften 168:423–446.

Kempe U, Bombach K, Matukov D, Schlothauer T, Hutschenreuter J, Wolf D, Sergeev S (2004) Pb/Pb and U/Pb zircon dating of subvolcanic rhyolite as a time marker for Hercynian granite magmatism and Sn mineralization in the Eibenstock granite, Erzgebirge, Germany: Considering effects of zircon alteration. Mineralium Deposita 39:646–669.

Korges M, Weis P, Lüders V, Laurent O (2018) Depressurization and boiling of a single magmatic fluid as a mechanism for tin-tungsten deposit formation. Geology 46:75–78.

Kroner U, Hahn T, Romer RL, Linnemann U (2007) The Variscan orogeny in the Saxo-Thuringian zone–Heterogenous overprint of Cadomian/Paleozoic Peri-Gondwana crust. Geological Society of America Special Paper 423:153–172.

Kroner U, Romer RL (2013) Two plates – Many subduction zones: The Variscan orogeny reconsidered. Gondwana Research 24:298–329.

Kroner U, Roscher M, Romer RL (2016) Ancient plate kinematics derived from the deformation pattern of continental crust: Paleo- and Neo-Tethys opening coeval with prolonged Gondwana-Laurussia convergence. Tectonophysics 681:220–233.

Kröner A, Willner AP, Hegner E, Frischbutter A, Hofmann J, Bergner R (1995) Latest Precambrian (Cadomian) zircon ages, Nd isotopic systematics and P-T evolution of granitoid orthogneisses of the Erzgebirge, Saxony and Czech Republic. Geologische Rundschau 84:437–456.

Kwak TAP (1983) The geology and geochemistry of the zoned, Sn-WF-Be skarns at Mt. Lindsay, Tasmania, Australia. Economic Geology 78:1440–1465.

Kwak TAP (1986) Fluid inclusions in skarns (carbonate replacement deposits). Journal of Metamorphic Geology 4:363–384.

Kwak TAP (1987) W-Sn skarn deposits and related metamorphic skarns and granitoids, Developments in Economic Geology, No. 24, Elsevier, Amsterdam, 451 p.

Kwak TAP, Askins PW (1981) Geology and genesis of the F-Sn-W (-Be-Zn) skarn (wrigglite) at Moina, Tasmania. Economic Geology 76:439–467.

Leake BE, Wooley AR, Arps CES, Birch WD, Gilbert MC, Grice JD, Hawthorne FC, Kato A, Kisch HJ, Krivovichev VG, Linthout K, Laird J, Mandarino JA, Maresch WV, Nickel EH, Rock NMS, Schumacher JC, Smith DC, Stephenson NCN, Ungaretti L, Whittaker EJW, Youzhi G (1997) Nomenclature of amphiboles: Report of the subcommittee on amphiboles of the international mineralogical association commission on new minerals and minerals names. Canadian Mineralogist 35:219–246.

Lefebvre MG, Romer RL, Glodny J, Kroner U, Roscher M (2019) The Hämmerlein skarn hosted deposit and the Eibenstock granite associated greisen, western Erzgebirge, Germany: Two phases of mineralization – two Sn sources. Mineralium Deposita 54:193–216.

Lefebvre MG, Romer RL, Glodny J, Roscher M (2017) Two stages of skarn formation in the Hämmerlein tin-skarn deposit, western Erzgebirge, Germany. 14th SGA Biennial Meeting 4:1305–1308.

Lentz DR (1998) Mineralized intrusion-related skarn systems. Mineralogical Association of Canada Short Course Series 26.

Leonhardt D, Geißler E, Engelhardt-Sobe A, Baumgart G (2004) Geologische Karte des Freistaates Sachsen 1:25 000. Blatt 5542 Johanngeorgenstadt. Sächsisches Landesamt für Umwelt und Geologie Abteilung Geologie (ed).

Leonhardt D, Geißler E, Engelhardt A, Baumgart G (2010) Geologische Karte des Freistaates Sachsen 1:25 000. Blatt 5541 Eibenstock. Sächsisches Landesamt für Umwelt und Geologie Abteilung Geologie (ed).

Leonhardt D, Geißler E, Fritzsche H (1999) Geologische Karte des Freistaates Sachsen 1:25 000. Blatt 5543 Oberwiesenthal. Sächsisches Landesamt für Umwelt und Geologie Abteilung Geologie (ed).

Linnemann U, McNaughton NJ, Romer RL, Gehmlich M, Drost K, Tonk C (2004) West African provenance for Saxo-Thuringia (Bohemian Massif): Did Armorica ever leave pre-Pangean Gondwana? – U/Pb-SHRIMP zircon evidence and the Nd-isotopic record. Internal Journal of Earth Sciences 93:683–705.

Lottermoser BG (1992) Rare earth elements and hydrothermal ore formation processes. Ore Geology Reviews 7:25–41.

Malyshev BI, Korzhanovskaya VS (1989) Behavior of tin in calcareous-skarn and greisen processes. Geokhimiya 2:216–226.

Malyshev BI, Mironova OF, Naumov VB, Savel'eva NI, Salazkin AN, Volosov AG (1997) Fluids of the Hemmerlein Skarn-Greisen Tin Deposit, Erzgebirge, Germany. Geokhimiya 1:179–188.

Matte P (1986) Tectonics and plate tectonics model for the Variscan belt of Europe. Tectonophysics 126:329–374.

McIver JR, Mihálik P (1975) Stannian andradite from "Davib Ost", South West Africa. Canadian Mineralogist 13:217–221.

Meinert LD (1995) Compositional variation of igneous rocks associated with skarn deposits – chemical evidence for a genetic connection between petrogenesis and mineralization. Mineralogical Association of Canada Short Course Series 23:401–418.

Meinert LD, Dipple GM, Nicolescu S (2005) World Skarn Deposits. Economic Geology 100th Anniversary Volume, 299–336.

Mingram B (1996) Geochemische Signaturen der Metasedimente des erzgebirgischen Krustenstapels. Scientific Technical Report, STR96/04, GeoForschungsZentrum Potsdam, 104 p.

Mingram B (1998) The Erzgebirge, Germany, a subducted part of northern Gondwana: geochemical evidence for repetition of early Palaeozoic metasedimentary sequences in metamorphic thrust units. Geological Magazine 135:785–801.

Mlynarczyk MSJ, Sherlock RL, Williams-Jones AE (2003) San Rafael, Peru: geology and structure of the world's richest tin lode. Mineralium Deposita 38:555–567.

Möller P, Maus H, Gundlach H (1982) Die Entwicklung von Flußspatmineralisationen im Bereich des Schwarzwaldes. Jahreshefte des geologischen Landesamtes in Baden-Württemberg 24:35–70.

Mueller AG, Campbell IH, Schiøtte L, Sevigny JH, Layer PW (1996) Constraints on the Age of Granitoid Emplacement, Metamorphism, Gold Mineralization, and Subsequent Cooling of the Archean Greenstone Terrane at Big Bell, Western Australia. Economic Geology 91:896–915.

Mueller AG, McNaughton NJ (2000) U-Pb Ages Constraining Batholith Emplacement, Contact Metamorphism, and the Formation of Gold and W-Mo Skarns in the Southern Cross Area, Yilgarn Craton, Western Australia. Economic Geology 95:1231–1257.

Mueller B, Seward TM (2001) Spectrophotometric determination of the stability of tin(II) chloride complexes in aqueous solution up to 300°C. Geochimica et Cosmochimica Acta 65:4187–4199.

Newberry RJ (1979) Systematics in W-Mo-Cu skarn formation in the Sierra Nevada: and overview. Geological Society of America, Abstracts with Programs 11:486.

Newberry RJ (1997) Skarn deposits of Alaska. Economic Geology Monograph 9:355–395.

Newberry RJ (1998) W-and Sn-skarn deposits: a 1998 status report. Mineralized intrusion-related skarn systems 289–335.

Ondruš P, Veselovský F, Gabašová A, Drábek M, Dobeš P, Malý K, Hloušek J, Sejkora J (2003) Ore-forming processes and mineral parageneses of the Jáchymov ore district. Journal of GEOsciences 48:157–192.

Pabalan RT (1986) Solubility of cassiterite (SnO_2) in NaCl solutions from 200°C-350°C, with geologic applications. PhD thesis, Pennsylvania State University, USA.

Robb L (2005) Introduction to ore-forming processes, first ed. Blackwell Science Ltd, Johannesburg.

Rojík P (2005) Tin deposits at Přebuz and Rolava in the Krušné hory/Erzgebirge, Czech Republic: classic localities, new challenges. Journal of GEOsciences 50:157–165.

Romer RL, Hahne K (2010) Life of the Rheic Ocean: Scrolling through the shale record. Gondwana Research 17:236–253.

Romer RL, Kroner U (2015) Sediment and weathering control on the distribution of Paleozoic magmatic tin-tungsten mineralization. Mineralium Deposita 50:327–338.

Romer RL, Meixner A (2014) Lithium and boron isotopic fractionation in sedimentary rocks during metamorphism – The role of rock composition and protolith mineralogy. Geochimica et Cosmochimica Acta 128:158–177.

Romer RL, Meixner A, Förster H-J (2014a) Lithium and boron in late-orogenic granites – Isotopic fingerprints for the source of crustal melts? Geochimica et Cosmochimica Acta 131:98–114.

Romer RL, Meixner A, Hahne K (2014b) Lithium and boron isotopic composition of sedimentary rocks – The role of source history and depositional environment: A 250 Ma record from Cadomian orogeny to the Variscan orogeny. Gondwana Research 26:1093–1110.

Romer RL, Thomas R, Stein HJ, Rhede D (2007) Dating multiply overprint Sn-mineralized granites – examples from the Erzgebirge, Germany. Mineralium Deposita 42:337–359.

Rötzler K, Plessen B (2010) The Erzgebirge: a pile of ultrahigh- to low-pressure nappes of Early Paleozoic rocks and their Cadomian basement. In: Linnemann U, Romer RL (eds) Pre-Mesozoic Geology of Saxo-Thuringia – From the Cadomian Active Margin to the Variscan Orogen. Schweizerbart, Stuttgart, pp 253–270.

Rötzler K, Schumacher R, Maresch W, Willner A (1998) Characterization and geodynamic implications of contrasting metamorphic evolution in juxtaposed high-pressure units of the Western Erzgebirge (Saxony, Germany). European Journal of Mineralogy 10:261–280.

Schmidt C (2018) Formation of hydrothermal tin deposits: Raman spectroscopic evidence for an important role of aqueous Sn (IV) species. Geochimica et Cosmochimica Acta 220:499-511.

Schuppan W, Hiller A (2012) Die Komplexlagerstätten Tellerhäuser und Hämmerlein. Bergbaumonografie, Freiberg Band 17, 162p.

Schwinn G, Markl G (2005) REE systematics in hydrothermal fluorite. Chemical Geology 216:225–248.

Selway J, Xiong J (2015) Tourmaline Recalculation: Developed by Julie Selway & Jian Xiong. Andy Tindle – Free Software. http://www.open.ac.uk/earth-research/tindle/AGTWebPages/AGTSoft.html. Accessed 31 May 2017.

Shapenko VV, Šmidel P (1991) Sn and W mineralization in skarn-greisen deposits at the northern margin of the Bohemian massif. Geokhimiya 5:724–732.

Sheppard RA, Gude AJ (1973) Boron-bearing potassium feldspar of authigenic origin in closed basin deposits. Journal of Research of the U.S. Geological Survey 1:377–382.

Spear FS (1995) Metamorphic phase equilibria and pressure-temperature-time paths, second ed. Mineralogical Society of America, Washington, D.C.

Stamatakis MG (1989) A boron-bearing potassium feldspar in volcanic ash and tuffaceous rocks from Miocene lake deposits, Samos Island, Greece. American Mineralogist 74:230–235.

Štemprok M, Blecha V (2015) Variscan Sn-W-Mo metallogeny in the gravity picture of the Krušné hory/Erzgebirge granite batholith (Central Europe). Ore Geology Reviews 69:285–300.

Sukhoruchkin SI, Soroko ZN (2009a) Atomic Mass and Nuclear Binding Energy for Fe-56 (Iron). In: Schopper H (ed) Landolt-Börnstein – Group I Elementary Particules, Nuclei and Atoms, Springer Berlin Heidelberg, pp 2276–2278.

Sukhoruchkin SI, Soroko ZN (2009b) Atomic Mass and Nuclear Binding Energy for Sn-119 (Tin). In: Schopper H (ed) Landolt-Börnstein – Group I Elementary Particules, Nuclei and Atoms, Springer Berlin Heidelberg, pp 6838–6840.

Tarantola A, Mullis J, Guillaume D, Dubessy J, de Capitani C, Abdelmoula M (2009) Oxidation of CH_4 to CO_2 by chloritization of detrital biotite at 270 ± 5°C in the external part of the Central Alps, Switzerland. Lithos 112:497–510.

Taylor SR, McLennan SM (1985) The continental crust: Its composition and evolution. Blackwell Scientific Publications Oxford 312p.

Taylor SR, McLennan SM (1995) The geochemical evolution of the continental crust. Reviews of Geophysics 33:241–265.

Taylor JR, Wall VJ (1993) Cassiterite solubility, tin speciation and transport in a magmatic aqueous phase. Economic Geology 88:437–460.

Tichomirowa M, Hofmann M, Schaltegger U, Sergeev S, von Quadt A, Whitehouse M (2016) The “Older” and “Younger” granites from the Western Erzgebirge – comparison of different zircon dating methods. Freiberg Online Geoscience 46:36–38.

Tichomirowa M, Leonhardt D (2010) New age determinations (Pb/Pb zircon evaporation, Rb/Sr) on the granites from Aue-Schwarzenberg and Eibenstock, Western Erzgebirge, Germany. Zeitschrift für Geologische Wissenschaften 38:99–123.

Tischendorf G, Förster HJ, Gottesmann B (2001) Minor and trace-element composition of trioctahedral micas: a review. Mineralogical Magazine 65:249–276.

Tischendorf G, Gottesmann B, Förster HJ, Trumbull RB (1997) On Li-bearing micas: estimating Li from electron microprobe analyses and an improved diagram for graphical representation. Mineralogical Magazine 61:809–834.

Tomascak S, Carlson SB, Shirey SB (1999). Accurate and precise determination of Li isotopic compositions by multi-collector sector ICP-MS. Chemical Geology 158:145–154.

Tonarini S, Pennisi M, Leeman WP (1997) Precise boron isotopic analysis of complex silicate (rock) samples using alkali carbonate furion and ion-exchange separation. Chemical Geology 142:129–137.

Velichkin VI, Chernyshov IV, Simonova LI, Yudintsev SV (1994) Geotectonic position, petrochemical and geochronological features of the Younger Granite Complex in the Krŭsné Hory (Erzgebirge) of the Bohemian massif. Journal of GEOsciences 39:116.

Villa IM, De Bièvre P, Holden NE, Renne PR (2015) IUPAC-IUGS recommendation on the half-life of 87Rb. Geochimica et Cosmochimica Acta 164:382–385.

Wang L, Shimazaki H, Wang J, Wang Y (2001) Ore-forming fluid and metallization of the Huanggangliang skarn Fe-Sn deposit, Inner Mongolia. Science in China Series D 44:735–747.

Wang RC, Xie L, Chen J, Yu A, Wang LB, Lu JJ, Jinchu Zhu JC (2013) Tin-carrier minerals in metaluminous granites of the western Nanling Range (southern China): Constraints on processes of tin mineralization in oxidized granites. Journal of Asian Earth Sciences 74:361–372.

Wenzel T, Mertz DF, Oberhänsli R, Becker T, Renne PR (1997) Age, geodynamic setting, and mantle enrichment processes of a K-rich intrusion from the Meissen massif (northern Bohemian massif) and implications for related occurrences from the mid-European Hercynian. Geologische Rundschau 86:556–570.

Werner O, Lippolt HJ (1998) Datierung von postkinematischen magmatischen Intrusionsphasen des Erzgebirges: thermische und hydrothermale Überprägung der Nebengesteine. Terra Nostra 98:160–163.

Werner O, Lippolt HJ (2000) White mica $^{40}Ar/^{39}Ar$ ages of Erzgebirge metamorphic rocks simulating the chronological results by a model of Variscan crustal imbrication. In: Franke W, Haak V, Oncken O, Tanner D (eds) Orogenic processes: quantification and modelling in the Variscan belt of Central Europe. Geological Society London Special Publications 179:323–336.

Werner O, Lippolt HJ, Hess JC (1997) $^{40}Ar/^{39}Ar$- and Rb-Sr-investigations of the cooling-history of metamorphic and plutonic rocks in the Erzgebirge (Mid-European Saxothuringian). Terra Nova 9:106–107.

Willner A, Rötzler K, Maresch W (1997) Pressure-temperature and fluid evolution of quartzo-feldspathic rocks with a relic high-pressure, granulite-facies history from the central Erzgebirge (Saxony, Germany). Journal of Petrology 38:307–336.

Wilson GA, Eugster HP (1990) Cassiterite solubility and tin speciation in supercritical chloride solutions, in: Spencer, R.J., Chou-I-Ming (Eds), Fluid-mineral interaction: a tribute to H.P. Eugster, The Geochemical Society, Special Publication 2:179–195.

Zartman RE, Doe BR (1981) Plumbotectonics – the model. Tectonophysics 75:135–162.

Zhao KD, Jiang SY, Jiang YH, Wang RC (2005) Mineral chemistry of the Qitianling granitoid and the Furong tin ore deposit in Hunan Province, South China: implication for the genesis of granite and related tin mineralization. European Journal of Mineralogy 17:635–648.

Zuleger E, Erzinger J (1988) Determination of the REE and Y in silicates materials with ICP-AES. Fresenius' Zeitschrift für Analytische Chemie 332:140–143.